UNIVERSITAT POLITÈCNICA DE VALÈNCIA

PhD in Biotechnology

Genetically modified peripheral neurons transplant aided activity maintenance and secretome modulation: a novel strategy for spinal cord injury treatment

VALENCIA BIOMEDICAL RESEARCH FOUNDATION
CENTRO DE INVESTIGACIÓN PRÍNCIPE FELIPE

PhD Supervisor: Dr. Victoria Moreno Manzano
UPV Mentor: Dr. Esther Giraldo Reboloso
Submitted by:
Sonia Hingorani Jai Prakash
April, 2024

UNIVERSITAT POLITÈCNICA DE VALÈNCIA

VALENCIA BIOMEDICAL RESEARCH FOUNDATION
CENTRO DE INVESTIGACIÓN PRÍNCIPE FELIPE

Dr Victoria Moreno Manzano, PhD in Pharmacy and Head of the Neuronal and Tissue Regeneration Laboratory at the Centro de Investigación Príncipe Felipe
CERTIFIES that the thesis titled:

"Genetically modified peripheral neurons transplant aided activity maintenance and secretome modulation: a novel strategy for spinal cord injury treatment"

has been developed by Sonia Hingorani Jai Prakash under her supervision in the Centro de Investigación Príncipe Felipe as her Thesis Project to obtain a PhD degree in Biotechnology from the Universitat Politècnica de València.

Valencia, April 2024

Victoria Moreno Manzano

To Mom & Dad,

Ankush, Mischa & Mahyr

“Two roads diverged in the woods, and I,

I took the one less travelled by,

And that has made all the difference”

Robert Frost

Acknowledgements

First and foremost, I´d like to thank my director and mentor, Dr. Victoria Moreno for her unwavering, constant support and encouragement throughout the development of this thesis. I am grateful for the freedom you provided and the faith you have placed in me during these years. For giving me the opportunity to work and develop this thesis in your lab, and for providing a space to learn from you and others. For your "never give up" attitude. But most importantly, for never losing hope when times are testing. Thank you.

To everyone at the I-44 laboratory, I take back a family. I feel lucky and proud to not only have learnt with you, but also to have laughed, cried, and loved. Carlos, for creating this project. Esther, for your kindness, for your advice in times of need and love for science. Ana, for your wisdom and for the best advice one could ever ask for; but also, for the being best vet one could possibly wish for, and for being one of the funniest persons I know. Mara, your capacity to love and your kindness is infinite. You spread joy wherever you go. Thank you for being our lab-mommy, but also thank you for being you. To María, thank you for your hugs, support, and love; but especially for your bubbling energy which brought joy and smiles, every day. To Guillem, for being so kind and patient; for always smiling no matter what and for all the help you have given me. To Marina and Pablo, the senior (now post) pre-docs with whom I have shared not only an office, a few tears and long working hours, but also a piece of my journey. To Eric, your support in the lab has been invaluable, but I am also fortunate and thankful to be your friend. Bea, in you I found a fellow scientist, a friend, a confidante and everything in between. I am so used to following my journey next to you that life in general will be different without you. To MariMar, my gym and Montaditos partner, I will miss being both healthy and unhealthy at the same time with you. To Anita, never stop smiling and radiating positivity. You are and deserve the best. To the newest additions to the I-44 family – Sahira, Samuel, Meri, Karolina and Loris – you have completely changed the lab for better. Wishing you the best in the lab but also hoping to meet you more outside!

To Frank Bradke & his lab for allowing me to undertake a 3 month internship in his laboratory, gifting me one of the most enriching experiences of my life, both professionally and

personally. To Seba, science needs people like you. Thank you for your infinite wisdom and huge heart. To Alba and Adri, for the unexpected friendships in foreign countries.

To the I-05 family, Susana, Carlos, Paco, & especially Juan. Thank you for illuminating our lives. Your infectious smile will forever be missed. To all the “young CIPF” members who have made these years fun. To “Destino Final: Science Edition”, for making everything funny, for sharing our joys and sorrows, and for making sure none of us is alone. Carmen, Ana, Yaiza, Isa & Valentina, thank you. To Ally, for making everything funnier, especially post-work beers. Finally, to Mili and Angie, who have put up with me during my worst, laughed with me during my best and listened to my long rants. Thank you for making everything better.

To my family and friends who have accompanied me even while being so far, especially Srishti, I miss you. Thank you for being there whenever I needed you.

To Ankush, Mischa and Mahyr, for loving me when I don’t deserve it, for believing in me more than I do, for making me laugh, and for all times we can’t stand each other. My life is incomplete without you three. Thank you for making me a better person.

Finally, to Mom&Dad, nothing I can write can do justice to what you mean to me, today and every day. Everything I am and will be, is because of you. Everything I do; is to make you proud.

RESUMEN

El sistema nervioso forma una red organizada de circuitos neuronales especializadas que son esenciales para una locomoción adecuada. El sistema nervioso central (que consiste en el cerebro y la médula espinal) recibe y transmite información de manera eficaz que es transmitida por el sistema nervioso periférico a los músculos, que conlleva a movimiento. Mientras el sistema nervioso periférico retiene su capacidad intrínseca de regeneración, el sistema nervioso central tiene una capacidad regenerativa limitada o nula en estadios adultos. Por ello, las lesiones en el sistema nervioso central son críticas y a menudo carecen de cura. Una de ellas es la lesión de la médula espinal, que es una condición devastadora y debilitante que altera la vida y que carece de una cura o tratamiento eficaz actualmente. Una lesión resulta en una interrupción de la entrada supraespinal en la médula espinal, lo que conduce a una disfunción locomotora debajo de la lesión. La relación alterada entre excitación e inhibición debajo de una lesión, con un aumento en la inhibición, junto con la capacidad limitada de regeneración endógena de los tractos neuronales afectados, limitan aún más la función locomotora. Como resultado, la parálisis completa puede ocurrir incluso en pacientes con lesiones anatómicamente incompletas. En esta tesis doctoral, nos centramos en estas ideas principales para definir una terapia combinada como estrategia para tratar la lesión de la médula espinal. Hipotetizamos que, para ayudar a la capacidad limitada de regeneración de los tractos, un trasplante neuronal periférico (ganglios de la raíz dorsal, DRG) que retiene la capacidad intrínseca de regeneración puede ser una estrategia de trasplante efectiva. Para alterar la inhibición, mejorar la supervivencia e integración del trasplante en los circuitos, se empleó la sobreexpresión del canal de sodio dependiente del voltaje bacteriano, NaChBac. Finalmente, para dirigir y mejorar la regeneración axonal de las células endógenas y trasplantadas, utilizamos medicamentos que modulan el citoesqueleto para mejorar la longitud axonal. Esta tesis doctoral estudia los efectos de esta estrategia combinada para tratar la lesión de la médula espinal.

En el Capítulo 1, describimos los estudios *in vitro* realizados para validar nuestra hipótesis. Primero estudiamos el efecto sinérgico de los medicamentos que modulan el citoesqueleto Epothilone B y Blebbistatin en la longitud de las neuritas *in vitro* y observamos que mientras el tratamiento individual con Blebbistatin aumenta la longitud de las neuritas, la combinación con Epothilone conduce a una morfología del cono de crecimiento alterada que resulta en una

disminución de la longitud de las neuritas. A continuación, describimos el efecto de la expresión de NaChBac en los DRG y las células Neuro-2A. En las DRG, la expresión de NaChBac conduce a un aumento en la actividad intrínseca y la secreción de factores neurotróficos, promoviendo la señalización pro-supervivencia y la señalización anti-apoptótica en las células Neuro-2A. Finalmente, describimos cómo el efecto combinado de la expresión de NaChBac y Blebbistatin mejora la longitud de las neuritas *in vitro*.

En el Capítulo 2, evaluamos la supervivencia, eficacia e interacción del trasplante de DRG con el tracto corticoespinal, el tracto más importante involucrado en la locomoción, en un estudio *in vivo* a corto plazo. Encontramos una integración y supervivencia adecuada del trasplante en el tejido huésped. Además, mostramos que la expresión de NaChBac aumenta la supervivencia del número total de células trasplantadas, así como mejora la preservación del tracto corticoespinal después de la lesión.

En el Capítulo 3, evaluamos el efecto del tratamiento combinado en un escenario de lesión crónica y severa. Demostramos que la combinación del trasplante que expresa NaChBac y Blebbistatin limita la recuperación funcional, mientras que el trasplante que expresa NaChBac mejora significativamente la función locomotora en ratones. Por lo tanto, centramos nuestra investigación en este último grupo y encontramos que los animales trasplantados con DRGs que expresan NaChBac tenían un aumento de fibras neuronales positivas para tubulina, con mayor preservación de mielina, aunque las fibras descendentes serotonérgicas y corticoespinales no mostraron cambios significativos entre los grupos experimentales. Encontramos que el trasplante de DRGs que expresan NaChBac aumentó significativamente el input excitatorio neto determinado por el aumento en el número de contactos de VGLUT2 y la disminución en los contactos de VGAT en los somas de las neuronas inmediatamente caudales a las lesiones.

Así pues, el trabajo de la presente tesis doctoral sugiere que el trasplante de DRGs disociados que expresan NaChBac rescata significativamente parte de la función motora perdida, contribuyendo a mantener una actividad neuronal remanente excitatoria inmediatamente caudal a la zona lesionada, poniendo en evidencia la relevancia del mantenimiento de la actividad neuronal como estrategia de terapia para el rescate funcional de lesiones medulares severas.

RESUM

El sistema nerviós forma una xarxa organitzada de circuits neuronals especialitzades que són essencials per a una locomoció adequada. El sistema nerviós central (que consistix en el cervell i la medul·la espinal) rep i transmet informació de manera eficaç que és transmesa pel sistema nerviós perifèric als músculs, que comporta a moviment. Mentres el sistema nerviós perifèric reté la seua capacitat intrínseca de regeneració, el sistema nerviós central té una capacitat regenerativa limitada o nul·la en estadis adults. Per això, les lesions en el sistema nerviós central són crítiques i sovint manquen de cura. Una d'elles és la lesió de la medul·la espinal, que és una condició devastadora i debilitant que altera la vida i que manca d'una cura o tractament eficaç actualment. Una lesió resulta en una interrupció de l'entrada supraespinal en la medul·la espinal, la qual cosa conduïx a una disfunció locomotora davall de la lesió. La relació alterada entre excitació i inhibició davall d'una lesió, amb un augment en la inhibició, juntament amb la capacitat limitada de regeneració endògena dels tractes neuronals afectats, limiten encara més la funció locomotora. Com a resultat, la paràlisi completa pot ocórrer fins i tot en pacients amb lesions anatòmicament incompletes. En esta tesi doctoral, ens centrem en estes idees principals per a definir una teràpia combinada com a estratègia per a tractar la lesió de la medul·la espinal. Hipotetizamos que, per a ajudar a la capacitat limitada de regeneració dels tractes, un trasplantament neuronal perifèric (ganglis de l'arrel dorsal, DRG) que reté la capacitat intrínseca de regeneració pot ser una estratègia de trasplantament efectiva. Per a alterar la inhibició, millorar la supervivència i integració del trasplantament en els circuits, es va emprar la sobreexpresió del canal de sodi dependent del voltatge bacteri, NaChBac. Finalment, per a dirigir i millorar la regeneració axonal de les cèl·lules endògenes i trasplantades, utilitzem medicaments que modulen el citoesquelet per a millorar la longitud axonal. Esta tesi doctoral estudia els efectes d'esta estratègia combinada per a tractar la lesió de la medul·la espinal.

En el Capítol 1, descrivim els estudis *in vitro* realitzats per a validar la nostra hipòtesi. Primer estudiem l'efecte sinèrgic dels medicaments que modulen el citoesquelet Epothilone B i Blebbistatin en la longitud de les neurites *in vitro* i observem que mentres el tractament individual amb Blebbistatin augmenta la longitud dels neurites, la combinació amb Epothilone

conduïx a una morfologia del con de creixement alterada que resulta en una disminució de la longitud dels neurites. A continuació, descrivim l'efecte de l'expressió de NaChBac en els DRG i les cèl·lules Neuro-2A. En les DRG, l'expressió de NaChBac conduïx a un augment en l'activitat intrínseca i la secreció de factors neurotròfics, promovent la senyalització pro-supervivència i la senyalització anti-apoptótic en les cèl·lules Neuro-2A. Finalment, descrivim com l'efecte combinat de l'expressió de NaChBac i Blebbistatin millora la longitud dels neurites *in vitro*.

En el Capítol 2, avaluem la supervivència, eficàcia i interacció del trasplantament de DRG amb el tracte corticoespinal, el tracte més important involucrat en la locomoció, en un estudi *in vivo* a curt termini. Trobem una integració i supervivència adequada del trasplantament en el teixit hoste. A més, vam mostrar que l'expressió de NaChBac augmenta la supervivència del nombre total de cèl·lules trasplantades, així com millora la preservació del tracte corticoespinal després de la lesió.

En el Capítol 3, avaluem l'efecte del tractament combinat en un escenari de lesió crònica i severa. Vam demostrar que la combinació del trasplantament que expressa NaChBac i Blebbistatin limita la recuperació funcional, mentres que el trasplantament que expressa NaChBac millora significativament la funció locomotora en ratolins. Per tant, centrem la nostra investigació en este grup i descrivim que els animals trasplantats amb DRGs que expressen NaChBac tenien un augment en la fibra neuronal positiva per a tubulina i la preservació de la mielina, mentres que les fibres descendents serotonérgics i corticoespinales van romandre sense alteració. Trobem que el trasplantament de DRGs que expressen NaChBac va augmentar l'entrada neuronal excitatoria, com es va observar per l'augment en el nombre de contactes de VGLUT2 i la disminució en els contactes de VGAT immediatament cabals a les lesions.

Així doncs, el treball de la present tesi doctoral suggerix que el trasplantament de DRGs dissociats que expressen NaChBac rescata una funció motora significativa en retindre una activitat de relé neuronal excitatoria immediatament cabal a les lesions en un model crònic i sever de lesió de la medul·la espinal i destaca la importància del manteniment de l'activitat com a teràpia efectiva per a la lesió de la medul·la espinal.

SUMMARY

The nervous system forms specialized neuronal circuitry and organization that are essential for adequate locomotion. The central nervous system (consisting of the brain and spinal cord) effectively receives and relay information which is then delivered by the peripheral nervous system to muscles to achieve locomotion. It is known that while the peripheral nervous system retains its ability to regenerate, the central nervous system has little to no regenerative capacity in adult stages. Therefore, injuries to the central nervous system are critical and often lack cure. One of them is spinal cord injury, which is a devastating, debilitating, and life-altering condition that lacks a cure or effective treatment as of today. An injury results in severing of supraspinal input into the spinal cord, which leads to locomotor dysfunction beneath the injury. Altered excitation inhibition ratio after an injury, with an increase in inhibition, together with limited endogenous regeneration capacity of the affected neuronal tracts further limit locomotor function. As a result, complete paralysis may occur even in patients with anatomically incomplete injuries. In this doctoral thesis, we focus on these major points to devise a combinatory approach as an effective strategy to treat spinal cord injury. We hypothesized that to aid the limited regeneration capacity of the tracts, a peripheral neuronal transplant (dorsal root ganglia, DRG) which retains the intrinsic ability to regenerate can be an effective transplantation strategy. To overcome inhibition, improve survival and integration of the transplant into circuits, the overexpression of bacterial voltage gated NaChBac sodium channel was employed. Finally, to target and improve the axonal regeneration of endogenous and transplanted cells, we use cytoskeleton modulating drugs to enhance axonal length. This doctoral thesis studies the effects of this combinatory approach to treat spinal cord injury.

In Chapter 1, we describe the *in vitro* studies performed to validate our hypothesis. We first study the synergistic effect of cytoskeleton modulating drugs Epothilone B and Blebbistatin on neurite length *in vitro* and find that while individual treatment with Blebbistatin increases neurite length, combination with Epothilone leads to an altered splayed morphology of the growth cone which results in decreased neurite length. Next, we describe the effect of NaChBac expression in DRGs and Neuro-2A cells. In DRGs, NaChBac expression leads to an increase in intrinsic activity and secretion of neurotrophic factors, promoting pro-survival

signaling and anti-apoptotic signaling in Neuro-2A cells. Finally, we describe how the combinatory effect of NaChBac expression and Blebbistatin further improves neurite length *in vitro*.

In Chapter 2, we evaluate the survival, efficacy, and interaction of the DRG transplant with the corticospinal tract, the most important tract involved in locomotion in a short-term *in vivo* study. We report a satisfactory integration and survival of the transplant into the host tissue. Furthermore, we show that NaChBac expression increases the survival of the total number of transplanted cells, as well as improves preservation of the corticospinal tract after the injury.

In Chapter 3, we study the effect of the combinatory treatment in a chronic, severe injury scenario. We find that the combination of the transplant expressing NaChBac and Blebbistatin limits functional recovery, while that of transplant expressing NaChBac significantly improved locomotor function in mice. Therefore, focusing our further research on this group, we report that animals transplanted with NaChBac-expressing DRGs had increased tubulin-positive neuronal fiber and myelin preservation, while serotonergic and corticospinal descending fibers remained unaffected. We found that transplantation of NaChBac-expressing DRGs increased the neuronal excitatory input, as seen by increased number of VGLUT2 contacts and decrease in VGAT contacts immediately caudal to the injuries. Together, the work in this doctoral thesis suggests that the transplantation of NaChBac-expressing dissociated DRGs rescues significant motor function by retaining an excitatory neuronal relay activity immediately caudal to injuries in a chronic, severe spinal cord injury model and highlights the importance of maintenance of activity as an effective therapy for spinal cord injury.

Acronyms

5-HT 5-Hydroxytryptamine

AAV Adeno-associated virus

AHP After-hyperpolarization

AKT Ak strain transforming

AraC Arabinoside cytosine

ASIA American Spinal Injury Association

BDNF Brain-derived neurotrophic factor

BMS Basso Mouse Scale

BSA Bovine serum albumin

cAMP Cyclic adenosine monophosphate

CGRP Calcitonin gene-related peptide

ChABC chondroitinase ABC

CNS Central nervous system

CNTF Ciliary-derived neurotrophic factor

CSPG Chondroitin sulphate proteoglycans

CST Corticospinal tract

DMEM Dulbecco´s Modified Eagle Medium

DREADD Designer receptor exclusively activated by designer drugs

EES Electric epidural stimulation

EGF Epidermal growth factor

FGF-2 Fibroblast growth factor 2

GABA Gamma-aminobutyric acid

GAP-43 Growth-associated protein 43

GDNF Glial-derived neurotrophic factor

GFAP Glial fibrillary acidic protein

GFP Green fluorescent protein

GPCR Cell-type–specific G protein-coupled receptor

HBS HEPES-Buffered Saline

HEK Human embryonic kidney

ICAM L1 Intercellular cell adhesion molecule L1

IFU Infectious units

IGF1 Insulin-like growth factor 1

IN Interneuron

KCC2 Potassium chloride co-transporter 2

MAG Myelin-associated glycoprotein

MBP Myelin binding protein

MN Motor neuron

MOI Multiplicity of infection

MSC Mesenchymal stem cell

mTOR Mammalian target of rapamycin

N2A Neuroblastoma 2A

NCX Sodium calcium exchanger

NG2 Nerve/glial antigen 2

NGF Nerve growth factor

NGS Normal goat serum

NMDAR N-methyl-D-aspartate receptors

NMMII Non-muscle myosin II

Nogo A Neurite growth inhibitor A

NPC Neural precursor cell

NSC Neural stem cell

NT-3 Neurotrophin-3

OPC Oligodendrocyte precursor cell

PAB Para-amino blebbistatin

PNS Peripheral nervous system

PTEN Phosphatase and TENsin homolog deleted on chromosome 10

PVDF Polyvinylidene fluoride

RAG Regeneration associated gene

RbSt Rubrospinal tract

RFP Red fluorescent protein

RNS Reactive nitrogen species

ROCK Rho-associate protein kinase

ROS Reactive oxygen species

RT Room temperature

RtSt Reticulospinal tract

RpST Raphespinal tract

SC Spinal cord

SCI Spinal cord injury

SEM Standard error mean

SOCS3 Suppressor of cytokine signalling 3

TRPC Transient receptor potential canonical

VGAT Vesicular GABA transmitter

VGLUT2 Vesicular glutamate transporter 2

VGLUT1 Vesicular glutamate transporter 1

VST Vestibulospinal tract

List of Figures:

Table List:

Contents

Introduction

1.1 Spinal cord: structure and function

Motor function, including walking and standing, is a complex amalgamation of several processes, neuronal circuits and cells that synchronize to form a response. Voluntary decision making and initiation of movement occurs in several areas of the brain, such as the motor cortex, midbrain, hindbrain, and cerebellum [1]. These areas of the brain send important information through descending tracts which are present in the spinal cord, where they form synapses with both motoneurons (MNs) and interneurons (INs). In turn, these neurons innervate target muscles which are responsible eventually for movement produced [2]. Therefore, movement is highly determined by the interpretation of these signals from the brain by the complex circuits in the spinal cord, as well as the peripheral feedback received [3].

The spinal cord (SC) is a highly complex and fundamental part of the central nervous system (CNS), and its main function is to transmit information from the brain to the periphery and vice versa [4].

The SC is organized into segments. In humans, this corresponds to 8 cervical, 12 thoracic, 5 lumbar, 5 sacral and one coccygeal segment (**Figure 1A, C**). This organization varies slightly within species, for example, the mouse spinal cord consists of 34 segments: 8 cervical, 13 thoracic, 6 lumbar, 4 sacral, and 3 coccygeal (**Figure 1B**) [5].

Anatomically, the SC is divided into two parts: grey matter and white matter. The grey matter comprises of cell bodies, which include motor and peripheral neurons, interneurons, glial cells, and unmyelinated axons. It can be divided into ventral and dorsal horns, intermediate grey and centromedial region (**Figure 1C, D**) [6, 7].

Along the transversal axis, the horn can be divided into laminas, also known as Rexed laminas, according to function and cytoarchitecture. These were first identified by Rexed in cat spinal

cord [8]. These range from laminas I-X (**Figure 1C, D**), and can be easily identified by the neuronal distribution, or even by some pre-synaptic marker pattern distribution [9] .

On the other hand, the white matter, consists of myelinated axonal tracts that may be of descending (carry information from the brain to the periphery) or ascending (from afferents to the brain) type.

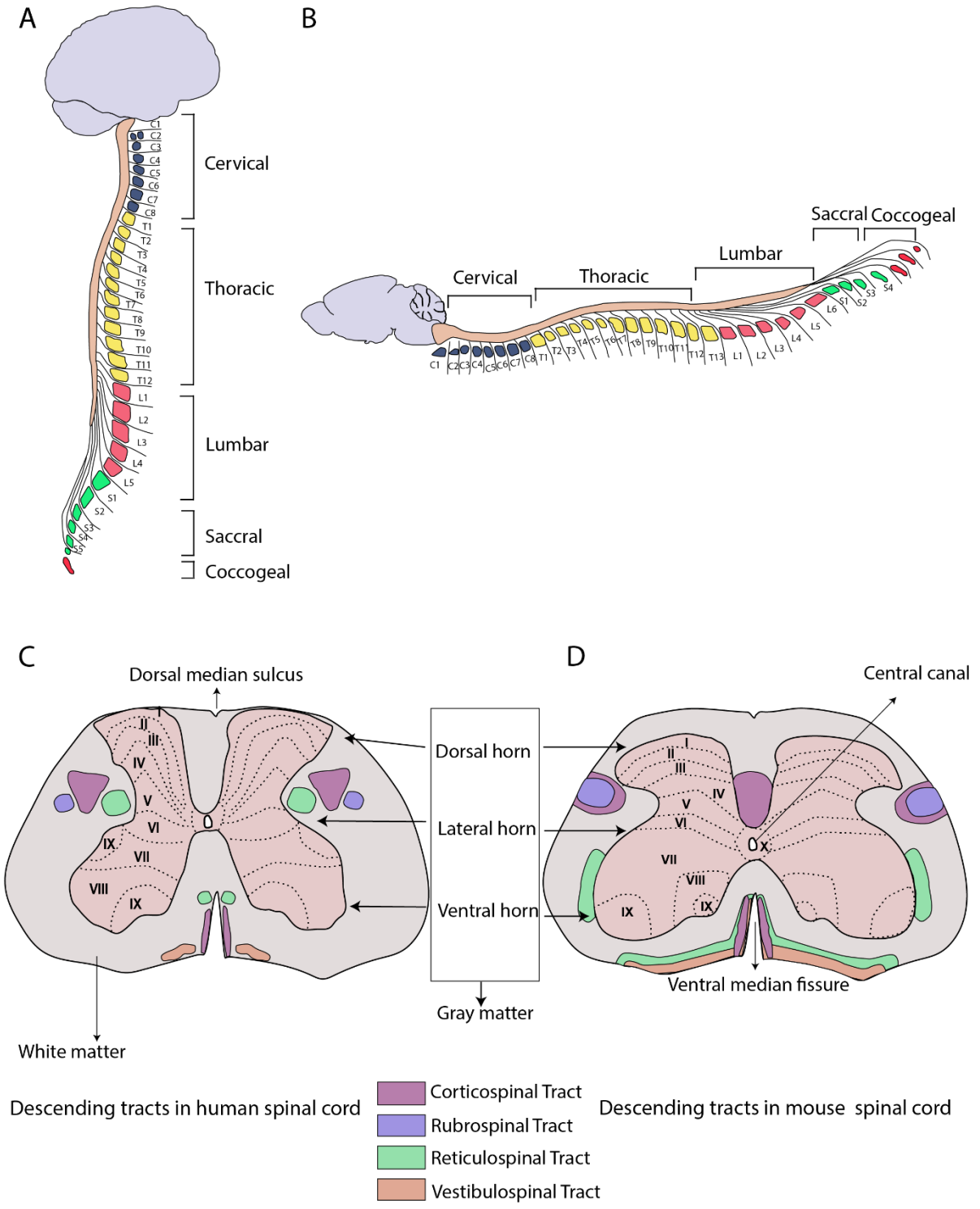

Figure 1*:* Representation of human spinal cord and segments as described by [6]. B) Illustration representing mouse spinal cord and its segments as described in *(Harrison et al., 2013*) *[10]*. C) Representation of a human spinal cross section along with the division into Rexed laminae (layers I-X) and the localization of major descending tracts as detailed in *(Saliani et al., 2017) [11]*. D) Illustration depicting a transversal section of a mouse spinal cord and its separation into Rexed laminae I-X, as well as the position of major descending tracts in the mouse, image created from information as shown in *(Saliani et al., 2017) [11]*.

1.2 Ascending and descending tracts in the spinal cord

Ascending tracts carry sensory information such as pain, temperature, touch and proprioception from the peripheral system – this information comes mainly from neurons of the dorsal root ganglia of the or the SC itself. These tracts carry information to the relevant areas in the brain (midbrain, hindbrain, brainstem, cerebellum). [12] These include the spinothalamic tract, spinocerebellar tract, spinomesencephalic, spinoreticular, spinobulbar, and spinocervical tracts [12].

Out of all **descending tracts** in the spinal cord, here we describe the major descending motor tracts that are present in the SC and have important contributions and consequences after an insult to the SC (**Figure 1C, D**). These are as following:

1.2.1 The corticospinal tract (CST)

The corticospinal tract (CST) is the largest tract originating mainly from the primary motor cortex neurons in the brain. It is an evolutionary conserved structure which is also the major voluntary tract controlling fine motor movements. A large percentage of the CST crosses the midline between the brain and the medulla and decussates before entering the SC [13]. Therefore, this part of the CST is present contralateral to its origin in the brain. In humans, the decussated CST is present at the dorso-lateral funiculus of the SC, contralateral to the point of origin [14] (**Figure 1A**); whereas the uncrossed CST is present at the ipsilateral to its origin [15]. In rodents, however, the crossed CST is present in the ventral part of the dorsal funiculus [14] , and the uncrossed CST is located at the ventral funiculus [16](**Figure 1B**).

It has been studied that contralateral CST innervates a specific, precise pool of MNs [17]. This anatomical feature explains the control of fine movements of the CST. While the importance of the CST in motor function has long been established [18], it is now known that it is also involved in the control of spinal reflexes [19], excitation and inhibition of motoneurons [18, 20], control of afferent input and autonomic control [21].

1.2.2 The rubrospinal tract (RbSt)

The RbST originates in the contralateral red nucleus in the brainstem[22]. The RbSt decussates at the ventral midbrain and descends in a contralaterally into the spinal cord. This tract is

especially developed in lower animals that rely on pectoral areas (eg. fins or upper limbs) for locomotion [23] but has also been shown to have a role in skilled functions such as grasping of food [24] Therefore, many of the fibres arising from the RbSt innervate mostly the cervical regions of the spinal cord [25], or the lumbosacral enlargement. Anatomically, RbSt fibres descend anteriorly to the CST. They innervate mainly interneurons that regulate large, flexor movements in the upper limb [26]. However, there is evidence to show direct connections of RbSt to MNs related to forepaw movement in both cats and rats [27, 28].

1.2.3 The reticulospinal tract (RtSt)

The reticulospinal tract (RtSt) is the second most important descending bilateral tract which originates in the reticular formation in the lateral brainstem [29], specifically, pontine caudal reticular nucleus, ipsilateral and rostral gigantocellular reticular neurons [30]. Unlike the CST, the RtSt does not decussate at any point before entering the SC.

The descending RtSt can be divided into lateral and medial tracts. The tract forms both direct synapsis with MNs and indirect (polysynaptic) connections to MNs [31]. This anatomy of the RtSt which enables bilateral innervation of MNs reaches a large pool of MNs, [31] in contrast to the CST. This anatomical feature of the RtSt explains its role in gross movements [32].

The RtSt has been identified as an important role for gross movements, such as postural control and locomotion [33, 34]; but also, in some finer reaching skill by interaction with the CST. It is mainly known thought to be involved in the process of initiation of movement. [32].

1.2.4 Vestibulospinal Tract (VST)

The VST tract originates in the vestibular nuclei of the brainstem. The main projections into the SC arise from the lateral vestibular nucleus [35]and the medial and spinal vestibular nuclei [36]. In humans, the medial VST connects to the cervical and thoracic segments of the SC whereas the lateral VST descends throughout the SC length [37, 38]. The lateral VST project in an ipsilateral manner into the SC whereas those arising from the medial and spinal vestibular nuclei project bilaterally [39]. The VST is largely associated with functions mainly to maintain and coordinate posture activity and muscle tones. In cats, it has been found to be responsible behind the initiation of extension in the limbs [40]. The lateral VST is controlled mostly by otolith signals [41].

The medial VST, on the other hand, receives input from semicircular canals and is related to maintaining position in space [42]. Most of the work on the VST has been carried out in cats, but some work in rats [43] and humans [44] show a similar anatomical structure.

1.2.5 Raphespinal (RpST) Tract

The raphespinal projections in the SC originate at the raphe in the brainstem, namely the raphe magnus, raphe pallidus nuclei and raphe obscurus [45].

Most of these neurons are serotonergic in nature, therefore constitute the major serotonergic, or 5-hydroxytryptamine (5-HT) fibre source in the SC [46]. These serotonergic projections from the raphe descend ipsilaterally and project into the vetrolateral white matter and innervate MNs in the ventral horn of all segments in the SC [47] but also have terminations in the dorsal horn [45]. The RpST plays an important role in the nociception modulation and response [48, 49], as well perform neuromodulatory control of rhythmic activity [50].

1.3 Spinal Cord Injury

1.3.1 Introduction and Prevalence

A spinal cord injury (SCI) occurs when sudden damage to the SC is produced, affecting the connections between the brain and one or more descending and/or ascending tracts, which leads to an interruption of the complex coordination between the brain and the SC [51].

SCI is a severely debilitating, life-altering injury which causes a wide range of symptoms, notably loss of motor, autonomic and sensory function. Other symptoms include dysfunction bladder, bowel sexual dysfunction, and pain [52]. It causes an economic burden to health systems, with an estimated cost of between 1-3 million USD throughout a patient´s life [53].. Typically, SCI is caused by a traumatic injury (90% of SCI cases) to the SC caused by accidents (38%), falls (32%) or injuries related to sports (8-17%) [54]. Non-traumatic SCI is caused mainly by cancer, infections, or degenerative diseases such as myelopathies [55, 56].

The global prevalence of SCI stands at about 1298 cases per million, or 250,000-500,000 thousand cases per year [57]. In Europe, the mean incidence is slightly lower than other developed countries, with about 16-19 cases per million habitants per year [58]; whereas it is 39 per million people in the US and 16 cases per million individuals in Australia [59]. SCI

exhibits a bimodal distribution, with one peak typically between 15-29 years of age, and the other above 50. It also has a higher prevalence in men than women (4:1) [58].

The outcomes of SCI vary depending on the location and severity of the SCI. Depending on the location, injuries to the upper cervical levels are associated with respiratory problems and quadriplegia, and lower segments (thoracic and lumbar) can lead to paraplegia. Injury severity, on the other hand is considered a more important factor for SCI outcome. To determine the severity of a SCI, the American Spinal Injury Association (ASIA) Impairment Scale is commonly used. This test assesses the grade of SCI and the remaining sensorimotor function [60] **(Table 1)**. SCI prognosis is greatly altered by acute treatment. In general, rapid intervention including spinal cord decompression within 24-36 hours after injury has been associated with improved sensorimotor preservation after injury [61]. It is therefore essential for any patients with suspected injuries to be treated efficiently and a quick diagnosis based on the AIS scale is essential. However, the AIS scale has some limitations and does not consider for example patients with sensory motor function preserved but not including sacral segments [62]. Additionally, initial spinal and neurogenic shock also further challenges the diagnosis. Nevertheless, a series of guidelines, including maintenance of adequate blood pressure, administration of methylprednisolone along with decompressive surgery are followed when treating with acute SCI patients. For SCI patients with cervical injuries, proper administration of oxygen and breathing supply is of utmost importance. The role of quick MRIs and scans to aid in diagnosis is also important. Lastly, the role of type and timing of rehabilitation is also essential to improve SCI prognosis [63].

Grade	**Description**
A (Complete)	No function (sensory or motor) present at S4-5 sacral segments.
B (Sensory incomplete)	Sensory function is present below the injury, including segments S4-5, but any motor function more than 3 levels beneath the injury is lost on both sides of the body.
C (Motor incomplete)	Motor function is present below the injury, at segments S4-5 OR patient presents sensory incomplete type injury and any motor function more than 3 levels beneath the injury is preserved on either side of the body.

D (Motor incomplete)	As C, but patient retains motor function in half or more essential muscle functions below the injury level.
E (Normal)	Both sensory and motor function are detected as normal in all segments.

Table 2: AIS scale adapted from *American Spinal Cord Injury Association*. The table shows the grade score (A-E) given to patients based on their sensory and motor function beneath the injury.

1.3.2 Pathophysiology

SCI can be divided into two distinct injury phases: primary injury and secondary injury.

1.3.2.1 Primary Injury

The primary injury phase comprises of the initial physical trauma including bone fracture and ligament tears which cause compression of the spinal cord leading to direct injury to neurons, astrocytes, endothelial cells, blood vessels and oligodendrocytes alike, disrupting neural pathways. The upsetting of the vasculature triggers haemorrhages and the formation of oedemas, as well as disrupts the blood brain barrier (BBB). There is an increase in pressure and consequent expansion of the SC [64].

1.3.2.2 Secondary Injury

The primary injury leads to a cascade cellular, molecular, and biochemical events which give rise to the secondary injury phase. This term refers to the subsequent, continuous damage and regeneration impediment in the SC. This phase can be further divided into acute (0-48h), sub-acute (48-2 weeks); and posterior chronic phases (>6 months) [65].

I. Acute phase

The acute phase begins shortly after the primary injury (within minutes) and is characterized by cellular changes caused due to vascular damage, ischaemia, spinal shock and cell death [66] (**Figure 2**). It is characterized by an imbalance in NMDA and Ca2+ regulation, together causing massive cell death.

Firstly, after SCI there is an increase in apoptotic signalling and an initial influx of pro-inflammatory cytokines, while a loss in the plasma integrity causes an influx of Ca2+ ions [67]. Increased cell death also leads to release of excitatory neurotransmitters, leading to an accumulation of glutamate and therefore, increased excitotoxicity [68]. Excessive glutamate accumulation also leads to ionic imbalance, causing an influx and disbalance of Ca2+ ions [69]. However, loss of plasma membrane integrity also contributes the sudden permeability to Ca2+ ions. Moreover, increase in glutamate leads to increase activity of N-methyl-D-aspartate (NMDA) of glutamate which also contributes to excessive Ca2+ influx in the mitochondria. Ca2+ is an important secondary messenger, therefore the intracellular accumulation of Ca2+ is directly associated to calcium dependent neuronal death [70].

Neuronal death also leads to an increase in the release of Na+, K+ and ATP. These further impair mitochondrial function, leading to a cyclic cell death. These factors contribute to the activation of microglial cells, which, in turn, activate other inflammatory cells such as lymphocytes and activated microphages. The role of inflammatory cell infiltration within the injury site is ambiguous since it has both detrimental and protective effects. On one hand, the inflammatory cells can clear off cell and myelin debris. On the other hand, they are responsible for the release of free radicals, which further lead to oxidation damage following into the acute phase [71].

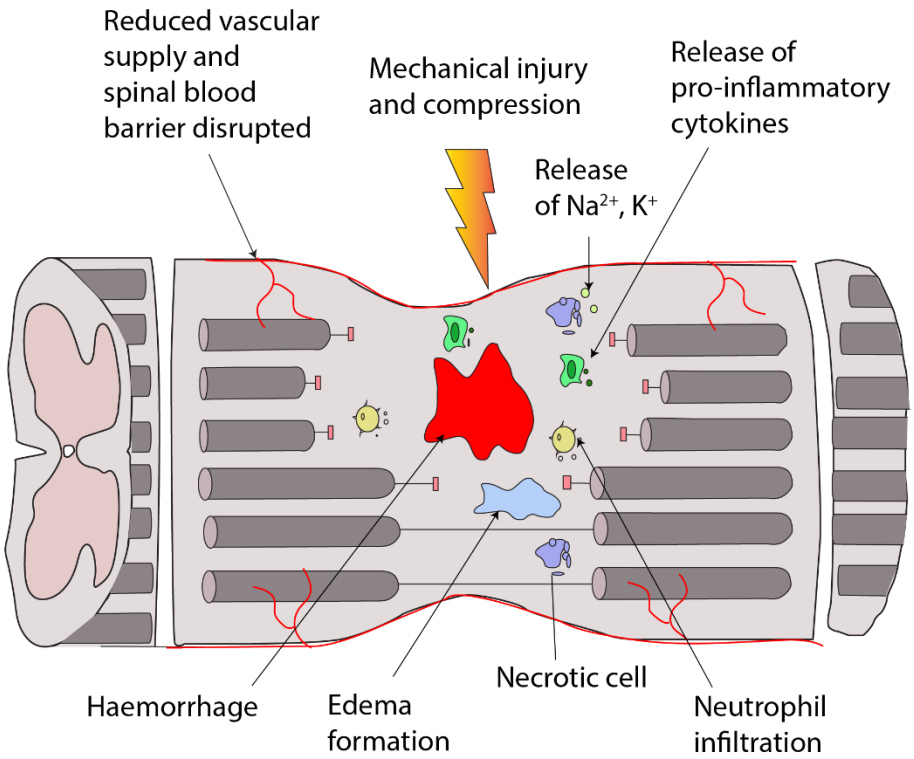

Figure 2: Schematic representation of the events that occur immediately (acute phase) after an injury. Figure created and based on *(Ahuja et al., 2017) [65]*.

II. Sub-Acute phase

Following the sub-acute phase, the acute phase is characterized by massive cell death and apoptosis and increased axonal degeneration (**Figure 3**). This includes Wallerian degeneration as well as axonal retraction [72], and demyelination [73]. Inflammatory cells begin to release free radicals, forming reactive oxygen species (ROS) and reactive nitrogen species (RNS), leading to lipid peroxidation [74]. Furthermore, large demyelination leaves axons exposed, which induces Wallerian degeneration of the axons. Wallerian degeneration is a compartmentalized, programmed degeneration which occurs first at distal parts of the axon near the injury up to the neuronal soma, followed by debris clearing by immune cells. At this stage, remodelling of the surrounding matrix characterized by the presence of inhibitory proteoglycans such as chondroitin sulphate proteoglycans (CSPGs) also occurs [75]. The glial cells begin their redistribution around the injury forming an impenetrable glial scar [76].

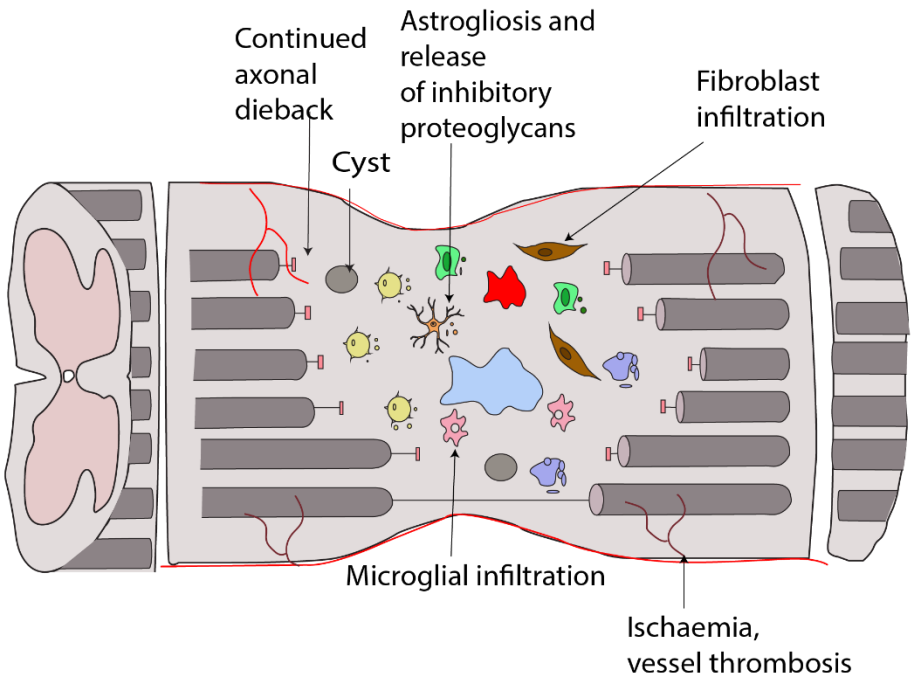

Figure 3: Illustration depicting the events that occur in the sub-acute phase after an injury. Figure created and based on *(Ahuja et al., 2017) [65]*.

III. Chronic phase

The chronic phase consists in the maturation and enlargement of the glial scar to an extremely inhibitory structure consisting of astrocytes that delimit the border [77], but also contains macrophages, pericytes, and fibroblasts [78] (**Figure 4**). It is also characterized by remodelling of neuronal circuits, including sprouting and spontaneous regeneration [79]. Wallerian degeneration continues to occur up to one year after SCI. It is largely considered that all these processes are stabilized one or two years after SCI in patients [80].

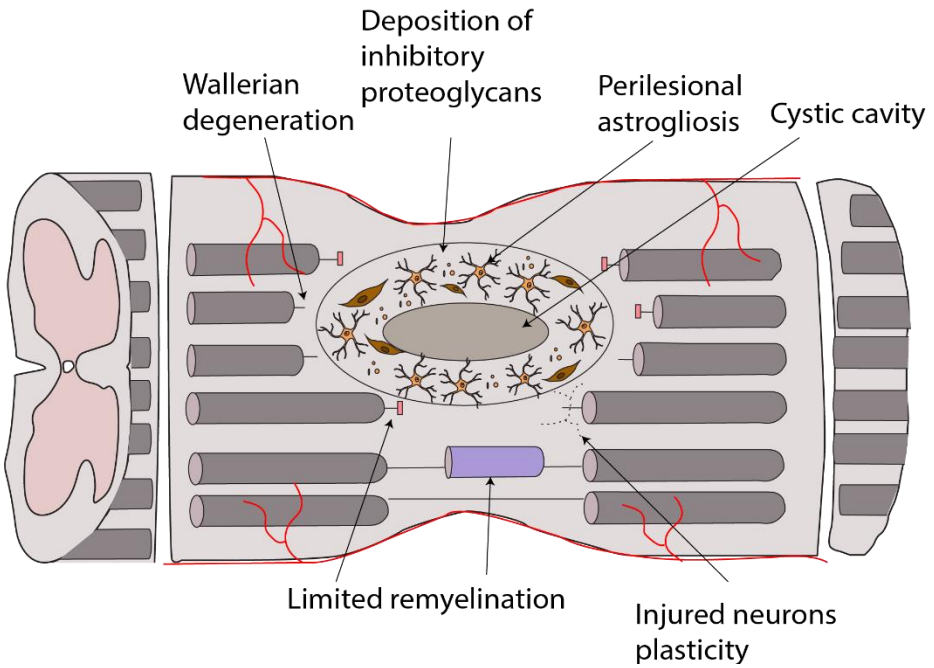

Figure 4: Representation of the hallmarks of the chronic phase of an injury. Figure created and based on *(Ahuja et al., 2017) [65]*.

1.4 Remodelling of SC after injury

Historically, it was believed that, unlike the peripheral nervous system (PNS), the CNS completely lacks intrinsic capacity for regeneration. More recently, however, this capacity of CNS regeneration is described as limited, but possible. CNS neurons often exhibit spasticity, sprouting and neuronal circuit rewiring in an attempt to overcome locomotor dysfunction, even years after the injury takes place [81]. While neurons do not regenerate, there is increase in proliferation of ependymal canal cells in rodents that produce precursor cells with the ability to proliferate into glial and even neuronal cells after SCI [82]. Additionally, early studies already revealed surviving neurons upregulate proteins such as growth-associated protein 43 (GAP-43) and cell adhesion molecules. GAP-43 is one of the first genes to be upregulated during development and, more importantly, during successful axonal regeneration [83]. Cell adhesion molecule L1 was found upregulated after SCI and showed a direct correlation with axonal regeneration in adult rats [84]. More recently, overexpression of L1 by transplanted NPCs further enhanced sprouting, preservation and re-myelination of serotonergic axons and CST axons [85]. Moreover, several gene profiling studies reveal the overexpression of regeneration associated genes (RAGs) such as GAP-43, nerve growth factor (NGF), brain-

derived neurotrophic factor (BDNF) and neurotrophin-3 (NT-3) [86, 87]. Additionally, growth promoting factors are released by macrophages and microglia into the injury, which could aid in limited axonal regeneration [88]. More importantly, it has been shown that spontaneous sprouting of important descending tracts such as the CST occurs in rats and leads to increased functional recovery [89]. This sprouting of the CST and other motor function relevant tracts such as the RtSt has been found to occur rostral to the injury, as well as caudal to the injury. Additionally, these collaterals have the ability to form "detour" circuits forming connections with propriospinal interneurons which can then form new intraspinal circuits to relay information [90].

However, these spontaneous changes in the SC alone do not seem to be enough to promote or provide relevant locomotor recovery. This is due a combination of factors which are described below.

1.5 Regeneration impediments

1.5.1 Lack of intrinsic regenerative capacity in the adult CNS:

During development, CNS axons display high intrinsic ability to grow and capacity to grow towards their target. However, as they mature, the CNS neurons lose this capacity, even after an insult or injury. This is attributed to several factors such as the lack of appropriate cues in the adult CNS and expression of regeneration or growth associated genes in adult CNS axons [91].

1.5.2 Glial scar:

Historically, the term glial scar has been referred to the astrocytic border formed surrounding the spinal cord injury, however it is additionally composed of non-neural cells such as fibroblast-like cells, glia and immune cells, and flibroblast-like cells [92]. The function of this border has contrasting views. In the initial phases of SCI, this structure is important to limit the injury site and infiltration of pro-inflammatory cells; as well as to prevent further injury to adjacent tissue [93]. However, after the injury is contained but the overall degenerative and reactive processes prevent effect tissue restoration, the scar becomes dysfunctional structure that encompasses an inhibitory environment for regeneration [94].

1.5.3 Presence of inhibitory matrix within inside and around the scar:

The presence of proteoglycans, especially CSPGs within the scar matrix has proved to be extremely effective blocking of axonal growth both *in vivo* [95] and *in vitro* [96]. CSPGs are thought to be secreted by astrocytes, and an increase in CSPG levels persists until months after an injury [97]. Lastly, the infiltration of fibroblasts and subsequent replacement of matrix with fibrous tissue also has detrimental effects to axon regeneration, which act as chemical barriers to axonal regeneration [98].

1.5.4 Inhibitory nature of myelin:

Damage caused to axons and molecules secreted by degenerating oligodendrocytes leads to accumulation of myelin-associated proteins which include, among others, Neurite growth inhibitor A (Nogo A), oligodendrocyte-myelin glycoprotein (OMgp) and myelin-associated glycoprotein (MAG). These molecules, in turn, bind to Nogo receptor and p75 receptor. Together, this leads to an activation of RhoA pathway and Rho-associate protein kinase (ROCK) [99]. This pathway causes an eventual collapse of growth cones and neurite retraction, leading to axonal degeneration and can also be activated by CSPGs [100].

Presently, SCI has no known cure. Patients with SCI are treated with palliative care. The most important intervention is the initial decompression of the SC as soon as it is possible. The effectivity is time-dependent, there is a direct correlation with delay in decompression and decreased sensorimotor function in patients [101]. Patients are often treated with methylprednisolone, and long rehabilitation process begins. Therefore, the path towards identifying targets and designing possible therapies for improved outcome of SCI is still under research [102].

1.6 Therapies for SCI

The current therapies employed to treat spinal cord injury, both at preclinical and clinical stages can be divided into 3 distinct categories:

1.6.1 Use of pharmacological agents:

The use of pharmacological drugs to modulate several different aspects related to SCI has long been described. Classically, pregabalin, an analog of gamma-aminobutyric acid (GABA), has

long been administered to patients to prevent neuropathic pain [103], and is known for its potential effect on locomotor improvement [104]. On the other hand, several NMDA antagonists such as MK801 and gacyclidine have been used to prevent excitotoxic effect of glutamate release [105]. Additionally, blockage of both NMDA and AMPA both show a synergistic neuroprotective effect in adult rats after SCI [106]. Intravenous administration of Rolipram, a phosphodiesterase-4 inhibitor, can enhance neural regeneration and function recovery after SCI in rats [107]. Similarly, a direct injection of cAMP is able to improve spinal axon regeneration after SCI [108].

Ion channel agonists, especially Ca^{2+} blockers and K^+ are also widely used. Nimodipine, a calcium channel blocker, has shown to improve spinal blood flow or improve neurological recovery after SCI [109]. Nevertheless, the most promising results are found with K^+ blockers. Using a K^+ channel agonist, potassium chloride co-transporter 2 (KCC2), researchers were able to inhibit the overactivation of inhibitory interneurons to restore normal activity and increase locomotor function in spinal cord in rats [110]. Another K^+ channel blocker, 4-AP exhibits high restoration rates of conduction in the SC after injury [111], and improved locomotor function has been reported even in human patients [112]. Modulation of the extracellular matrix by delivery of chondroitinase ABC (ChABC) enzyme at injury site to degrade CSPGs promotes increased regeneration of the CST and ascending sensory tracts, promoted post-synaptic activity and subsequently motor recovery in mice [113] and monkeys alike [114].

Finally, several pharmacological agents to block RhoA signalling, and its downstream effects are also exploited as potential therapy. Therefore, intraperitoneal injection ROCK inhibitor Y-27632 showed improved locomotor function after SCI by modulating astrocyte phenotype [115]. Administration of a stabilized fasudil conjugate, a Rho/ROCK inhibitor, improved axonal elongation *in vitro* and prevented apoptosis and induced neuroprotective and axonal growth signalling after SCI in rats [116]. In this aspect, the use of cytoskeleton modulating drugs that modulate the growth cone to overcome axonal retraction and promote axonal regeneration are also used. Non-muscle myosin II (NMMII) is a downstream effector of the Rho/ROCK pathway and is responsible for retrograde actin flow in the growth cone. Blebbistatin, a pharmacological inhibitor of NMMII effectively enhances enhanced axonal growth in presence

of CSPGs and myelin *in vitro* [117, 118]. However, possibly due to the highly phototoxic nature of Blebbistatin, there are currently no *in vivo* studies using this drug in this context.

Epothilone B, a microtubule stabilizing agent which can cross the BBB improved axonal regeneration after SCI in rats [119]. More recently, we have shown that Epothilone B alone reduced fibrotic scarring, as well as decreased the infiltration of cells into the injury area. Additionally, it significantly improved serotonergic regeneration and increased vesicular glutamate transporter 1 (VGLUT1) excitatory input into central pattern generator, thereby improving functional recovery. In combination with rehabilitation, all of these parameters were further enhanced [120].

1.6.2 Gene therapy

On of the limitations of CNS regeneration is the loss of activity in the mammalian target of rapamycin (mTOR). Perhaps one of the most important advances in the use of gene therapy in SCI has been the deletion of Phosphatase and TENsin homolog deleted on chromosome 10 (PTEN), a negative regulator of mTOR. This dramatically increased the sprouting of uninjured CST axons as well as the intrinsic regenerative capacity of injured CST axons in adult mice [121]. Co-deletion of PTEN and Suppressor of cytokine signaling 3 (SOCS3) further enhanced this sprouting and resulted in significant functional recovery after SCI in adult mice [122]. Adeno-associated virus (AAV) mediated over expression of several growth factors, namely, ciliary-derived neurotrophic factor (CNTF), glial-derived neurotrophic factor (GDNF), osteopontin, fibroblast growth factor 2 (FGF2), insulin-like growth factor 1 (IGF1), and epidermal growth factor (EGF) resulted in an exaggerated 100 fold increase in axonal growth [123]. On the other hand, acting upon the inhibitory glial scar by temporal controlled expression of ChABC solved the problem of continuous and uncontrolled administration of ChABC and improved locomotor function in both short and long term expression of ChABC, but only long term expression promoted improvement in skilful movements such as grasping [124]. Similarly, selective deletion of RhoA in neurons promoted axon regeneration after injury [125]. Cell adhesion molecules such as intercellular adhesion molecule 1 (ICAM-1) play an important role in supporting axonal regeneration. AAV mediated expression of L1 resulted in reduced astrogliosis and reduction of CSPGs marked by a decrease in glial fibrillary acidic protein (GFAP) and nerve/glial antigen 2 (NG2); and an increase in locomotor recovery [126].

Gene therapy is often also used for the overexpression of growth factors since they are well known growth trophic factors. This was highlighted in a recent study where neural precursor cells were transplanted, and brain derived neurotropic factor (BDNF) was injected 3 segments caudal to the injury. Transplanted cells exhibited a 5 and 3 fold increase in the axonal density in gray and intermediate gray matter, forming functional connections with host MNs [127]. Similarly, AAV- lentiviral driven expression of BDNF improve the formation of functional synapses [128]; whereas short- term expression of BDNF in the spinal motor neurons decreased apoptosis and improved axonal growth and oligodendrocyte progenitor cell proliferation [129].

1.6.3 Cell therapy

Cell therapy is an attractive approach aiming to replace the lost cells during an injury, re-establish circuits and provide trophic support. Currently, it is one of the most widely used therapies in SCI. Collectively, there are several potential targets that cell therapy can address as a therapeutic option in SCI (**Figure 5**).

The earliest known transplantation into the CNS was of neural tissue in the brain in 1890. In this work, Thompson successfully grafted cortical tissue obtained from cat brain into dog brain [130]. This was followed by a series of successful attempts transplanting fetal cortex tissue, postnatal cervical ganglion and neonatal cerebral cortex into adult brains [131]..

This was soon followed by the revolutionary transplant in 1979 in a Parkison's disease model. Fetal dopamine-producing neurons were transplanted into the animal models and were able to integrate into host tissue, leading reduction in motor dysfunction [132].

In the SC, early attempts using intraspinal grafts of peripheral segments were rendered ineffective [133-135]. It was not until the 1980´s that pioneering work by Aguayo and colleagues demonstrated that CNS axons could regenerate when provided by sciatic nerve grafts [136, 137].

This was followed by studies in which donor spinal cord transplants were able to bridge axonal repair and improve axonal regeneration [138] and serotonergic sprouting [139] and studies highlighting the importance of the age of transplant became clear. E14 fetal spinal cord

transplants were able to integrate into host tissue, and even extend upto 5 mm into host tissue [140].

Cell therapy can be divided into non neural precursor cell therapy and neural precursor cell (NPC) therapy. Non neural precursor cell transplantation includes, amongst others, oligodendrocytes precursor cells (OPCs) and mesenchymal stem cells (MSCs); as described below.

OPCs were first identified after their proliferation following Wallerian degeneration [141]. These cells are able to differentiate into both oligodendrocytes and astrocytes, but a preferent differentiation into oligodendrocytes under demyelination exists [142]. Earlier studies showed OPC transplantation into the injury site have exhibit increased survival, proliferation, and differentiation into oligodendrocytes, and improved motor functional recovery [143]. OPCs can be obtained from human embryonic stem cells [143]; which when transplanted after contusive SCI; doubled remyelination and improved motor function [144], decreased cavitation and improved gray and white matter preservation[145]. OPCs can also be derived from induced pluripotent stem cells [146]. Like previous results, OPCs derived from induced pluripotent stem cells enhanced axonal remyelination and reduced cavitation [147].

Nevertheless, use of OPCs also has some important limitations to take into consideration. Given the rapid proliferation of OPCs in and around the injury site after transplantation, there is evidence supporting that they may contribute to the formation of the glial scar, of which NG2 cells are an important component [148]. Another concern is the contribution to the secretion of CSPGs, and other inhibitory molecules such as ephrin tyrosine kinases and semaphorin 3, creating an increasing inhibitory matrix for axonal regeneration. Furthermore, the presence of CSPGs may also have a limiting effect on OPCs [149].
Therefore, while OPC transplantation may aid in remyelination after SCI, the complex interactions with scar, glia and matrix may hinder the pro-regenerative potential of OPCs as an effective therapy for SCI [150].

Other widely used cells for transplantation are MSCs. MSCs are a good candidate due to their easy and quick isolation and obtention [151]. This has also led to widespread use of

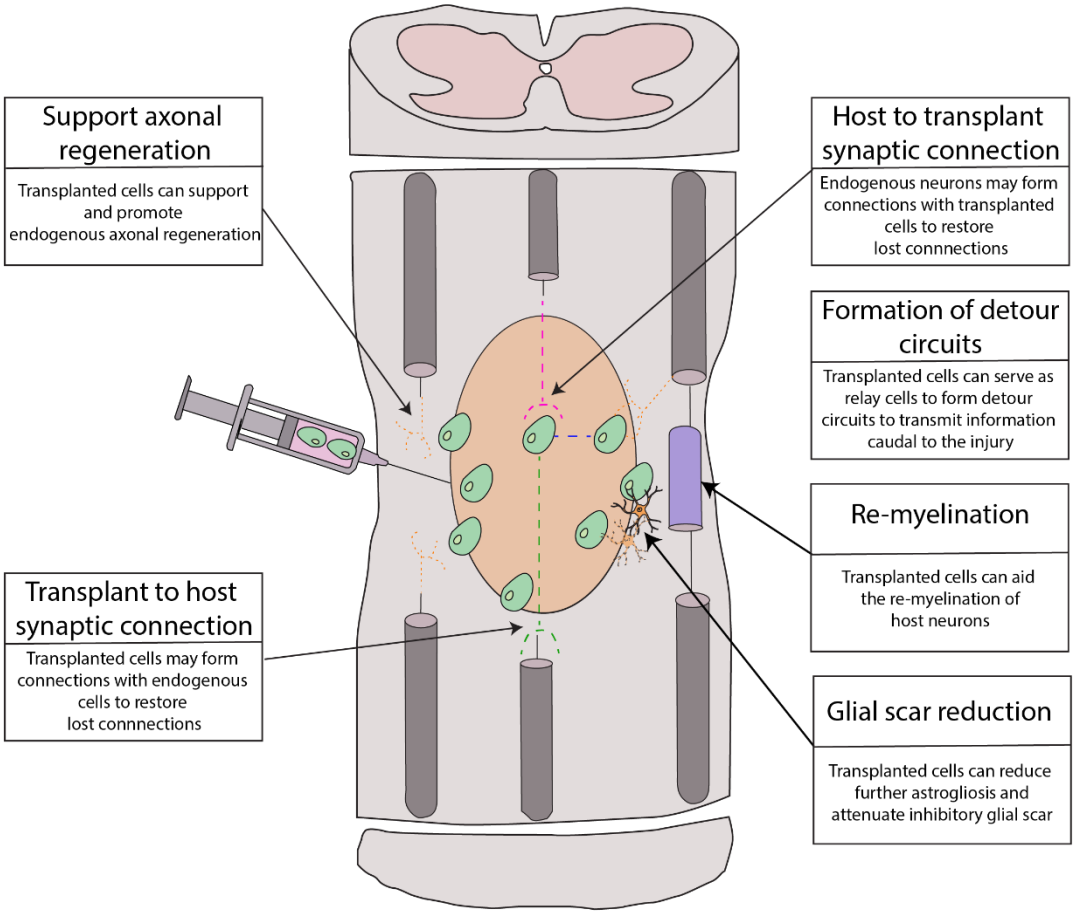

Figure 5: Figure representing the current postulated potential targets and effects of cell therapy through various mechanisms. Figure created obtaining information from *(Lane, Lepore, & Fischer, 2016) [152].*

MSC transplantation with several clinical trials ongoing or taken place [153]**.** Historically, their regenerative potential was thought to be the ability to proliferate and differentiate in several types, including glial and neuronal cells, making them ideal candidates for SCI cell transplantation [154]. However, more recently, the therapeutic potential of MSC transplantation has been identified to be the paracrine effect that they exhibit. MSCs secrete GDNF, NGF, BDNF and VEGF; which can promote neuronal repair and regeneration, as well as reduce scar formation [155]. They also have immunomodulatory effects and can stimulate angiogenesis due to the secretion of interleukin-10, interleukin-6, b fibroblast growth fact, transforming growth factor-β and placental growth factor, among others. MSCs can be isolated from bone marrow, umbilical cord, or adipose tissue [156, 157].

Given these factors, MSCs use is spread out along various clinical trials, many of them which have successfully reported neurological, motor, and sensory recovery (reviewed by [153]).

Despite their widespread use, MSCs transplantation has been associated to tumour formation and progress, including in patients. Also, survival of MSCs in the hostile SCI environment seems to hamper their paracrine effects, as well as their survival. This increases release of toxic molecules by dead MSCs, instead contributing to the damage caused by SCI [158, 159].

Finally, use of neural stem cells (NSCs) and NPCs and has recently emerged as the most promising and effective cell transplantation therapy for SCI. NPCs are considered a more restricted source of oligodendrocytes, astrocytes and neurons, whereas NSCs are self-renewing cells with a capacity to differentiate into all types of neuronal lineages [160]. NSCs were first identified in the developing mammalian SC and brain [161]; and were later identified in the dentate gyrus and lateral ventricle of adult mammalian brain and the central ependymal canal of the SC [162, 163]. However, given the general limited regenerative ability of adult CNS systems, the focus has shifted to NPC transplantation derived from fetal tissue. The potential use of NPCs can be seen in the phrenic circuit network; where they exhibit integration with the host tissue and establish synaptic connections, improving respiratory activity [164]. Leading work by the Tuszynski laboratory has revealed the numerous benefits of NPC transplantation, both in rodents and non-human primates. They demonstrated that fetal derived NPC tissue transplantation, along with a cocktail of matrix and growth factors can extend robustly and form long distance (up to 25 mm) connections with host axons in rats [165] and rhesus monkey, as well improve locomotor function [166]. Furthermore, their studies show increased CST regeneration and interaction with the graft by transplantation of fetal NPCs in adult rats derived from embryonic rat and human tissue [167]. More recently, they have even showed the transplanted NSCs were able to integrate into host circuits and relay information below the injury [168]. Work from our laboratory also consistently highlights the improvement in connectivity, integration of host tissue and functional recovery obtained by NPC transplantation strategies in rats after SCI [116, 169].

Despite all the described advances in NSCs/NPCs cell therapy; there are several limitations to be taken into consideration. Firstly, the survival of these cells into the inhibitory environment of SCI is limited [170]; and their capacity of differentiation into neurons is also reportedly low in several studies. This limits the integration into circuits and establishment of connections [171].

1.7 New trends - Importance of maintaining activity after SCI

Half of the total incomplete spinal cord injuries in patients exhibit complete paralysis [172]. This phenomenon may have a dual cause. First, surviving axons undergo degeneration due to the hostile injury environment and second, the loss of activity in the axons activates a degradation of these axons [173]. During development, loss of activity in neurons is associated with pruning of neurons [174]. Similarly, SCI induces several activity changes in the SC. This includes the complete or partial loss of supraspinal input into the spinal cord and leads to circuit rearrangements by sprouting and/or formation of detour/relay circuits [90, 114, 173, 175]. In chronic situations, motor neurons caudal to the injury significantly exhibit low excitatory pre-synaptic input; thereby attenuating their activity and function [176], further emphasized by reports suggesting that excitatory neurons play a direct role in motor function activity [177]. Additionally, neurotransmitters of surviving endogenous neurons undergo a switch from excitatory phenotype to inhibitory phenotype after SCI, further disrupting their activity and consequently, motor function [178]. Axonal sprouting is also associated and enhanced with increase in activity and regeneration [179]. During development, an increase in activity positively enhances formation of new circuits is also linked to decrease in apoptosis [180-182]. Since injury induces rearrangement of circuits, it is crucial to prevent loss of activity surrounding the injury to facilitate or induce sprouting, prevent degeneration of surviving axons, and facilitate the formation of new circuits. Overall, the interruption of pathways and over inhibition restricts the connections to effector muscles severely limiting locomotion recovery. Altogether, this points to the importance of maintaining the activity of neurons caudal to the injury, not only to maintain function of neurons caudal to the injury, but also to improve the formation of detour circuits after SCI [183].

Consequently, several therapeutic approaches for SCI focus on the maintenance and generation of activity in the spinal cord. Several studies highlight the link between exercise induced activity which is capable of improving axonal regeneration [179], associated with an increase in the expression of pre-synaptic markers [184, 185], and specifically, pre-synaptic excitatory markers such as VGLUT1 [120, 186]; and vesicular glutamate transporter 2 (VGLUT2) [110, 187]. While the exact mechanism behind exercise induce locomotor function are not yet fully understood, various studies suggest exercise induced recovery is due to

sprouting of 5-HT [188] and RtSt [189]. Modulation of activity by Cell-type–specific G protein-coupled receptor (GPCR) also promoted axon regeneration after injury to retinal ganglionic cells [190]. Following this theory, several treatments aiming to alter synaptic changes after injury may also activate dormant pathways [191, 192]. Other strategies focus on the maintenance of excitation to inhibition ratio post injury, for example, inhibition of inhibitory interneurons by the administration of KCC2 or designer receptor exclusively activated by designer drugs (DREADDs) re-establishes E/I ratio in the SC and promotes activation of dormant relay circuits [110].

Another such example is electric epidural stimulation (EES). Early studies in cats revealed hindlimb locomotor function in decapitated cats when stimulated at lumbar levels [193, 194]. An outstanding example is the work from the Courtine lab where they have shown that electrical epidural stimulation of the spinal cord dramatically improves motor function in rats [195, 196], monkeys [197] and humans with chronic SCI alike [198].

Finally, till an effective cure for SCI is not discovered; strategies aimed to improve current options will be constantly re-invented and improved. Keeping in mind the described commonly used strategies and their limitations, as well as the growing knowledge of the importance of activity based intervention, it is possible that a single, effective treatment may not be possible, rather a combination of two or more strategies may the key.

1.8 Use of DRGs as a potential therapy for spinal cord injury

As described earlier, there are several disadvantages to cell therapy. The use of DRGs as a potential transplantation target aims to overcome these limitations. In case of OPCs, the major drawbacks are the differentiation of the transplanted cells into glial cells which can contribute to further formation of glial scar and secretion of CSPGs [148, 149] . Regarding MSCs, it is the possible formation of tumours and secretion of harmful factors by MSCs when present in a hostile environment [158, 159]. For NPCs, it has been the low survival rate and differentiation into neurons [170, 171]. DRG transplantation can be an effective way to overcome these handicaps since the direct transplantation of neurons, which do not have the ability of differentiation nor proliferation, would avoid most of these drawbacks. Limitations of cell therapy also include the low differentiation rate into neurons, and consequently, the limited

ability to support or integrate into re-establishment of neuronal circuits [171]. Another of the biggest rationales behind cell therapy is the replacement of neural cells. The direct transplantation of neurons into the SC aims to ensure most transplanted cells are neurons. However, in case of DRGs, we include the added beneficial regenerative potential of peripheral neurons. Several instances of neuronal transplantation been studied in the brain. Young cortical neurons mature and easily integrate into brain tissue, extending axons when transplanted in a stroke damaged cortex model in adult rats [199]. Similarly, cortical neurons transplanted into damaged visual cortex of adult mouse re-established the connections and responded to visual stimuli [200]. As described earlier, early stage dopaminergic neurons have been long transplanted into Parkinson´s disease model. These studies eventually led to the use of human fetal ventral mesencephalic derived dopamine grafts survived into rat brain, restoring dopamine release, and forming synaptic connections with host tissue. These studies have led to interventions in patients with positive results and long-term assessment [201].

This is in stark contrast to studies in the SC, where only a few instances of neuronal transplants in the context of SCI are known. Studies suggest GABAergic cortical precursor cells were successfully transplanted in adult mice and survived up to 4 weeks after transplantation, with a survival rate of approximately 6%, which was enough to exert a functional difference and reduce injury-induced pain [202, 203]. Other studies revealed that human derived GABA expressing neurons DREADDs were able to survive long term, mature and integrate into host circuits in rhesus monkey, and were functionally active as shown by the activation of excitatory DREADDS by CNO administration. This study highlights the capacity of integration of neurons into spinal circuits [204].

Offhand, exploitation of increased regenerative potential and support of the peripheral nervous system has been described in early SCI studies, where it is established by Aguayo and colleagues that peripheral nerve grafts provide adequate support for CNS regeneration [136, 137]. The role of the peripheral nervous system as a potentiator for CNS repair is further highlighted by the "conditioning lesion paradigm", a well-studied phenomenon where a previous insult to the peripheral axon of DRG leads to a switch in the regenerative capacity of the central axon, is mediated by the upregulation of several RAGs after increased levels of

intracellular Ca^{++} and cyclic adenosine monophosphate (cAMP) at the DRGs, even after SCI [205, 206].

Early studies co-transplanted embryonic neural tissue with peripheral neural grafts to potentiate regeneration after SCI. In this study, the different survival and integration capacity from various sources was also studied by transplanting embryonic tissue grafts from the SC, DRG or cortex along with a peripheral nerve graft. They found that DRGs increased ability of axon extension DRGs, while a non-existing capacity for cortical tissue and moderate ability for SC tissue [207]. Furthermore, when adult or fetal DRGs where transplanted along with peripheral nerve grafts into injured cervical SC, both survived up to 2 months after transplantation and extended long axons [208] and even expressed peripherin [209]. Other studies also demonstrated the efficacy of DRG transplants only, revealing survival and integration of allografts of ganglia in adult mouse spinal cord [210]. Additionally, fetal DRGs transplants were found to mature and differentiate into functional, mature DRGs in the SC [211]; as well as survive upto 9 months after transplantations; and extend both axons towards both PNS and CNS in the SC. This is especially relevant because it revealed the capacity of transplanted DRGs to cross into the CNS and extend axons [212]. It was further revealed that xenograft mouse DRGs transplanted into adult rat SC survived and integrated into the SC similar to allografts, with axons that could extend upto 4 cm [213]. Finally, studies revealed that human, fetal dorsal root ganglia were able to differentiate and migrate in adult rat SC, even bypassing the inhibitory dorsal root entry zone after crush injury [214].

Interesting studies by Silver´s lab concluded that minimally damaging transplants by microinjections of postnatal or adult dissociated DRGs, rostral to the injured brain, project long axons and robustly integrate, forming multiple collaterals into the white matter of the host adult rat brain [215]. In the adult spinal cord, micro transplanted dissociated adult DRG neurons, when transplanted distal to the primary trauma, were able to survive and extend up to 4-5 mm in rats, however, they were unable to invade the inhibitory scar limiting their capacity to cross over the injury and contribute to denervated circuits caudal to the lesion in this case [216].

1.8.1 NaChBac sodium channel induced expression in DRGs can modify the neuronal behaviour

NaChBac is a bacterial sodium gated channel first identified in 2001 [217]. Structurally, it consists of 6 helices, four S1-S4 voltage sensor domains; and S5 –S6 pore domains [218] (**Figure 6**). Its overexpression in mammalian systems has provided an insightful tool into the role of Na_vs [219]. Expression of NaChBac in granule neurons revealed that its activation threshold was about 15 mV lower than in endogenous sodium channels. Additionally, the channel exhibits slow inactivation, up to hundreds of milliseconds, compared to one millisecond in mammalian channels [220]. Finally, the NaChBac sodium channel produces long depolarization waves when expressed in granule cells, around 600 ms [221]. These findings were consistent in visual cortical neurons [222], arcuate neurons [223] and developing cortical neurons in the cortex [180], where it has also shown to elevate spontaneous calcium currents [224].

As described previously, neuronal survival and integration into circuits during development is activity dependent [180-182, 225, 226]. However, this mechanism is also true for granule cell neurons in adult olfactory bulb, the only other adult circuit formation under normal physiological conditions [227]. Additionally, the expression of NaChBac by viral injections into the SVZ in the developing neurons has been shown to decrease apoptosis and thus increases the survival rates of newly formed olfactory neurons. In contrast, inhibition of these newly formed neurons prevented their integration into existing circuits. [221] Cortical interneurons in the developing cortex undergo activity-dependent death; NaChBac expression aided in escaping apoptosis with an increasing cell survival [180].

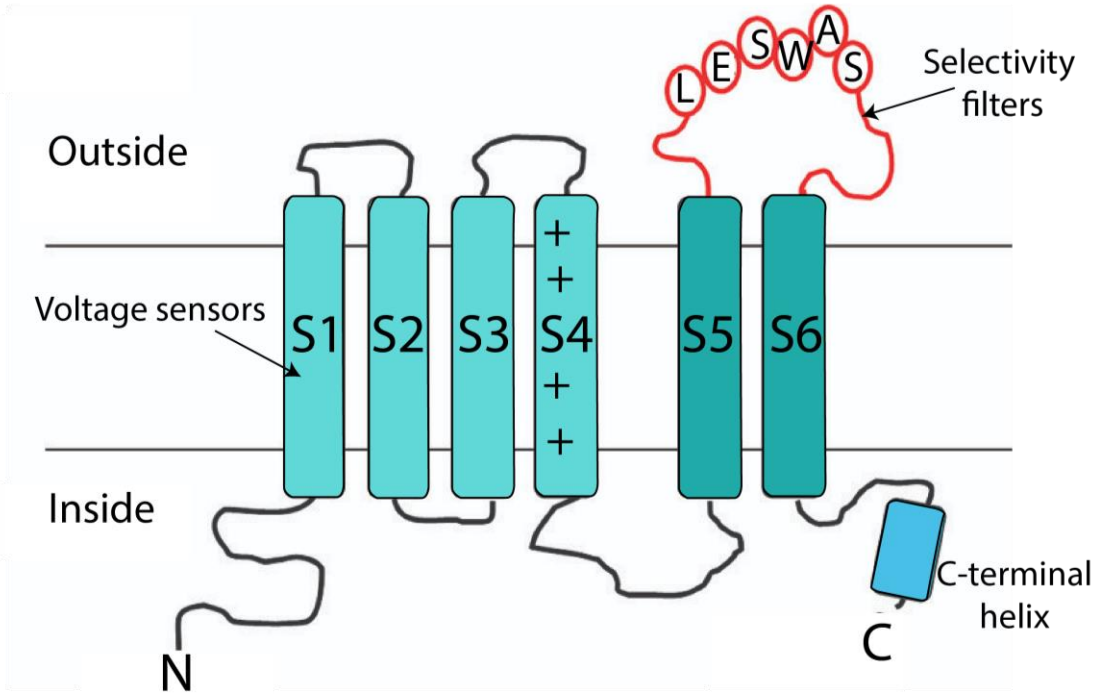

Figure 6: Structure of prokaryotic NaChBac sodium channel. S1-S4 domains are voltage sensors, S6-S6 are selectivity pores. Image created based on *(Charalambous & Wallace, 2011*) *[218]*.

Hypothesis and objectives

Transplantation of dissociated dorsal root ganglia (DRGs) for spinal cord injury treatment can provide an alternative strategy by exploiting their regenerative potential. Considering the importance of maintaining activity for neuronal survival, integration and reorganization into pre-existing circuits, the additional expression of NaChBac would provide enhanced regenerative capabilities to the transplanted DRGs. We also hypothesize that a combinatorial approach by including the cytoskeleton modulating drugs like Epothilone B and Blebbistatin to overcome the inhibitory environment formed after SCI and enhance the damaged axonal growth.

Based on the hypothesis described above, we draw specific objectives which are described in the following order and chapters of this manuscript.

Chapter 1:

Objective 1: Study the ability of cytoskeleton modulating drugs to enhance axonal length, alone or in combination with NaChBac expression in neuronal cultures:

1.1. To characterize a possible synergistic effect of cytoskeleton modulating drugs Epothilone B and Blebbistatin on *in vitro* DRG culture by simulating conditions similar to those encountered in an injury environment by creating a permissive and non-permissive substrate.

1.2. To characterize the effect of NaChBac expression on neuronal activity and neuronal survival.

1.3. Evaluate the effect of NaChBac and cytoskeleton modulating drug on DRGs.

Chapter 2:

Objective 2: Evaluation of DRGs expressing NaChBac transplant in a moderate spinal cord injury

2.1. Analysis of localization, cell survival and migration of the transplant.

2.2. Examine the interaction of the transplant with the corticospinal tract (CST).

Chapter 3:

Objective 3: Evaluation of DRGs expressing NaChBac transplant in a chronic, severe injury scenario

3.1. To study the functional motor rescue of mice of all the groups representing the combinatory and individual treatments.

3.2. To analyze the structural modifications in the injured spinal cord influencing neuronal preservation and neuronal activity.

Materials and methods

1.1 NaChBac stable overexpression

NaChBac fused to enhanced green fluorescent protein (eGFP) sequence was extracted from the plasmid NaChBac FRSW kindly given by Dr Carlos Lois lab [228] and cloned into pLL3.7 (#11795, Addgene, Watertown, Massachusetts, USA) lentivirus vector.

1.1.1 Production of pLL3.7-NaChBac-eGFP:

Briefly, the endogenous eGFP sequence from the plasmid was eliminated and NaChBac-eGFP was inserted in its place, under the CMV promoter. For that, NaChBac-eGFP sequence was amplified using PCR using primers NACHBAC Fwd (5`-TTT TTG AAT TCT TAC TTG TAC AGC TCG TC -`3) and NACHBAC Rev (5`-TGC TAG CCA CCT CCA AGC TC-`3), to add restriction sites for XbaI/ BsrGI and double digested with these enzymes in Neb Buffer 2.1 for 1 hour at 37ºC; run in a 1% agarose gel and purified using QIAquick PCR & Gel Cleanup Kit (#28506, Qiagen, Hilden, Germany). Similarly, pLL3.7 plasmid was digested with NheI/BsrgI, run in a 1% agarose gel and purified. Ligation of both digested products was done in 1:6 (1 digest plasmid, 6 insert) was ligated using T4 ligase overnight at 16ºC (#M0202S, New England Biolabs, Ipswich, Massachusetts, United States).

1.1.2 Generation of pLL3.7-NaChBac-mScarlet:

For the generation of pLL3.7-NaChBac-mScarlett, eGFP sequence from pLL3.7 was eliminated and mScarlett and NaChBac sequences were inserted by LIC method.

1.1.3 Obtention of pLL3.7-mScarlet:

pLL3.7-mScarlet was generated by eliminating NaChBac sequence from pLL3.7-NaChBac-mScarlett using and re-ligation.

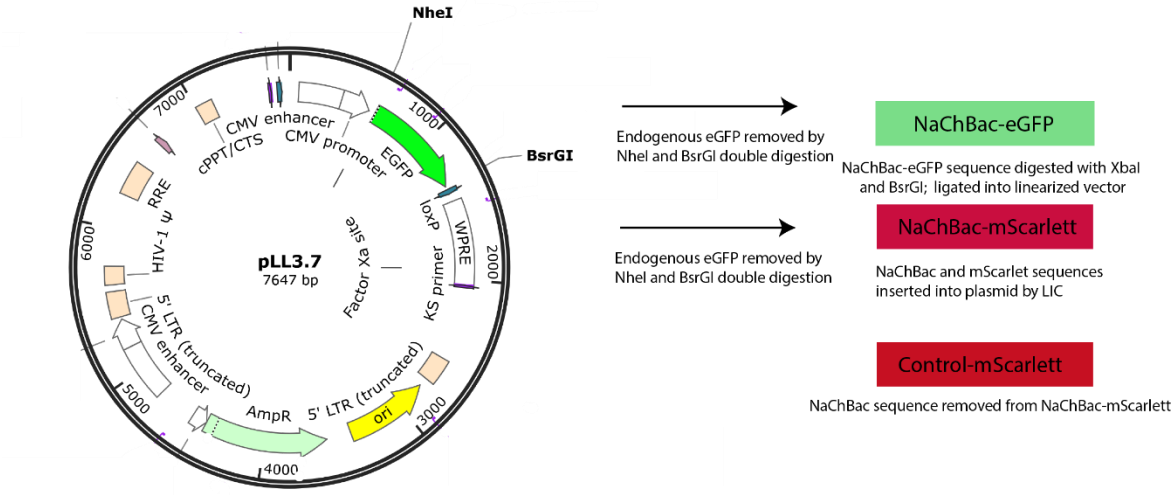

Figure 7: Schematic representation of generation of pLL3.7-NaChBac-eGFP (NaChBac-eGFP), pLL3.7-NaChBac-mScarlett (NaChBac-mScarlett) and pLL3.7-mScarlett (Control-mScarlett).

1.1.4 Lentiviral production

For lentiviral production, human embryonic kidney 293T (HEK-293T) cell line was transfected with the desired plasmid construct pLL3.7-NaChBac-eGFP construct or pLL3.7 empty vector (for control samples) together with packing vector (#22036, Addgene, Watertown, Massachusetts, USA) and envelope vector (#12259, Addgene, Watertown, Massachusetts, USA) using calcium phosphate method [229] as previously described [230, 231].

1.1.4.1 Calcium phosphate protocol:

2 million HEK-293T cells were plated in a 10 cm dish using DMEM + 10% FBS + 1% P/S medium. Next day, between 1-3 hours before transfection medium was changed. A transfection mix was prepared as follows:

20 ug of vector desired construct

15 ug packing vector

6 ug envelope vector

62.5 mL of 2M calcium chloride

Made upto 500 mL

2X HEPES-Buffered Saline (HBS) was added to this mix dropwise while vortexing, pipetting to form bubbles and incubated at room temperature (RT) for 40 minutes. Next, this was added

dropwise to the dish, evenly distributing all over the dish and dishes were kept back into the incubator. 4 hours later, medium was changed.

1.1.5 Virus collection and concentration:

Virus was collected only when transfection efficiency reached approx. 90%. Virus particles were harvested 48 and 72 h after transfection. For this, media was carefully collected and centrifuged at 2000 rpm to remove cell debris. Virus was concentrated by ultracentrifugation at 26000 rpm at 4ºC for 2 hours, and supernatant was carefully aspirated. Virus pellet was then resuspended in cold PBS and kept on ice for 30 minutes. Next, virus was stored at -80ºC until further use.

1.1.5.1 Virus titre:

To calculate the titer, HEK cells were seeded at a density of 70,000 cells/well in a P24 cell culture plate. Next day, confluency was checked to be around 60%. To infect the cells, serial dilutions were prepared as follows:

5 ul stock virus + 495 ul media = 10-2

50 ul of 10-2 virus + 450 ul media = 10-3

50 ul of 10-3 virus + 450 ul media = 10-4

50 ul of 10-4 virus + 450 ul media = 10-5

50 ul of 10-5 virus + 450 ul media = 10-6

50 ul of 10-6 virus + 450 ul media = 10-7

HEK cell line was infected with above mentioned serial dilutions. Next day, medium was changed completely. 48 hours after that, (i.e, 72 hours after infection) and checked for infection under a fluorescent microscope. The dilution with around 20% infected was selected, trypsinized and sorted by FACS.

Finally, the formula $T=(P\times N)/(D\times V)$ was used to calculate the titer of the virus as described in [229]; where T = titer (infectious units (IFU)/ml), P = % GFP positive cells), N = number of cells determined at the time of viral transduction, D = dilution factor and V = volume of viral inoculum.

For our experiments, we used multiplicity of infection (MOI) 10 volume of virus to be added was calculated using the following formula: Volume of virus added = Number of cells x MOI / Titer (IFU/mL).

1.2 DRG and Neuro2A infection

Dissociated DRGs or Neuro2A were transformed for overexpression of pLL3.7-NaChBac-eGFP (referred to as NaChBac-GFP), pLL3.7 empty vector containing eGFP (referred as Control-GFP hereon), pLL3.7-NaChBac-mScarlet (referred to as NaChBac-mScarlet) or pLL3.7-mScarlet (depending on the experiment as described for every experiment) by infecting the cell cultures 4 hours after plating with pLL3.7-NaChBac-eGFP or pLL3.7 empty vector lentiviral derived particles at MOI 10.

Media was completely refreshed 16 hours after infection. In case of DRGs, this consisted of medium with AraC (5uM) hours after infection. GFP expression was detected 48-72 hours later.

In the case of neuroblastoma 2A (N2A) cells, these cells were sorted with FACs to obtain a pure line and used for all subsequent experiments at similar passage.

1.3 Dissociated dorsal root ganglia (mixed) culture

1.3.1 Coatings

Firstly, 12 coverslips mm were placed in P24 cell culture plates and coated with poly-L-lysine (#P2636, Sigma, St. Louis, Missouri, USA) at a concentration of 20 µ g/ml overnight at 37ºC, washed with ddH_2O and then coated with laminin (#L2020, Sigma, St. Louis, Missouri, USA) at a concentration of 10 µ g/mL for 3 hours at 37ºC.

In case of neurite length assay experiments where CSPGs; assays were carried out over permissive and non-permissive coatings, therefore; the previous coating protocol was modified slightly, following 10.1073/pnas.1011258108. In short, after washing of poly-L-lysine coating with ddH_2O; coating laminin plus CSPGs coating was prepared for the non-permissive condition, whereas laminin plus bovine serum albumin (BSA) coating was prepared for the permissive condition. For permissive substrate, A coating solution of 10 µg/mL of laminin and

2 ug/mL BSA (#10735078001, Roche, Basel, Switzerland) was prepared in 1x phosphate-buffered saline for permissive substrate and added to the coverslips mL for 3 hours at 37ºC.

Similarly, for non- permissive substrate; a coating solution of 10 µg/mL of laminin and 2 ug/mL CSPGs (#CC117, Sigma, St. Louis, Missouri, USA) was prepared in 1x phosphate-buffered saline for non-permissive substrate and added to the coverslips mL for 3 hours at 37ºC.

1.3.2 Dorsal root ganglia isolation and culture

Dorsal root ganglia (DRG) were isolated from decapitated neonate rats at P3-P4 as previously described [96]. Briefly, DRGs from 4-5 pups were dissected from all medullar segments, pooled, and collected in cold HBBS (#24020091, Gibco, Thermo Fisher Scientific, Waltham, Massachussetes, USA). After removal, residual spinal roots and nerves attached to the DRG were carefully cut under a stereoscope, DRGs were collected and allowed to settle to remove HBBS solution. Then, they were digested in Collagenase IA (#C9891, Sigma, St. Louis, Missouri, USA) for 35 min. Collagenase solution was removed by allowing DRGs to settle, followed by 7 min digestion with Tryple (#12563-011, Gibco, Thermo Fisher Scientific, Waltham, Massachussetes, USA). Tryple solution was carefully discarded and digested DRGs were suspended in complete medium (MM**:** Dulbecco´s Modified Eagle Medium (DMEM) F12 (+ 10% fetal bovine serum (FBS) + 1% (penicillin/streptomycin) P/S (#15140122, Gibco, Thermo Fisher Scientific, Waltham, Massachussetes, USA) and 25 ng/µL NGF (#13257-019, Gibco, Thermo Fisher Scientific, Waltham, Massachussetes, USA), and mechanically dissociated with a 1000 µL blue pipette tip and seeded plated at various densities as described below:

1.4 DRG Experiments

1.4.1 Neurite assay experiments:

In order to successfully analyze the neurite length of the DRG neurons, we used low-density cultures. DRGs were seeded at a concentration of 10,000 cells/ well, in 500 mL of complete MM and NGF over chondroitin sulphate proteoglycans (CSPGs, non-permissive) or bovine serum albumin (BSA, permissive) substrates. Four hours after plating, drug of choice (Blebbistatin, Epothilone B or a combination of both) was added. The following concentrations were used: Epothilone B (Epo B) at 0.1 nM; Blebbistatin (Blebb) at 1.5 and 15 µM; and the

combinations of both. Cells were fixed 20 hours after drug application using 4% PFA and 4% sucrose for 20 minutes and washed with PBS three times.

In case of replating experiments, DRGs were first plated at high density in P12 well format (85000 cells/ cm2). Next, they were infected at MOI 10 four hours after plating as described above. 72 hours after infection, correct expression was ensured, cells were trypsinized with Trypsin-EDTA 0.05% for 5 min, recovered in MM, centrifuged at 300g for 7 min and counted. Since re-plating experiments required higher cell density, 35,000 cells/well of a P24 plate were re-plated over Permissive or Non-Permissive substrates (as described above). In case of Control-GFP + Blebbistatin or NaChBac-GFP + Blebbistatin condition, Blebbistatin 15 µM was added 4 hours after re-plating. Cells were fixed 20 hours after addition of Blebbistatin.

Following this, immunocytochemistry for the visualization of β-III-tubulin and actin was performed. Cells were first permeabilized and blocked in Blocking Solution: 0.5% Triton-TX100 + 3% normal goat serum (NGS) for an hour at RT. Primary antibody for β-III-tubulin used was mouse Anti-alpha-Tubulin Purified (1:400, #11-250-C100, Exbio, Vestec, Czechia), and was added in blocking solution overnight at 4ºC. Actin (1:400, #ab176756, Abcam, Cambridge, UK) was added with secondary antibody; AlexaFluor 488 anti-mouse for an hour at RT and washed. Coverslips were counterstained with 4',6-diamidino-2-phenylindole DAPI (1;1000, #D9542, Sigma, St. Louis, Missouri, USA) and mounted with Mowiol® (#81381, Sigma, St. Louis, Missouri, USA).

1.4.2 Electrophysiology experiments

For electrophysiological recordings (described in detail below) cells were seeded at a density of 21000 cells/cm^2 in 12 mm coverslips over 24 well plates and infected (as described below). Cytosine arabinoside (AraC) (#C1768, Sigma, St. Louis, Missouri, USA) (5µM) was after for 16 h to reduce Schwann cell growth. Half media volume was refreshed every 3 days.

It should be noted that dissociated dorsal root ganglia culture is a mixed culture type which includes glial cells and DRG neurons. Even though AraC is added to the cultures in all cases except neurite assay length assay experiments (due to the short duration); glial cells were only controlled, not eliminated.

Small-diameter (<30 µm) DRG neurons were recorded in voltage and current-clamp modes using an EPC10 amplifier controlled by Patchmaster software (HEKA Elektronik). Experiments

were performed in whole-cell configuration at ≈22ºC. Briefly, patch pipettes from borosilicate glass with OD 1.5 mm x ID 1.17 mm (Warner Instruments) were pulled using a Flaming/Brown micropipette puller P-97 (Sutter Instruments) to have 2-5 MΩ resistance. Seal-resistance was between 200 MΩ - 2 GΩ and series resistance was compensated for at around 80 %.

Infected cells were selected and visualized with a fluorescent microscope (Axiovert 200 Inverted Microscope, Carl Zeiss). Extracellular solution contained (in mM): 140 NaCl, 4 KCl, 2 CaCl2, 2 MgCl2, 10 HEPES, 5 Glucose, 20 Mannitol, pH 7.4 adjusted with NaOH. Pipette internal solution contained (in mM): 144 KCl, 2 MgCl2, 10 HEPES, 5 EGTA, pH 7.2 adjusted with KOH.

Resting membrane potential (RMP) was determined without any current injection after establishing whole-cell access. To calculate the rheobase and the firing frequency, 1 s-current depolarizing pulses from 0 to 300 pA in 10 pA intervals were applied. The minimum current required to evoke the first APwas considered as the current rheobase. The AP parameters were measured in the action potential fired at the minimum current injected using 10 ms depolarizing pulses from 0 to 300 pA in 10 pA steps. The voltage threshold (V_{th}) of the action potential was set when the upstroke slope was ≥ 10 V/s. The AP amplitude was calculated between the RMP and the AP peak.

For voltage clamp recordings, a series of 300 ms voltage steps from -80 to 60 mV in 10 mV intervals were applied.

Data were acquired at 20 kHz for all the protocols. Only one cell per dish was recorded and analysed.

1.4.3 Calcium live imaging

For live calcium imaging experiments, dissociated DRGs were seeded at a density of 21000 cells/cm^2 in 24 well plates with glass surface (662000-06, Greiner Bio One) ideal for imaging cells *in vivo* infected with either NaChBac-mScarlet or Control-mScarlet four hours after plating (as described above). 4 days after seeding and infection, cells were treated with Fluor 4AM (#F14201, Thermo Fisher Scientific, Waltham, Massachussetes, USA) at 3 µM for 30 min and washed according to manufacturer´s instructions. The confocal microscope Leica TSP-SP8 was used since it has resonant scanning mirrors required for real time live imaging [232]. Cells

were transferred to the confocal microscope with adequate CO_2 setup. Recording started around 10-20 seconds before depolarization. Cells were depolarized by directly adding 100 mM KCl into the well and recording was continued for 60s.

The change in fluorescence of the cells was then determined using LasX software by change in green fluorescence (Fluor4AM intensity). Data was screened so that neurons that did not respond to depolarization by KCl were discarded from the analysis.

1.4.4 cAMP Determination

Dissociated DRGs were seeded at a density of 85000 cells/ cm^2 in a 12 well plate and infected with either NaChBac-GFP or Control-GFP four hours after plating at MoI 10. 4 days after infection, cAMP was extracted from cells using perchloric method [233]. Briefly, media from cell culture was removed and cells were washed twice with PBS 1x. Next, 150-200 µL of 0.4M perchloric acid was added to the wells and cells were scrapped off using a cell scraper. Next, the solution was homogenised by sonicating once, centrifuged at 20000 rpm at 4ºC for 10 minutes. The supernatant obtained was stored at -80ºC until use and the pellet was dissolved in 1M NaOH and measured for protein using BCA assay kit (23227, Pierce™ BCA Protein Assay Kit, Thermo Scientific).

The chromatographic conditions were optimized to our instrument XBridge C18 2.1x75 2.5 ((#186005626, BEH Technology, Waters, USA) based on [234]. The mobile phase composition was as follows: component A) 0.1% formic acid in water component B) 100% acetonitrile. The conditions for chromatographic run were flow rate 0.4 ml/min, gradient was 0.5 min: 100 %A; 1 min: 10% A; 2.2 min: 10% A, 2.3 min: 100% A; 3.5 min: 100 % A. Volume injected was 25 µL.

cAMP levels were measured by chromatography in nanomolar concentration; and normalized to the total protein content obtained by BCA kit. Hence, data was represented as cAMP nM/µg of protein.

1.4.5 Secretome Analysis

For secretome analysis *in vitro* dissociated DRG cultures were used. Three days after infection with NaChBac-GFP or Control-GFP, culture media was changed to low serum media: MEM + 2% FBS + 1% P/S. Media was collected 24 hours later and stored at -20ºC until use. Array

analysis was performed using Rat Growth Factor Array 1 (#AAR-GF-1-2, RayBiotech, Georgia, USA). Briefly, undiluted culture media was directly incubated over membrane well, followed by washes, antibody incubations and visualized using Uvi-Tech Alliance Q9 chemiluminescence imaging system. Data was analysed as per manufacturer´s instructions; (n=2). BDNF secretion was additionally validated this data using ELISA kit (CC-SEA011Hu, Biogen Científica, Madrid, Spain) for BDNF in a different set of samples (n=2). Similar data was obtained when media from N2A culture was employed using the same array and the BDNF ELISA (data not shown).

1.5 Neuro2A experiments

Neuroblastoma 2A (N2A) cell experiments were performed with pLL3.7-NaChBac-eGFP (NaChBac-GFP) or empty pLL3.7 (Control-GFP) line. Cell culture medium used in N2A experiments was DMEM+ 10% FBS+ 1% P/S.

1.5.1 Proliferation curve

N2A cells expressing either NaChBac-GFP or Control-GFP were plated at a density of 300,000 cells/well in a P6 plate. On days 2, 3, 4 and 5 each, cells were trypsinized and counted in a Neubaeur chamber. To distinguish dead cells, Trypan blue (#15250061, Thermo Fisher Scientific, Waltham, Massachusetts, USA) was added to the cell suspension.

1.5.2 Hypoxia experiments

NaChBac-GFP and Control-GFP cells were seeded at a density of 150,000 cells/well in a P12 plate and then placed in a hypoxia chamber set at 1% oxygen for 24 hours and posteriorly trypsinized and counted in a Neubaeur chamber after adding Trypan blue. Two types of counting were done: Total number of cells and number of dead cells. Data was then represented as the % of dead cells = Number of dead cells/Total number of cells *100.

1.5.3 Protein extraction

Cells were plated at a density of 300,000 cells/well in a P6 culture plate and protein was extracted on day 3.

1.5.4 Western Blotting

Total protein from N2A cells was extracted using a lysis buffer containing 1 × Protease Inhibitor Cocktail (#11836153001, Roche Diagnostics, San Diego, CA, USA), 50 mM Tris–HCl, pH 7.5, 150 mM NaCl, 1% NP40, and 1 mM orthovanadate. The protein concentration was determined using BCA Protein Assay Kit (23225, Thermo Fisher Scientific, Waltham, Massachusetts, USA). Equal amounts of protein were separated by 10% SDS-PAGE and transferred to a polyvinylidene fluoride (PVDF) membrane.

The membrane was blocked with 5% bovine serum albumin in TBST buffer (20 mM tris-HCl pH7.4 150 mM NaCl with 0.1% Tween-20) for 1 h at room temperature and incubated at 4 °C overnight with the following primary antibodies: rabbit phospho mTOR 1:1000 (#2971, Danvers, Cell Signalling, Massachusetts, USA); rabbit mTOR 1:1000 (#2972, Cell Signalling, Massachusetts, USA); mouse Bcl2 1:100 (#sc-7382, Santa Cruz Biotechnology, Dallas, Texas, USA); mouse phospho AKT 1:1000 (sc-293125, Santa Cruz Biotechnology, Dallas, Texas, USA); rabbit Caspase3 1:1000 (#9622s, Cell Signalling, Massachusetts, USA), rabbit AKT 1:1000 (#4691s, Cell Signalling, Massachusetts, USA); mouse β-actin 1:10,000 (#A1978, SIGMA). Signal detection was performed with an enhanced chemiluminescence kit (ECL Plus Western blotting detection reagent—GE Healthcare, Piscataway Township, NJ, USA), and bands developed using Uvi-Tech Alliance Q9 chemiluminescence imaging system. Relative protein expression was quantified using the Uvi-Tec NineAlliance Q9 h software.

1.6 Animal models

All *in vivo* procedures were performed in female C57BL/6 mice (approx. 20 g, 8 weeks old) bred at the Animal Experimentation Unit of the Research Institute Príncipe Felipe (CIPF, Valencia, Spain). The maintenance and use of all animals were by guidelines established by the European Communities Council Directive (86/609/ECC) and the Spanish Royal Decree 53/2013. All experimental procedures were approved by the Animal Care and Use Committee of the Research Institute Prince Felipe (2020/VSC/PEA/0120). The experimental protocol included humane endpoint criteria when severe signs of distress were observed. Mice were housed under standard temperature conditions with controlled 12 h light/dark cycles with ad libitum access to food and water. All animals were managed by professionally trained staff.

Only female mice were used for this study, mainly due to easier bladder emptying due to shorter tract and decreased infection susceptibility [235].

1.6.1 Chapter 2 mouse model

To perform the SCI, mice were subcutaneously administered 5 mg/kg morphine 30 min before the surgery and anesthesia was maintained throughout the surgery by continuous flow of 2% isoflurane and oxygen of 1L/ min. A single T8 hemisection was performed as described in 10.1038/s41586-022-05385-7. Briefly, laminectomy was performed to expose T8 and a lateral right hemisection uptil the spinal cord midline was performed using a micro scalpel blade (#72-2201 Sharpoint Angiotech, Reading, USA). This incision was performed twice to ensure complete severing of the spinal cord. The muscle and skin layers were then separately sutured using 4/0´s monosyn suture (#G2022004, Braun, Kronberg im Taunus, Germany), followed by drop of Histoacryl over the skin to prevent opening of wound.

Animals from this study were distributed into 2 groups: 1) SCI and DRG neuron transplant expressing eGFP (Control-GFP) and b) SCI and DRG neuron transplant expressing NaChBac-eGFP (NaChBac-GFP); (*n*= 9-10 animals/group were in each group for histological analysis). Dissociated DRG cell transplant was performed by single injection in 3ul (see section DRG cell transplantation below) immediately after hemisection and below the injury.

1.6.2 Chapter 3 mouse model

This model consists of a double lateral, opposite hemisection model that ensures a complete injury but maintains a relay zone between two lateral hemisections (See Chapter 2, Introduction). This was achieved by a T7-T10 double unilateral complete hemisection model as described in[236]. Briefly, a T7-T10 laminectomy was performed to expose the spinal cord and an incision was made using a micro scalpel blade (#72-2201 Sharpoint Angiotech, Reading, USA) on the right T7 side until the midline. This incision was performed twice to ensure complete severing of the spinal cord. Similarly, an incision was done from left T10 level until the midline. The muscle and skin layers were then separately sutured using 4/0´s monosyn suture (#G2022004, Braun, Kronberg im Taunus, Germany), followed by drop of Histoacryl to prevent opening of wound.

Animals were distributed into 3 groups: 1) SCI and no cell transplant (Non-Transplanted);

2) SCI and DRG neuron transplant expressing GFP (Control-GFP) and 3) SCI and DRG neuron transplant expressing NaChBac-eGFP (NaChBac-GFP); (*n*= 8-12 animals/group for locomotion analysis; *n*=4-7 for histological analysis). Dissociated DRG cell transplant or medium for control group was performed immediately after the double lesion in a single injection at T8 of 3 µL (see section DRG cell transplantation below).

Following surgery, mice were kept warm using heating pads and food was kept on the cage floor. All animals were subcutaneously administered buprenorphine twice a day (0.1 mg/kg) for 4 days after surgery and enrofloxine once a day for a week after surgery (5mg/kg). Manual bladder drainage was performed twice or once a day until recovery (if any) or experimental endpoint. Immunosuppressant cyclosporine (once a day, 20 mg/kg) was administered from one day before transplant until experimental endpoint. Animals were carefully checked for endpoint symptoms.

1.6.3 DRG cell transplantation

For dissociated DRG transplantation, dissociated DRGs were first seeded at a density of 85000 cells/ cm^2 in a 12 well plate and infected as described above. They were further kept in culture until DIV 5 with AraC to reduce other cell contamination. Cells were trypsinized with Trypsin-EDTA 0.05% for 5 min, recovered in MM, centrifuged at 300g for 7 min and counted. This was followed by further centrifuging at 200g for 7 min two times to compact the pellet and finally resuspending the cells in a final total volume of 3 µL MM. Each animal was transplanted with 150,000 cells. Cells were transplanted intramedullary in a single injection using a Hamilton (#80308, Hamilton Syringe) coupled to a siliconized sharpened glass capilar; attached to a Nanoliter injector (Harvard Apparatus, Manchester, UK). DRGs were infused at the rate of 2 µl/min and allowed to deposit for 2 minutes before removing the syringe.

1.6.4 Neuroanatomical tracing

Tracing of hindlimb corticospinal tract (CST) was performed as described [237].

Mice were subcutaneously administered 5 mg/kg morphine 30 min before the surgery and anesthesia was maintained throughout the surgery by continuous flow of 2% isoflurane and oxygen of 1L/ min. First, mice were placed on the stereotaxic instrument so that the head was completely straight, and flat skull position was achieved. Next, briefly, a small incision at the head of mice was done to expose the skull. Once the skull was exposed, bregma was identified

and marked. Next, the coordinates AP -0.50, ML +-1.50, DV -0.70 from bregma using a stereotaxical instrument were marked to drill holes into the skull avoiding bleeding. Once the d holes were drilled, careful injection of virus a described below were injected at the rate of 200 nanolitre per min.

For Chapter 2 model: In the single hemisection SCI model, 1.5 µL of pAAV-hSyn-RFP was injected in both right and left motor cortex each. Tracing was performed two weeks before SCI and transplant.

For Chapter 3 model: In the complete SCI by double hemisection model, 1.5 µL of pAAV-hSyn-EGFP (#50465; Addgene, Watertown, Massachusetts, USA) (titer $3.75x10^{11}$) was injected into the right hemisphere and 1.5 µL pAAV-hSyn-RFP ((#22907; Addgene, Watertown, Massachusetts, USA) (Titre $3.75x10^{11}$) into the left hemisphere. Tracing was performed one week before SCI and transplant.

1.7 Functional Evaluation

Since SCI affects several functions, namely sensory, locomotor and autonomic, behavioral tests have been a primary method used to evaluate recovery after SCI and the potential effects of several therapies. These include motor functions such as grasping, open field testing or established scales such as Basso Mouse Scale. Sensory function is evaluated with neuropathic pain models such as Von Frey´s test or test for hot and cold sensation. Sensorimotor functions are evaluated by tests such as horizontal ladder, grid walking and rope climbing tests [238].

Therefore, in our studies of **Chapter 3**, we have selected one of each (motor, sensory and sensorimotor) tests to analyze accurately the behavioral changes brought about by the experimental therapies we used in our models.

1.7.1 Basso Mouse Scale:

Motor function was evaluated by using Basso Mouse Scale (BMS) [239], an established scale which evaluates locomotor function based on the specific guidelines described by the scale. This scale evaluates ankle and paw movement, trunk stability and step coordination of mice. (**Table 2**). For this test, animals were placed in an open field twice a week and recorded for 3 minutes only. Videos were analysed by trained blinded investigator and a maximum score was

given for each paw according to the scale. Data was represented then as the score of the mice in time.

Score	BMS SCALE
0	No ankle movement
1	Slight ankle movement
2	Extensive ankle movement
3	Plantar placing of the paw with or without weight support OR Occasional frequent or consistent dorsal stepping but no plantar stepping
4	Occasional plantar stepping
5	Frequent or consistent plantar stepping, no coordination OR Frequent or consistent plantar stepping, some coordination, paws rotated at initial contact and lift off (R/R)
6	Frequent or consistent plantar stepping, some coordination, paws parallel at initial contact (P/R, P/P) OR Frequent or consistent plantar stepping, mostly coordinated, paws rotated at initial contact and lift off (R/R)
7	Frequent or consistent plantar stepping, mostly coordinated, paws parallel at initial contact and rotated at lift off (P/R) OR Frequent or consistent plantar stepping, mostly coordinated, paws parallel at initial contact and lift off (P/P), and severe trunk instability
8	Frequent or consistent plantar stepping, mostly coordinated, paws parallel at initial contact and lift off (P/P), and mild trunk instability OR Frequent or consistent plantar stepping, mostly coordinated, paws parallel at initial contact and lift off (P/P), and normal trunk stability and tail down or up & down
9	Frequent or consistent plantar stepping, mostly coordinated, paws parallel at initial contact and lift off (P/P), and normal trunk stability and tail always up.

Table 2: Table describing the score and characteristics of mice movement in order to evaluate locomotor function using BMS Scale. Table derived from *Basso et al., 2006 [239] .*

1.7.2 Horizontal ladder beam test:

Sensorimotor function and fine forelimb and hindlimb coordination was evaluated by the horizontal ladder beam test [240]. Animals were recorded crossing a horizontal ladder for a

minimum of 3 rounds once a week, throughout the experiment [241]. For this test, mice were trained before undergoing SCI. Mice were put on a horizontal ladder, with rings placed at a distance of 1 cm and were given a treat after passing the ladder. On the last week before sacrifice, all animals were considered fit to undergo this test and were made to pass the test. After careful consideration of the videos, a scaling method adapted from [240] was employed (**Table 3**); where instead of names, we assigned score values to the terms described.

Score	Movement
Drag (0 points)	Paw does not exhibit any movement so that the dorsal part of the paw is pulled along.
Miss (0.5 points)	Paw does not contact rung, however the hind passes two rungs so that it attempts a step cycle.
Slip (1 points)	Paw contact on the first rung, however, falls on the second rungs so that an incomplete step cycle.
Skip (2 points)	Paw pad does not contact first rung but recover contact rung and completes step cycle.
Toe step (3 points)	Paw unable to support weight, in a manner that the toes are not visible above the rung until the end of step cycle.
Plantar step (4 points)	Plantar surface contacts the rung, in a manner that the toes are visible above the rung.

Table 3: Table describing the score value assigned and the description for the ladder beam evaluation based on *Cummings et al., 2007 [240]* .

1.7.3 Von Frey test:

The sensory test to detect allodynia that was performed was Von Frey´s test, using the "ascending stimulus" method [242]. Briefly, animals were placed on a mesh with an open bottom which allowed to insert Von Frey filaments (**Table 4**). Monofilaments were applied on the plantar of the hind paws of mice in ascending order until a withdrawal response was recorded. The force of this filament that elicits a response was marked as the "response evoking threshold (g)". Data was presented as mean of both hind limbs.

Force (g)	0,02	0,04	0,08	0,16	0,4	0,6	1	1,4	2	4	6	8

Table 4: Table showing the ascending stimulus force in grams of the filaments used for the Von Frey test.

1.8 Sacrifice and tissue processing

At every experimental endpoint (in Chapters 2 and 3), animals were transcardially perfused to harvest tissue [243]. Briefly, animals were anaesthetized with fentanyl (0.05 mg/kg) and pentobarbital (100 mg/kg) via intraperitoneal injection. Once anesthesia effects became evident, animals were checked for paw reflex. Ensuring the lack of reflex, the heart was exposed so that transcardial perfusion could be performed in two steps: transcardial perfusion with 0.09% w/v saline to clear blood from organs followed by 4% PFA in PB 0.1M. Spinal cords were dissected out and kept in PFA 4% solution for an additional 4 hours (post-fixation) and then stored in PB 0.1M and 0.02% sodium azide.

1.8.1 Chapter 2 Tissue processing

After careful removal of meninges, SC were placed on a ruler and cut so that a piece ranging from thoracic segments from T2-T10 were then obtained and cryopreserved in 30% sucrose during 2 weeks for inclusion in Tissue-Teck OCT (Sakura Finetek Europe BV, Flemingweg, Netherlands), stored at -80ºC till sectioning. Similarly, for CST sprouting, 1.5 mm immediately above the T2 segment (i.e C8 and T1) were cut, cryopreserved and included in OCT as described above (**Figure 8**).

Cryopreserved tissue, in longitudinal or coronal sections (as specified for each analysis below) sections (35 µm) of the tissue were sectioned in 6 series using HM 340E microtome (Thermo Fisher Scientific, Waltham, Massachussetes, USA) and collected in wells containing cryoprotectant solution (25% v/v glycerol, 30% v/v ethylene glycol in 0.1 M PB).

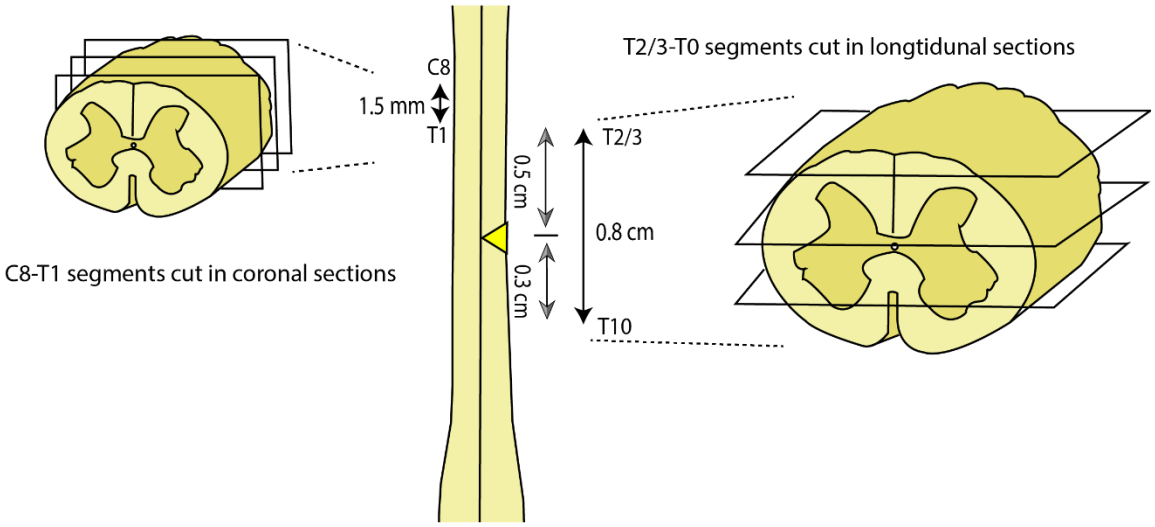

Figure 8: Schematic illustration of the segments and sections of spinal cord employed for Chapter 2 histological analysis.

1.8.2 Chapter 3 Tissue processing

For histological evaluation in Chapter 3, spinal cord samples were processed in the following manner: After careful removal of meninges, spinal cords were placed on a marked ruler and the centre point between both hemisections (at T7 and T10) was identified. From thereon, 0.75 cm rostral and caudal was marked and cut, therefore isolating an injury zone and the immediate rostral and caudal area for histological analysis and study from T2-T13 approximately (**Figure 9**). The other segments of the SC were stored in PB 0.1M and 0.02% sodium azide. The injury section in paraffin embedded tissue were included in paraffin in histology cassettes after dehydration. These were further processed in Leica ASP 300 tissue processor (Leica Microsystems, Nussloch, Germany) and sectioned in longitudinal sections (8 µm) of the tissue were and collected on gelatin coated slides in 5 series [244].

The lumbar segments, however, were selected from L1 to L6 and cryopreserved in 30% sucrose during 2 weeks for inclusion in Tissue-Teck OCT (Sakura Finetek Europe BV, Flemingweg, Netherlands), and further coronal sections of the tissue (35 µm) were sectioned in 6 series using the HM 340E microtome (Thermo Fisher Scientific, Waltham, Massachussetes, USA) collected in wells containing cryoprotectant solution (25% v/v glycerol, 30% v/v ethylene glycol in 0.1 M PB).

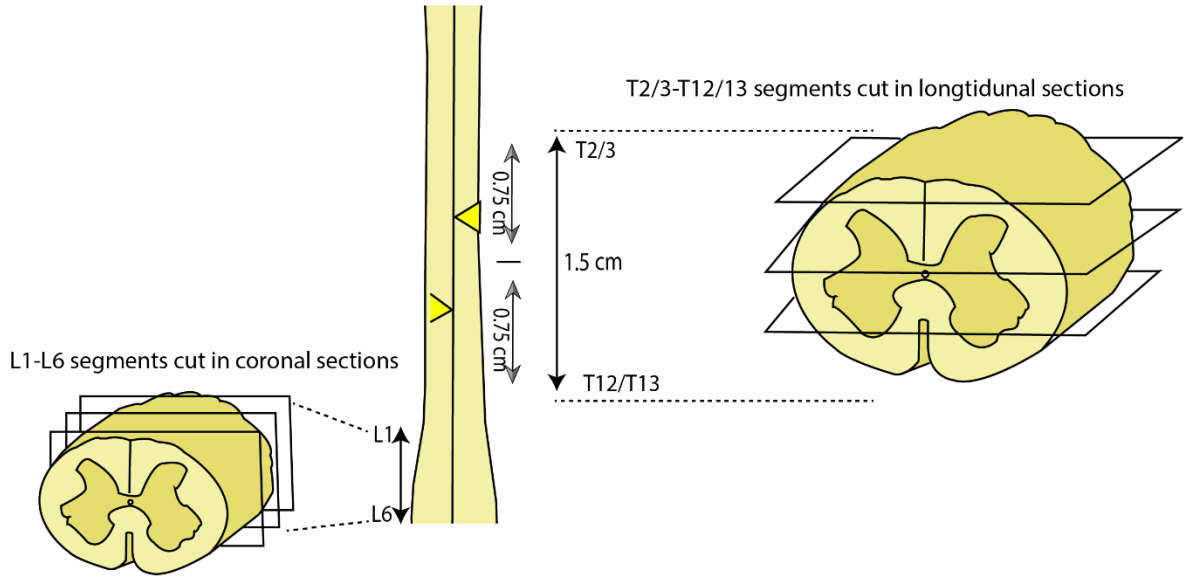

Figure 9: Schematic illustration of the segments and sections of spinal cord employed for Chapter 3 histological analysis.

1.9 Immunohistochemistry

For sections embedded in paraffin, previous steps were performed before the staining. A first heating step at 65ºC for 30 min to remove excess paraffin, followed by rehydration and deparaffinization steps done in the Leica AutoStainer (Leica Microsystems, Nussloch, Germany). Next, to unmask the epitopes, we employed the following antigen retrieval procedure: sections were incubated for 25 min in Tris-EDTA Buffer (10 mM Tris Base, 1 mM EDTA Solution, 0.05% Tween 20, pH 9) at 97ºC, as described in [245].

In case of cryopreserved tissue, no previous steps were performed.

Sections were then blocked and permeabilized with a solution of 10% FBS, 5% horse serum, and 0.1% Triton X-100 in PBS for 1 h at room temperature and then incubated with primary antibody solution overnight in a humid chamber. Primary antibodies were employed using the following dilutions: Rabbit anti-GFAP (1:600, Z0334, DAKO, California, USA); mouse anti-β-III tubulin (1:400, 11-264-c100, EXBIO, Vestec, Czechia); chicken anti-GFP (1:1000, ab13970, Abcam); guinea pig anti-RFP (1:1000, 390004, Synaptic Systems, Gottingen, Germany); rabbit anti- serotonin (1:400, S5545, Sigma, Missouri, USA); rabbit anti-MBP (1:400, ab69863, Abcam, Cambridge, UK); guinea pig anti-VGLUT1 (1:400, 135305, Synaptic Systems, Göttingen,

Germany); rabbit anti-VGLUT2 (1:400, 135402, Synaptic Systems, Gottingen, Germany); rabbit anti-VGAT (1:400, 131002, Synaptic Systems, Göttingen, Germany) and chicken anti-NeuN (1:600, ABN91, Merck Millipore, Massachusetts, USA).

Conjugated secondary antibodies AlexaFluor 488, 555, and 647 were used against the respective IgG for 1 h at room temperature. Slides were counterstained with DAPI (1;1000, #D9542, Sigma, St. Louis, Missouri, USA) and mounted with Mowiol® (#81381, Sigma, St. Louis, Missouri, USA).

1.10 Image Analysis

Images were acquired from Aperio Versa Scanner, Zeiss Apotome unless specified otherwise and visualized and analysed using Leica AperioScope or ImageJ.

1.10.1 Quantifications from Chapter 1

1.10.1.1 Total neurite length:

Images were obtained in 20x magnification using Zeiss Aperio Apotome microscope. Total neurite length of was defined as total length of all dendrites was measured using NeuronJ pluggin in ImageJ software in microns using the adequate scale. Briefly, images were opened and passed to 8 bits. Same threshold was applied to all images. Images were then opened in NeuronJ and dendrites were manually traced. Total dendrite length per neuron in microns was expressed per neuron. A minimum of 20 neurons were analysed per condition per sample (n).

1.10.1.2 Growth cone quantification

Growth cone images were obtained by imaging at 100x using Zeiss Aperio Apotome microscope. Growth cone area was defined as the actin positive area at the microtubule end of the growth cone. This was manually traced and expressed as area in μm^2.

1.10.2 Quantifications from Chapter 2

1.10.2.1 Quantification of number of cells

Images of (cryopreserved) longitudinal sections were taken using Aperio Versa Scanner and visualized using AperioScope software at 20x magnification.

As described in Chapter 2 results (**Figure 20F**), two types of cells were identified – glial cells and neurons.

For longitudinal sections, the total number of cells were counted manually across an entire series of each animal, then multiplied by the total volume of the series to estimate the total number of cells in the entire spinal cord.

Additionally, in some animals, the number of cells were counted in clarified spinal cords using IMARIS. To compare the analysis, each analysis was first normalized to the mean of their control. Data was presented as total number of cells raw numbers.

Number of neurons were properly distinguishable only in longitudinal sections, therefore total number of neurons were counted manually across an entire series of each animal, then multiplied by the total volume of the series to estimate the total number of neurons in the entire spinal cord, and clarified spinal cord date was not included. Data was presented as total number of neuron raw numbers.

1.10.2.2 Rostral migration

Images of (cryopreserved) longitudinal sections were taken using Aperio Versa Scanner and visualized using AperioScope software at 20x magnification.

The lesion and injection center were manually marked as the starting point (or 0) as per the damage to the tissue, and a horizontal line till the furthest transplanted cell (GFP positive) in both directions, caudal and rostral was drawn.

Additionally, in some animals the distance from the injury center was analysed in clarified tissue sections using IMARIS. To compare the analysis, each analysis was first normalized to the mean of their control. Data was presented as the maximum rostral migration in µm for every animal.

1.10.2.3 CST passing through transplant

Images of (cryopreserved) longitudinal sections were taken using Aperio Versa Scanner at 20x magnification and visualized using ImageJ software.

Transplanted area was traced manually in ImageJ as shown in Figure 21E and the area of CST passing through this area was calculated applying the same threshold for all sections. This area was then normalized to the total transplanted area. Data was presented as the ratio of CST positive area and the total transplant area for every animal.

1.10.2.4 CST preservation after lesion

Images of (cryopreserved) longitudinal sections were taken using Aperio Versa Scanner at a 20x magnification and visualized using ImageJ software.

To calculate the positive pixels of CST after injury, first, the midpoint of every injury (identified by the degradation of the CST and the tissue) was marked as 0 (no pixel value). Next, the same threshold values were applied to the images. Using Dynamic ROI Profiler in ImageJ, the positive pixels for CST per column of the image were obtained. This was then represented as positive pixels/microns of image from the midpoint of the injury.

1.10.2.5 CST Sprouting analysis

For the single lateral hemisection model, coronal (cryopreserved) sections immediately rostral to the lesion site, (T3) were analysed. Positive area of the descending CST fibers, expressing RFP, transduced by the injection of the pENN.AAV.hSyn.TurboRFP.WPRE.RBG particles in both hemispheres of the motor cortex area was measured using the Dynamic ROI profiler in ImageJ to obtain the positive pixels for RFP for every pixel column in the image, represented as positive pixels at every micron.

1.10.3 Quantifications from Chapter 3

1.10.3.1 GFAP – area

Images were taken using Aperio Versa Scanner at 20x magnification and visualized using AperioScope software.

The injured and scar area is characterized by the delimiting border forming astrocytes [94, 246]. Therefore, the extension of the scar was taken as glial fibrillary acidic protein (GFAP) negative area delimited by the GFAP positive border, manually traced using the AperioScope software. The analysis was performed in paraffin longitudinal sections of T2-T13 zone in at

least 6-7 slices, throughout the dorso-ventral axis of the spinal cord per animal. This was normalized to the total tissue area marked from the first appearance of a GFAP negative area till the last. Data was presented as ratio of GFAP negative area and the total transplant area for every animal.

1.10.3.2 Neuronal fibres analysis

Images were taken using Aperio Versa Scanner and visualized using ImageJ software.

The global preservation of ascending and descending neuronal fibers was identified by β-III-tubulin immunostaining rostral and caudal to the injury and in the epicenter of the lesion, excluding the somas in the grey matter. Preservation of serotonin fibers was also evaluated by 5-HT immunostaining. Similarly, the global preservation of myelin was analysed using MBP immunostaining. In all the cases, sections were evaluated in an entire series of every animal, in paraffin longitudinal sections. Positive signal was measured applying the same threshold for images taken at the same intensity and exposure every 1mm for β-III-tubulin or 1.5 mm for 5-HT staining, in the rostral region (including T6) and caudal region (including T11) as well as in the lesion site (including T7-T10). For myelin fiber analysis, this region was defined as in a region of interest starting from1 mm rostral to the injury epicenter to 1 mm caudal (including T6-T11 segments) Each of these measurements (in pixels/mm2) were then expressed as a % of positive area normalized to the total area analysed.

1.10.3.3 CST sprouting analysis

Images were taken using Aperio Versa Scanner at 20x magnification and visualized using ImageJ software.

CST sprouting analysis in the T7-T10 double lateral hemisection model was analysed in the following manner: Positive area of the descending CST fibers, expressing GFP, transduced by the injection of the AAV9-Synaptophysin-GFP particles in the right hemisphere of the motor cortex area was measured and normalized to the total traced tract area.

The analysis was done in an entire series of every animal throughout the dorsoventral axis from T3-T6 (rostral to lesion) at least in 7 paraffin longitudinal slices per animal. Data was represented as ratio of total sprouting area/total tract area.

1.10.3.4 NeuN quantification

Images were taken using Aperio Versa Scanner at 20x magnification and visualized using ImageJ software.

In order to quantify the number of neurons, NeuN staining was employed in and around the lesion site in longitudinal (paraffin) sections 1.5mm rostral and caudal to the lesion, and the lesion site. Each of these measurements (in pixels/mm2) were then expressed as a % of positive area relative to the tissue area quantified [247] since there were slight differences among animals.

1.10.3.5 Excitability and inhibitory neuronal input analysis

For analysis of contacts per neuron, longitudinal sections of ventral zone from were chosen. Images were taken in a Leica TCS SP2 at 63x magnification in the confocal microscope at step size of 1 µm. VGLUT2, VGLUT1 and VGAT immunostaining were respectively used for excitatory and inhibitory input analysis when co-localized with NeuN positive neurons. At least 15-20 neurons per section per zone (injury or immediately caudal) were analysed in a minimum of 2 sections per animal, in 4 animals per group. The values for every neuron were then plotted individually as contacts per neuron.

For lumbar analysis, an entire series of coronal (cryopreserved) sections was analysed. Images were taken using Aperio Versa Scanner and analysed using ImageJ software. Spinal cords were divided into laminae I-X as described by [9]. Similar threshold in all animals was applied in all sections for VGLUT2 and VGLUT1 positive area for every lamina, which was then normalized to the total area of each lamina respectively. Data was presented as the ratio per animal.

1.11 Statistical Analysis

All statistical analysis was performed using GraphPad Prism Software. The Shapiro-Wilk normality test was performed to ensure the dataset normality (Gaussian). Outliers were identified using ROUT's test (Q=1%). Comparisons between the two groups were carried out using the two-tailed *t*-test. The Mann-Whitney test was performed for datasets that did not follow a normal distribution. One-way ANOVA was performed to compare more than two groups with single variables, followed by Tukey's post-test for typical data sets. Kruskal-Wallis One-way ANOVA with Dunn's post-hoc correction was used for data sets that did not follow a normal distribution.

Two-way ANOVA was performed for repeated measurements with two variables, followed by a Tukey post-hoc test. The confidence level for all tests was set as 95%. All bar plots are represented as mean ± standard error mean (SEM). P values are represented as: * $P < 0.05$; ** $P < 0.01$; *** $P < 0.001$; and **** $P < 0.0001$. # and + were used following the same rule as * for different group comparisons.

Chapter 1 – Study the ability of cytoskeleton modulating drugs to enhance axonal length, alone or in combination with NaChBac expression in neuronal cultures

1.1 Introduction

As described earlier (See Use of pharmacological agents, Introduction) several cytoskeleton modulating drugs are actively used as an effective therapy for SCI. During SCI, axons are severed and have limited their ability to extend again to reach their targets. Therefore, the use of cytoskeleton modulating drugs mainly focus on the alteration of the complex cytoskeleton dynamics of the growth cone to modulate its activity and consequently, axonal growth.

Growth cones are structures present in the tip of dendrites and axons which modulate the migration process of the cone, and by default, the length of the axon or dendrite. It is a fan-like structure consisting of lamellipodia, composed of filamentous actin (F-actin) and filopodia, composed of actin fibres. Within this mesh framework of actin fibres are intertwined microtubules which also play an important role in the regulation of growth process. Structurally, the growth cone can be divided into 3 distinct domains: The central (C) domain, the transition (T) domain and the peripheral (P) domain. The (C) domain is made up of microtubules that stick out from the axon tip (shaft), with their plus end facing the axon ends. The T domain is composed of actomyosin arcs (actin arcs attached to NMII). The P- domain is made up of actin, consisting of lamellipodia, composed of filamentous actin (F-actin) and filopodia, composed of actin fibres [248](**Figure 10**).

Currently, there are two major consensuses on the governing mechanisms behind growth cone dynamics: actin dynamics and microtubule dynamics. Actin dynamics is maintained by the polymerization and depolymerization of F-actin in the P domain. Actin polymerization pushes the actin from the P domain forward, resulting in axonal growth. Depolymerization of actin leads to retrograde movement of the growth cone. Polymerization and depolymerization rates of actin are decisive for the growth cone growth direction [249]. Another important player is the T domain, where actomyosin arcs act as retrograde contractile force that opposes action extension [118]. Indeed, use of Blebbistatin, an inhibitor of NMMII can revert this effect

[117, 118, 250], and genetic deletion of NMMII promotes axonal extension after optic nerve crush [251] (**Figure 11A**).

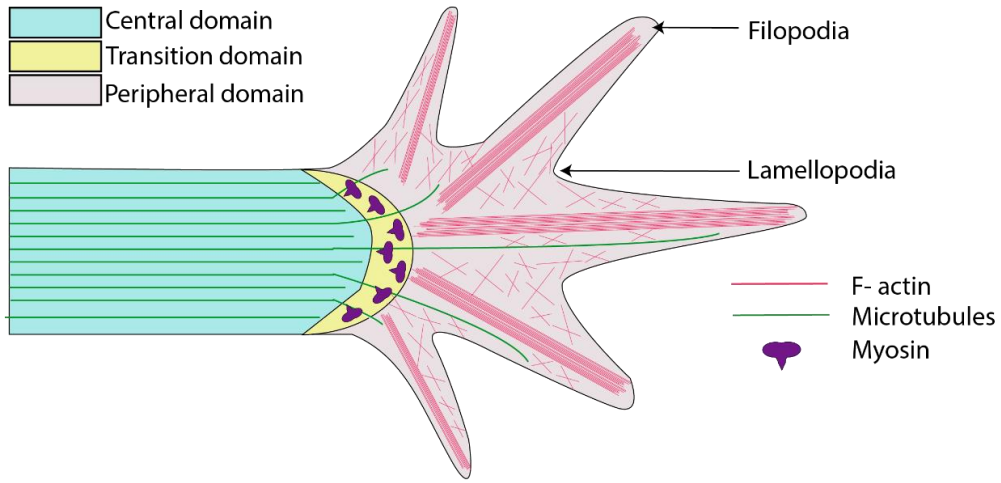

Figure 10: Structure of growth cone. Central domain is enriched in microtubules, whereas transition zone is where actin-microtubule interaction takes place, as well as acto-myosin interactions. Peripheral domain is rich in F-actin filaments, forming filopodia and lamellopodia. Figure created based on information from *(Franze & Guck, 2010) [248]* and *(Leite, Pinto-Costa, & Sousa, 2021) [249]*.

Microtubule (composed of tubulin) movement is ruled by the assembly or polymerization (rescue) of tubulin fibres at the plus (distal) end of the axon, leading to forward protrusion of microtubules passing from T to P domain, or rapid disassembly (catastrophe) of the tubulin fibres, leading to microtubule retraction. Assembly and disassembly regulate axonal growth and extension [252]. Several studies have shown that microtubule stabilising drugs such as Taxol, Epothilone B can promote axonal extension [96, 253] (**Figure 11B**). Use of Epothilone has also been shown to have positive results *in vivo* in SCI models, however it is now believed it is due to the effect dual effect on other cell types due to effects such as reduced fibrotic scarring rather than only axonal extension of neurons [120, 254].

Focusing on our **first objective** for this chapter, which is to characterize the dual effect of cytoskeleton modulating drugs on *in vitro* DRG culture simulating conditions like those encountered in an injury environment by creating a permissive and non-permissive

substrate; we make use of neurite length assays to study the potential neurite elongation effects of our treatments.

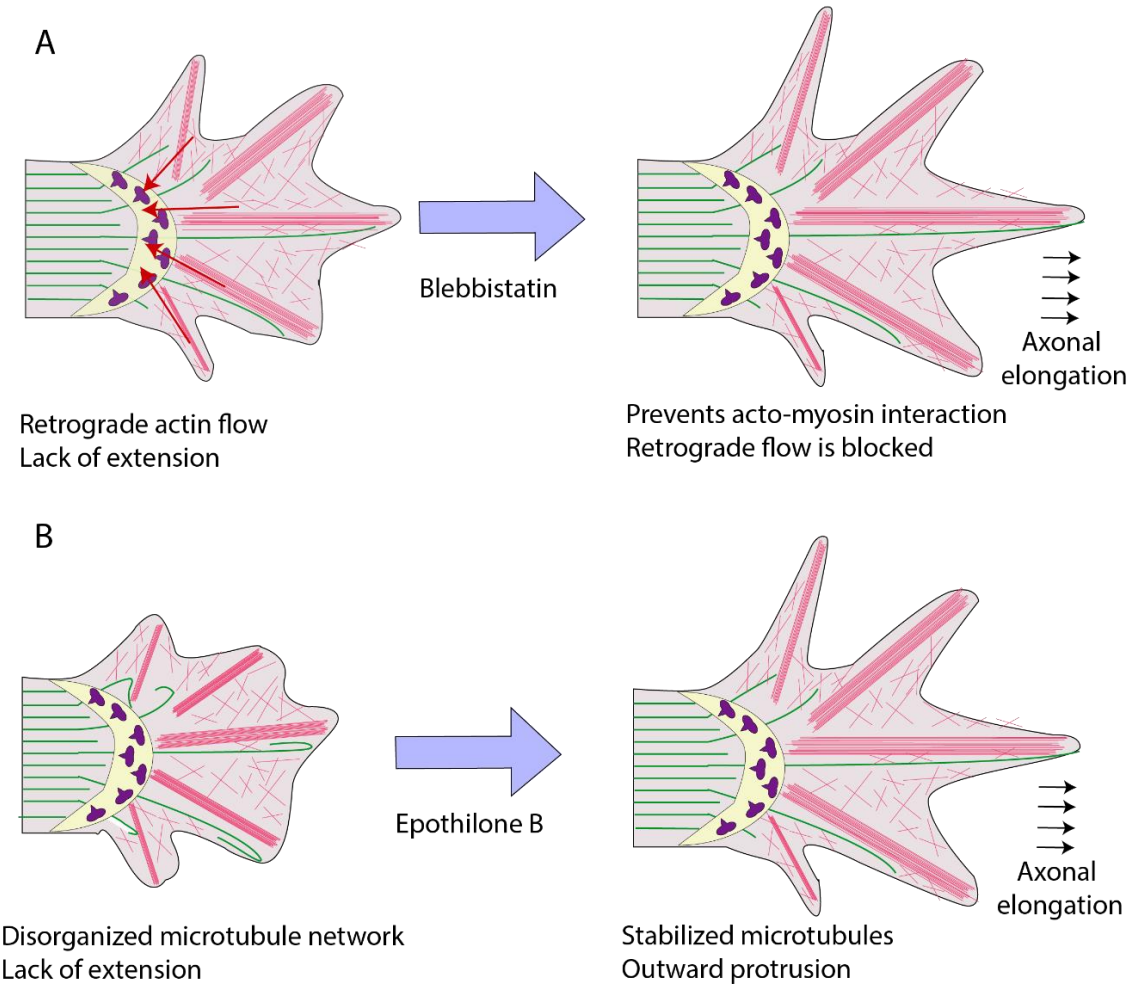

Figure 11: Blebbistatin and Epothilone B effect on growth cone. Action of Blebbistatin (**A**) and Epothilone B (**B**) over the growth cone and consequent axonal elongation.

1.1.1 Neurite length assays as a method to evaluate neuronal response to cytoskeleton altering drugs:

Neurite outgrowth assays are an effective means of understanding how neurons may be affected by a treatment and its effect on the axonal length of cultured neurons *in vitro*. Primary neuronal cultures isolated from tissue, may be cultured over substrates that are known to inhibit CNS growth *in vivo,* creating an environment similar to the inhibitory environment in *vitro* to further understand the potential of a drug to overcome this negative inhibition [255]. Therefore, using an inhibitory molecule such as CSPGs as substrates, which is known to be an important component of the SCI environment, as well as is a well-known axonal growth inhibitor; can effectively produce an *in vitro* model that could allow us to study the effect of

neurite retraction [256]. This allows us creates a “non-permissive” environment for neurite growth *in vitro.* This contrasts with a control “permissive” condition, generally laminin, a major component of basal laminae, which has been shown to be essential to initiate neurite outgrowth *in vitro* [257, 258].

The second objective of this chapter is to characterize the effects of NaChBac overexpression on neuronal activity and survival. For that, we first evaluate the expression of NaChBac in DRGs followed by the expression in a neuronal cell line, neuroblastoma 2A line.

1.1.2 NaChBac sodium expression in DRG neurons, relationship between Na+, Ca2+ and cAMP

Classically, the electrophysiological profile of the cells can be determined by techniques such as single cell patch clamp techniques. Typically, part of the cell membrane can be isolated by attaching onto a micro tip, forming a continuity between the tip and the cell, allowing the measurement of conductance of ion channels present in the membrane. By controlling the ions that pass through the pipette, several parameters relating to the voltage, conductance, currents can be determined [259]. Studies have effectively shown a change in the electrophysiological profile of several neuronal types expressing NaChBac – such as developing granule cells [221], arcuate neurons [223], developing cortical neurons [180], and cell lines such as HEK and HeLa [217]. These include additional sodium current corresponding and specific to NaChBac, which activates at around -40 ± 10 mV, leading to an increase in intrinsic activity as well as spontaneous firing in some of the neurons expressed [221]. Some even identify an increase in Ca^{2+} influx in the neurons expressing NaChBac [224]. This could be explained by the fact that Na^{+} and Ca^{2+} signalling is closely linked and tightly regulated to prevent overload and consequent apoptosis. One of the most important regulators of Na^{+} and Ca^{2+} signalling is the sodium calcium exchanger (NCX), exchanging three Na^{+} for one Ca^{2+} [260]. Furthermore, Na^{+} influx can also activate voltage gated Ca2+ channels, leading to increased Ca^{2+} influx. Another important regulator of Ca^{2+} influx into cells are N-methyl-D-aspartate receptors (NMDARs); which are permeable to both Ca^{2+} and Na^{+} but are largely linked to activation by Na^{+}. In fact, an influx of Ca^{2+} alone acts as an inhibiting factor for the activation of NMDAs. However, when the influx of Na^{+} is above a certain threshold, the influx of Ca^{2+} is immediately increased to overcome the Ca^{2+}-inhibition of NMDARs [261]. Ca^{2+} signalling is essential to for the regulation of apoptosis and autophagy, consequently, cellular

homeostasis. This balance is a delicate one since an increase in Ca^{2+} is known to increase cell survival and proliferation. However, excessive Ca^{2+} accumulation leads to the activation of apoptotic and/or autophagy signalling [262]. Ca^{2+} ions also act as axonal outgrowth regulators and are important for its mediation and motility. Transient receptor potential canonical (TRPC) channels, a family of channels that are permeable to Ca^{2+} ions are important for the guidance of axonal outgrowth at the growth cone [263]. Recently, it has been demonstrated that Ca^{2+} controls the growth cone cytoskeleton, thereby controlling motility of neurons [264]. Since Ca^{2+} is also an important modulator of cAMP [265, 266], a known regeneration-associated factor, NaChBac expression as a therapy for SCI seems promising. However, to our knowledge, none of these experiments have been carried out in DRG neurons; and therefore, we aim to characterize the electrophysiological profile of NaChBac. For this purpose, we performed single cell patch clamp experiments. We also aim to identify possible alterations that NaChBac overexpression may bring about related to Ca^{2+} and cAMP.

1.1.3 Use of murine neuroblastoma 2A (N2A) cell line:

We take use of a neuronal-like cell line neuroblastoma 2A (N2A) cell line, a well characterized cell line known for its capacity to differentiate into neurons and exhibit neuronal cell characteristics; originally was derived from mouse neural crest. N2A cell line can spontaneously differentiate into neurons by culturing the cells in low serum conditions, exhibiting some typical neuronal signalling and morphological features such as neurite formation [267]. Therefore, this line is widely used as a neuronal model to study differentiation into neurons [268], including dopaminergic neurons [269] and cholinergic neurons [270]. N2A cell line is also commonly used for neurite and axonal length assays [271]. Additionally, N2A have also been used studies to elucidate signalling pathways, including genetically modified to mimic some alterations found in Alzheimer´s disease [272]. Moreover, given the proliferative properties of this cell line, it is also commonly used to understand survival mechanisms in neurons, including apoptosis [273].

Together, N2A proves to be a reliable and good model for neuronal signalling and survival studies. Since NaChBac expression has shown to decrease apoptosis and increase survival of newly formed olfactory neurons [221] and cortical interneurons [180], we use N2A cell line to study this increased survival and identify the possible mechanisms behind the signaling.

Graphical Abstract:

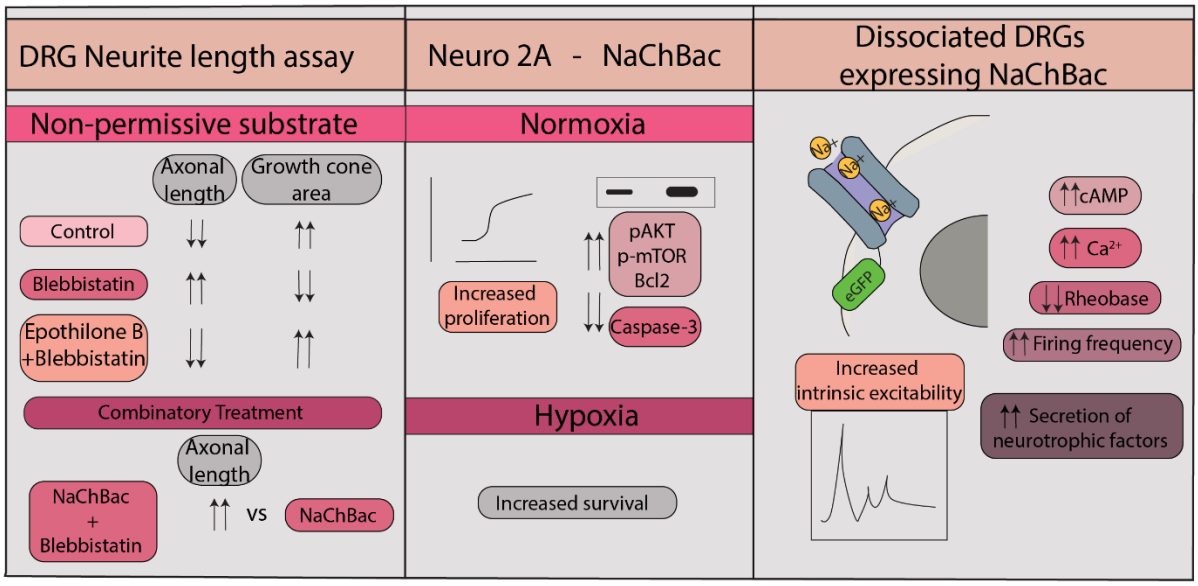

Figure 12: Chapter 1 graphical abstract.

1.2 Results

1.2.1 Blebbistatin alone rescues the neurite length of neurons plated over of CSPGs, whereas a combination with Epothilone B reverts this effect

As part of objective (1.1) of Chapter 1, we evaluate the effect of cytoskeleton modulating drugs Epothilone B and Blebbistatin over neurite length of DRGs.

Since cytoskeleton modulating drug Epothilone B has been described to enhance neuronal length *in vitro* [96], as well as *in vivo* [119, 120] , and Blebbistatin has been shown previously to improve axonal length [117, 118, 125, 250]; our first objective was to observe if there was a synergistic effect by the application of both drugs that act upon different components of the growth cone cytoskeleton, microtubules and NMMII. We first verified that the non-permissive chondroitin sulphate proteoglycans (CSPGs) did indeed create an inhibitory environment and reduced neurite length and outgrowth, like that found in the environment surrounding the injury. We added “Permissive” coatings of laminin + bovine serum albumin (BSA), and “Non-Permissive” coatings of laminin + CSPGs; for 3 hours at 37ºC. We found a significant decrease in neurite length when comparing Permissive (laminin and 2 µg/mL BSA coating) and Non-Permissive (laminin and 2 µg/mL CSPGs) (**Figure 13A, B**). Since our main objective was to observe a synergistic effect with the drugs, we analysed in parallel the effect of Blebbistatin

(Blebb) and Epothilone B (Epo) both separately and together. Based on literature, we used two concentrations of Blebbistatin (1.5 and 15 µM) and 0.1 nM for Epothilone B. Our studies showed a significant increase in neurite length and % of DRG neurons with neurites treated with 15 µM Blebbistatin, whereas the combination of both drugs seemed to revert this effect. Indeed, we found a significant decrease in the neurite length of DRGs treated with a combination of 15 µM Blebbistatin and 0.1 nM Epothilone B (**Figure 13C,** representative images**; D,E** quantifications of neurite length and % neurons with neurites **).**

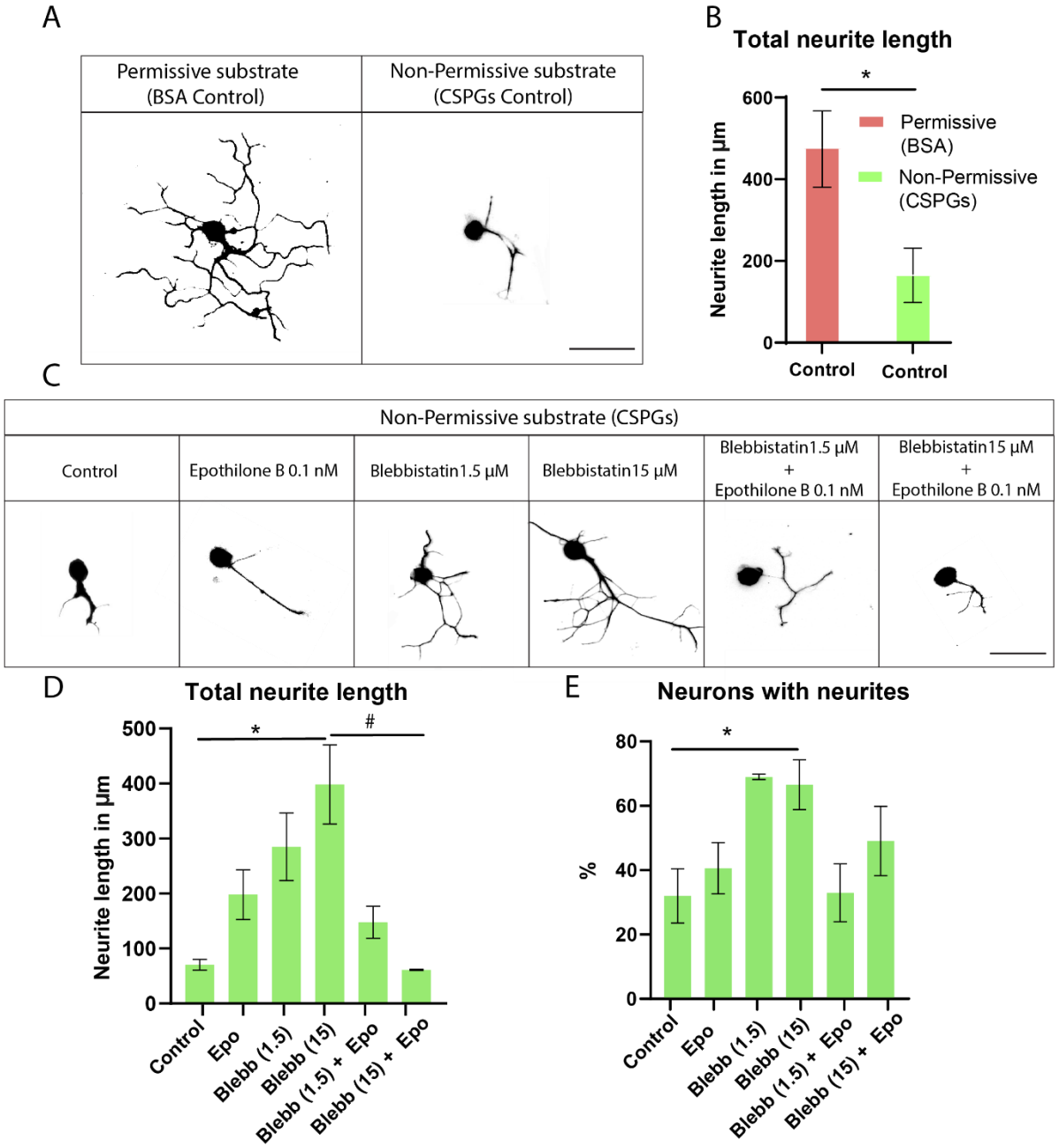

Figure 13: Blebbistatin 15 µM alone increases neurite length of dissociated DRG neurons. **A)** Images illustrating the neurite length of neurons plated over permissive (laminin + BSA) and non-permissive substrates (laminin + CSPGs). Concentration of both BSA and CSPGs used

was of 2 µg/mL. Coatings were added for 3 hours at 37ºC. **B)** Graphical quantification of neurite length in micron, *p=0.04, Student´s t-test. **C)** Images illustrating the neurite length of neurons plated over non-permissive substrates (CSPGs) and treated with drug. Cells were fixed 20 hours after treatment with drug. **D)** Quantification of neurite length of DRG neurons plated over CSPGs with treatment. *p=0.04, #p=0.01; One-way ANOVA followed by Tukey´s test. **E)** Quantification of % neurons with neurites of DRG neurons plated over CSPGs with treatment. *p=0.01, One-way ANOVA followed by Tukey´s test. All data are represented as Mean ± SEM. N=4.

1.2.2 Growth cone area increases with presence of CSPGs, Blebbistatin reverts back to normal conditions whereas the combination with Epothilone B fails to do so

Since we observed that the combination of both drugs resulted in a decrease in axonal length, we decided to get insight into the possible mechanisms behind this effect. It has been previously reported that an increase in the growth cone area, namely a "splayed" growth cone structure leads to shorter axonal lengths, observed when plated over CSPGs. Treatment with Blebbistatin can revert this structure to a thinner tightly bundled growth cone which facilitates axonal outgrowth [117]. We analysed the growth cone structure of the neurons when treated with either Blebbistatin, or the combination of Epothilone B and Blebbistatin. For that, we studied the area of the growth cone, defined as the actin positive area of the growth cone. We found that coating with CSPGs (Non-permissive) substrate significantly increased the area of growth cone of DRGs, leading to a "splayed structure". (**Figure 14 A,** representative images; magenta, actin; gray, tubulin **B,** graphical representation of growth cone area quantification). However, treatment with 15 µM Blebbistatin reverts this effect, which is again increased when combined with 0.1 nM Epothilone B (**Figure 14 C** representative images; magenta, actin; gray, tubulin; **D** graphical representation of growth cone area quantification).

Our studies suggest that the combination of Epothilone B and Blebbistatin presents an undesired effect rather than the expected synergistic one and reverts axonal length similar to those found in Non-permissive conditions without any treatment. Therefore, for the purpose of further study, we discard the combination of Epothilone B and Blebbistatin and focus on Blebbistatin alone.

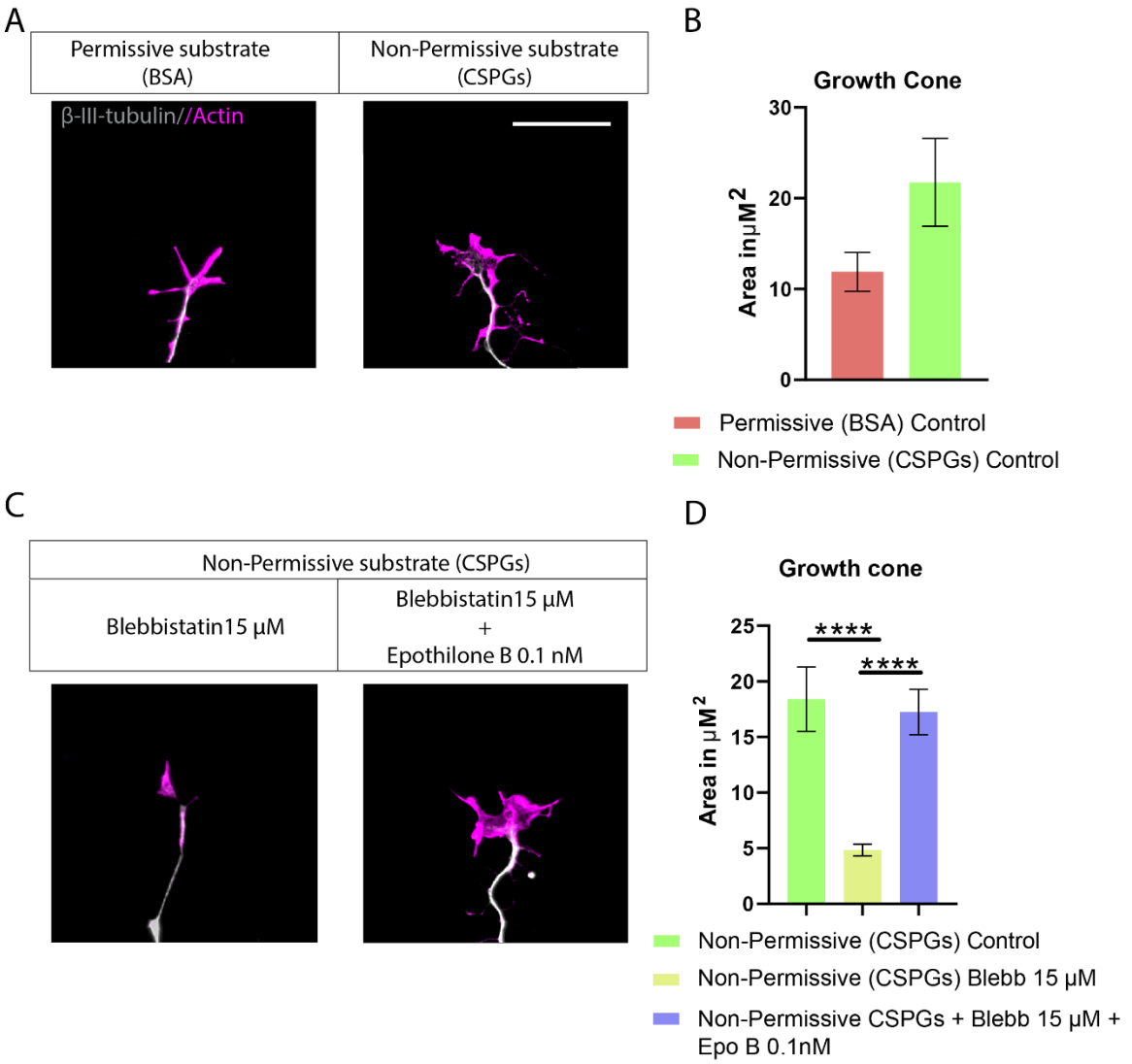

Figure 14: Blebbistatin decreases growth cone area whereas CSPGs and combinatory treatment increases area. A) Images illustrating the neurite length of neurons plated over permissive (BSA)and non-permissive substrates (CSPGs). **B)** Differences in growth cone area when CSPGs are added, $^{****}p<0.0001$, T-test. N=4. **C)** Images illustrating the neurite length of neurons plated over non-permissive substrates (CSPGs) and treated with Blebbistatin 15 µM (left), and combination of Blebbistatin 15 µM + Epothilone B 0.1 nM (right). **D)** Changes in the growth cone area treated with only Blebbistatin, or the combination of Blebbistatin 15 µM and Epothilone B 0.1 nM, $^{****}p<0.0001$, One-way ANOVA followed by Tukey´s test, N=4. All data are represented as Mean ± SEM.

1.2.3 NaChBac expression increases the excitability of neonatal rat DRG neurons

To evaluate Objective (1.2) of Chapter 1, we studied the effect of NaChBac expression on neuronal activity. For that, DRGs were transduced with lentiviral particles with Control-GFP or NaChBac-GFP constructs.

NaChBac expression fused to GFP in rat neonatal DRG neurons was predominantly located at the cytosolic membrane (**Figure 15A**), and modulated DRG activity as characterized by

intracellular electrophysiological recordings (**Figure 15B-I**). Single-cell patch clamp recordings of NaChBac-GFP DRG neurons demonstrated a slow inward current opening at -50 mV, which was absent in Control-GFP DRG neurons (**Figure 15B, C**). This confirms the presence of the sodium current specific to the NaChBac sodium channel. Additionally, we observed a modified action potential waveform in NaChBac-GFP DRG neurons (**Figure 15D**), resulting in a significantly smaller after-hyperpolarization (AHP) phase compared to Control-GFP DRG neurons (**Figure 15E**). These alterations induced an altered action potential firing in NaChBac-GFP DRG neurons (**Figure 15F**), a decrease in the rheobase (**Figure 13G**), and a significant increase in the firing frequency (Hz) (**Figure 15H**). NaChBac-GFP DRG neurons did not display altered properties such as the resting membrane potential (**Figure 15I**). These findings agree with those previously reported for CNS neurons [223, 224].

Together, these findings revealed that NaChBac-GFP expression in sensory DRG neurons leads to higher intrinsic excitability which correlates with previously published data about the electrophysiological profile of NaChBac sodium channel. This not only confirms the adequate and correct expression of NaChBac in our system, but also validates the changes brought about by NaChBac expression for the first time in DRG neurons.

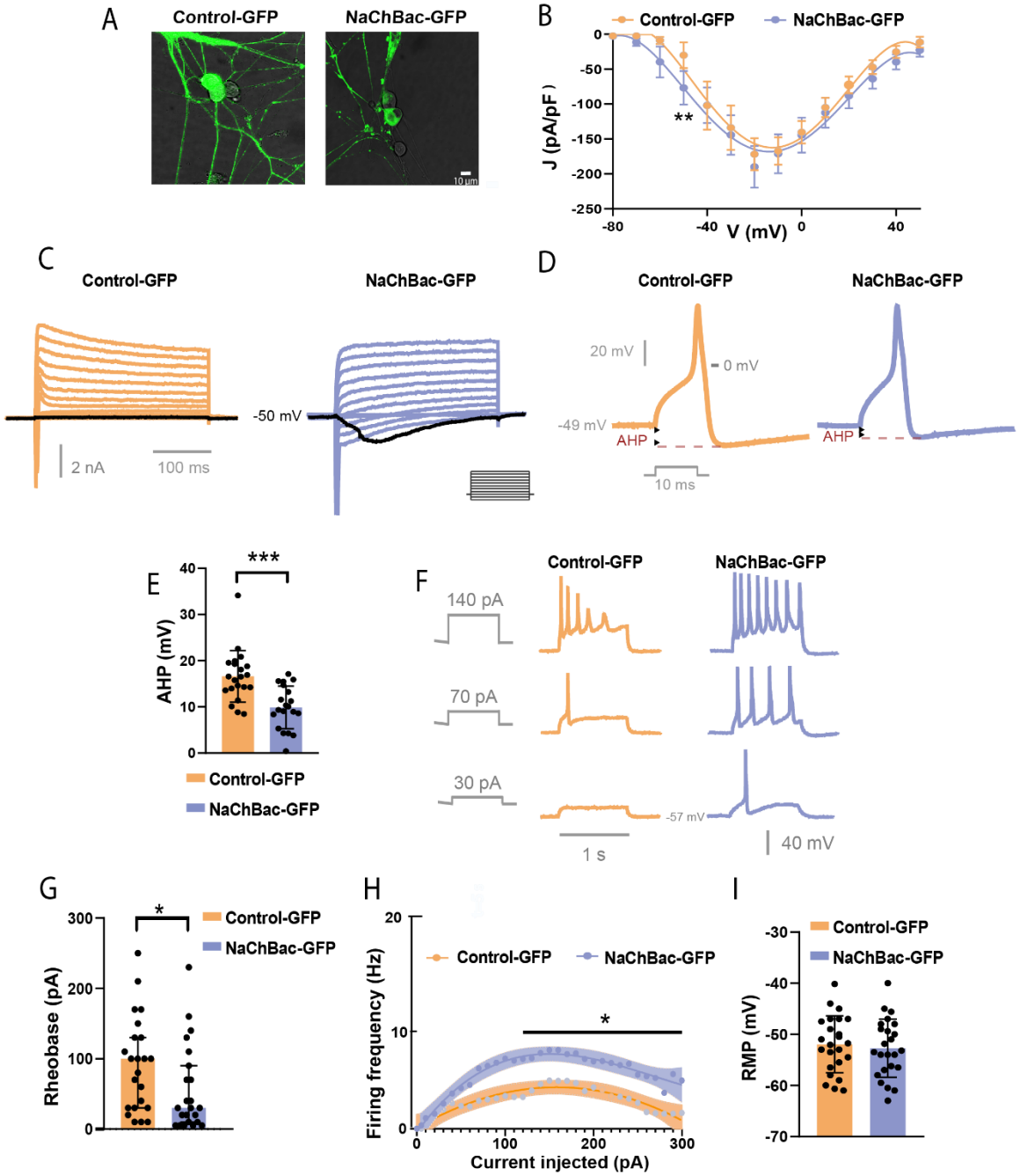

Figure 15: Impact of NaChBac expression in rat neonatal DRG neurons. **A)** DRG neurons expressing Control-GFP or NaChBac-GFP 72 h after lentiviral transduction. **B)** Representative family of current traces evoked by a 300 ms voltage steps protocol from -80 to 50 mV in 10 mV increments in Control-GFP and NaChBac-GFP DRG neurons. Holding potential = 60 mV. The black trace displays the current elicited at -50 mV. **C)** Current density-voltage (J-V) relationships were obtained with the protocol described in **B** in Control-GFP and NaChBac-GFP DRG neurons. **p = 0.0025, Mann-Whitney test. **D)** Representative action potentials recorded in Control-GFP and NaChBac-GFP DRG neurons. Action potentials were evoked with a 10 ms depolarizing current pulse. **E)** Amplitude of the AHP in Control-GFP and NaChBac-GFP DRG neurons. ***p=0.0002, Mann-Whitney test. **F)** Representative action potential firing evoked by 1 s depolarizing current pulses for Control-GFP and NaChBac-GFP DRG neurons. **G)** Rheobase for eliciting action potential in Control-GFP and NaChBac-GFP DRG neurons. *p=0.0302, Mann-Whitney test. **H)** Action potential firing frequency induced by increasing

current pulses applied (0-300 pA) in Control-GFP and NaChBac-GFP DRG neurons with the protocol described in **B**. Mann-Whitney test. *p<0.005. **I)** Resting membrane potential for Control-GFP and NaChBac-GFP DRG neurons. For electrophysiology experiments, each dot represents a neuron; n=25-30, N=3.

1.2.4 NaChBac expression elevates Ca^{2+} currents and cAMP in DRG neurons

As NaChBac expression elevates spontaneous calcium (Ca^{2+}) currents in developing cortical neurons [224], we next performed real-time imaging of Ca^{2+} dynamics using Fluor4AM reporter conjugated with Alexa488 in NaChBac-mScarlet or Control-mScarlet DRG neurons. When depolarized with KCl, NaChBac-mScarlet neurons displayed higher Ca^{2+} signaling, which persisted for at least 60 s (**Figure 16A,** representative images of Fluor4AM intensity before adding KCl, t=0s, and t=5s after; **16B** graph of Fluor4AM intensity change**; 14C** area under graph of **B**). Given that Ca^{2+} signaling modulates adenyl cyclases and cAMP generation [265], we consistently found an increase in cAMP levels detected by chromatography in NaChBac-GFP dissociated DRGs compared to Control-GFP dissociated DRGs (**Figure 16D**).

Together, these findings provide evidence that ectopic NaChBac-GFP expression in DRG neurons leads to an increased influx of intracellular Ca^{2+} and elevated cAMP levels.

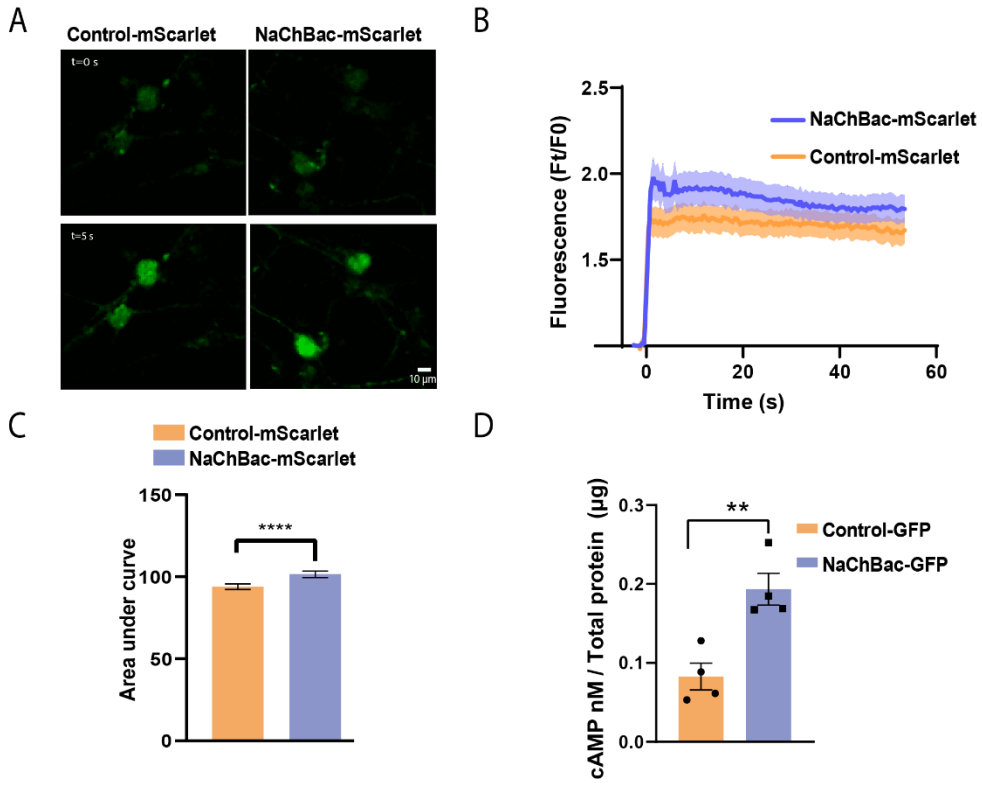

Figure 16: NaChBac expression increases internal Ca^{2+} and cAMP in DRG neurons. A) Representative images of Control-mScarlet and NaChBac-mScarlet DRG neurons at t=0 s

(before the addition of KCl) and t=5 s after the addition of 100 mM of KCl, previously treated with Fluo-4AM (Green). Scale bar = 10 µm. **B)** Graph showing change in Ca^{2+} as measured by the difference in fluorescence intensity of Fluo-4AM (green) after adding 100 mM KCl to culture throughout imaging timeframe (60s). **C)** Area under the curve of **B**. Unpaired t-test, p<0.0001, n=3. **D)** cAMP quantification normalized to total protein content in Control-GFP and NaChBac-GFP dissociated DRGs. N=4, *p=0.0056, Unpaired student's t-test. Data presented as mean ± SEM, n=3 (unless specified).

1.2.5 NaChBac expression enhances cell survival and pro-survival signaling in murine neuroblastoma cells and growth factor secretion in DRGs

As second part of objective (1.2), we next evaluated the effect of NaChBac expression over survival. For that, we next verified the ability of NaChBac expression to increase cell survival using the immortalized murine neuroblastoma line Neuro-2A (N2A). After achieving stable expression in N2A cells by lentiviral transduction, we found NaChBac-GFP expression restricted to the N2A cell membrane but a uniform cytoplasmic GFP expression pattern for Control-GFP N2A cells (**Figure 17A**), as shown for DRG neurons (**Figure 15A**). Analysis of cell proliferation revealed that NaChBac-GFP expression significantly increased the number of N2A cells after four and five days in culture before reaching confluency and under standard growth conditions (**Figure 17B**). In addition, NaChBac-GFP expression significantly prevented N2A cell death after exposure of sub-confluent N2A cultures to hypoxia (1% oxygen) for 24 h (**Figure 17C**).

To further evaluate the effect of NaChBac expression in cell survival signaling pathways, we evaluated active phosphorylation levels (p) of protein kinase B (also known as Ak strain transforming, AKT) and mTOR proteins [223, 274] and total levels of Bcl2 and Caspase 3 proteins [275, 276]. NaChBac-GFP expression led to a significant increase in the active forms of AKT (pAKT, **Figure 17D**), mTOR (p-mTOR, **Figure 17E**) and in total levels of the antiapoptotic Bcl2 protein (**Figure 17F**). Conversely, NaChBac-GFP expression significantly reduced the levels of the cleaved Caspase 3, a pro-apoptotic marker (**Figure 17G**). As shown in **Figure 17** our findings reveal that NaChBac expression increases N2A proliferation, prevented hypoxia-induced cell death, and increases cell survival-related signalling.

Finally, because cAMP can increase brain derived neurotrophic factor (BDNF) levels [277], as well as it is known that Ca^{2+} signaling is closely related to several growth factors including vascular endothelial growth factor [278] and glial derived neurotrophic factor [279], we

further explored the role of NaChBac expression in DRGs and the potential effect on the secreted factors. Therefore, we performed a multiarray using the media obtained from Control-GFP or NaChBac-GFP DRG culture. We found a significant increase in several growth factors, including BDNF, nerve growth factor (NGF), GDNF, granulocyte macrophage colony-stimulating factor (GM-CSF), insulin-like growth factor 1 (IGF-1), platelet-Derived Growth Factor (PDGF) isoform AA, insulin-like growth factor binding protein 5 (IGFBP5), and vascular endothelial growth factor (VEGF) (**Figure 17H**).

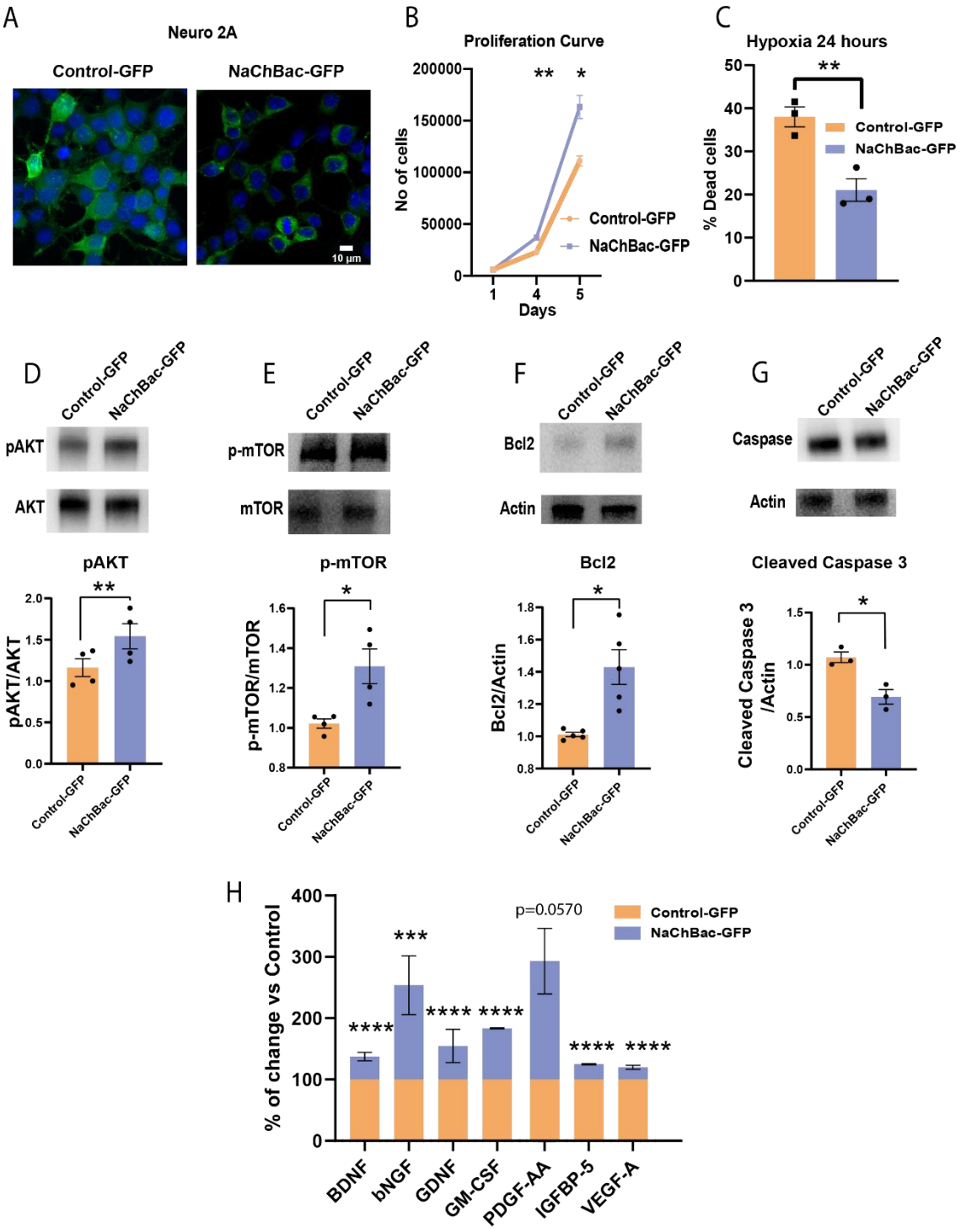

Figure 17: NaChBac expression enhances neuroblastoma cell survival and pro-survival signaling. A) Representative images of N2A cells expressing Control-GFP (left, green) or NaChBac-GFP (right, green). Cell nuclei stained with DAPI (blue); Scale bar = 10 µm. **B)** Proliferation curve for Control-GFP and NaChBac-GFP N2A cells, absolute number of cells counted; n=3. **p=0.0038 Day 4; *p= 0.013 Day 5, Unpaired t-test. **C)** Percentage of N2A cell death after 24 h of hypoxia (1% O_2) n=3; **p=0.0082, Unpaired t-test. **D-G**) Representative Western blots (Upper panels) and semiquantitative analysis (Lower Panels) in Control-GFP and NaChBac-GFP N2A cells of **D)** pAKT (normalized to total AKT protein levels); **p=0.001, n=3, **E)** p-mTOR protein (normalized to total mTOR protein levels) *p=0.01, n=4, **F)** Bcl2 protein

(normalized to Actin) *p=0.01, n=5, and **G)** cleaved caspase 3 (normalized to Actin); *p=0.04, n=3. Ratio paired T-Test; two-tailed. Data presented as mean ± SEM. **H)** Graph showing the increase in the levels of neurotrophic factors of NaChBac-GFP compared to Control-GFP after quantification of array. Multiple unpaired t-test, BDNF **** p<0.000001, bNGF *** p=0.0082, **** p= 0.000727, **** GM-CSF p<0.000001, PDGF-AA p=0.057, IGFBP-5**** p= 0.000002, VEGF-A **** p= 0.000226.

After ensuring proper expression, we replated the DRGs over Permissive (BSA) or Non-permissive substrates (CSPGs). We additionally, added Blebbistatin at 15 µM four hours after replating to Control-GFP DRGs (Control-GFP + Blebb), or NaChBac-GFP DRGs (NaChBac-GFP + Blebb) to analyse the effect of NaChBac expression with Blebbistatin treatment.

Over Permissive substrate (BSA), we observed no significant changes between Control-GFP and NaChBac-GFP conditions, indicating that the expression of NaChBac did not alter neurite length under permissive conditions. However, the addition of Blebbistatin significantly increased neurite length of Control-GFP + Blebb compared to Control-GFP, and NaChBac-GFP + Blebb condition compared to NaChBac condition alone (**Figure 18A**, representative images; **C** total neurite length quantification). This outcome elucidates that neither GFP nor NaChBac expression has an effect over Blebbistatin; which is able to significantly increase neurite length in permissive condition.

When plated over Non-permissive substrate (CSPGs); we also did not observe any differences between Control-GFP and NaChBac-GFP conditions. This again highlights that the expression of NaChBac did not change neurite length under Non-permissive conditions either. Also, the addition of Blebbistatin significantly increased neurite length of NaChBac-GFP + Blebb condition compared to NaChBac condition alone but failed to do so in Control-GFP + Blebb condition compared to Control-GFP (**Figure 18B**, representative images; **D** graphical representation of total neurite length quantification). This result elucidates that NaChBac expression has an effect over Blebbistatin; which can significantly increase neurite length of DRGs expressing NaChBac over non-permissive condition. However, Blebbistatin fails to increase neurite length of Control-GFP neurons under non-permissive conditions, possibly due to high sample variability.

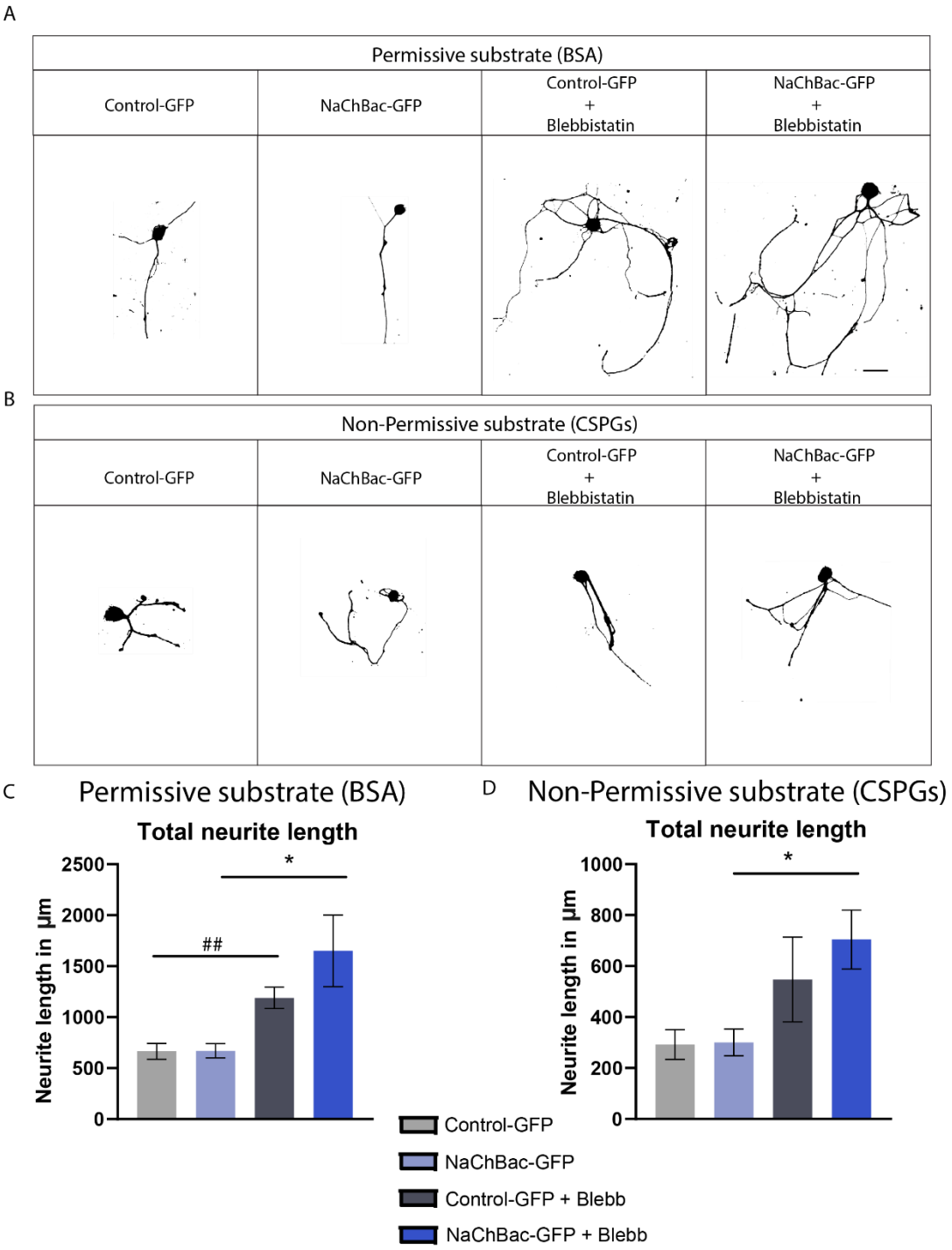

Figure 18: Effect of combinatory treatment of NaChBac and Blebbistatin over dissociated DRG neurons. **A)** Images illustrating the neurite length of neurons plated over permissive (BSA) and **B)** non-permissive substrates (CSPGs). **C)** Changes in the neurite length of DRG neurons replated over permissive (BSA) substrate, expressing Control-GFP or NaChBac-GFP; and treated with or without Blebbistatin. (Control-GFP vs Control-GFP + Blebb) $^{\#\#}p= 0.0018$, (NaChBac-GFP vs NaChBac-GFP + Blebb) $^{*}p=0.016$; Kruskal Wallis test followed by Dunn´s post-test. **C)** Changes in the neurite length of DRG neurons replated over Non-permissive (CSPGs) substrate, expressing Control-GFP or NaChBac-GFP; and treated with or without Blebbistatin. (NaChBac-GFP vs NaChBac-GFP + Blebb) $^{*}p=0.011$; Kruskal Wallis test followed by Dunn´s post-test. N=3. Data presented as mean ± SEM.

Chapter 2 – Evaluation of DRGs expressing NaChBac transplant in a moderate spinal cord injury

2.1 Introduction

Chapter 2 focuses on understanding the effect of transplanting DRG neurons in an SCI environment. For this, we transplanted the cells obtained from the culture immediately after performing an injury. The cells were transplanted at the injury site. This contrasts with previous studies by Silver´s lab where DRGs were transplanted rostral to the injury in a manner that they were away from the injury environment. Indeed, their studies revealed that the DRG neurons survived and extended until the injury site, but not beyond it. Because our aim by transplanting DRG neurons is not only to provide local support, but also enhance, maintain, and integrate if necessary to prevent the lost circuits within the injury site to prevent the complete ablation of crucial information caudal to the injury. Additionally, by expressing NaChBac we aim to enhance survival and the integration of the transplanted neurons into the existing circuits. For the purpose of this study, we chose a single lateral hemisection SCI model, which we explain further ahead. Additionally, we traced the CST with adenovirus associated virus (AAV) with a specific promoter for neurons, synaptophysin fused to red fluorescent protein (RFP) reporter gene. Therefore, AAV-hSyn-RFP was injected in the motor cortex of mice one month before the injury and transplant.

2.1.1 Spinal cord injury models: Single lateral hemisection model

A single lateral hemisection is an incomplete, partial injury to the spinal cord. It is a widely used model due to its reproducibility and reduced mortality. It is also associated with simpler and shorter postoperative care since this injury model does not destroy bladder function [280]. This type of injury severs and interrupts all the descending and ascending tracts of one side of the spinal cord until the midline. This leads to typical Brown-Séquard syndrome, which is defined by loss of locomotor function and loss of sensation on the ipsilateral side of the performed injury, with some deficits (especially proprioceptive) in the contralesional side [281]. To perform a single lateral hemisection, the desired segment (in this case thoracic segment 8, T8) is exposed by a laminectomy. Next, a complete lateral cut passing through dura matter from the lateral until the midline of the spinal cord is performed on the desired injury

site. Typically, the single lateral hemisection is performed with a surgical scalpel to obtain a clear, neat cut in the selected segment [282]. It is important to reach the midline accurately to severe all the tracts present in the midline and ensure reproducibility. Lateral hemisections provide a good model for the study of regenerative characteristics, since contralateral side of the injury is untouched, providing sufficient capacity of sprouting and regeneration. In fact, it has been demonstrated that the supraspinal information that crosses caudal to the injury on the contralateral side of the injury is responsible for functional recovery. Indeed, animals receiving lateral hemisections quickly recover locomotor performance after around 2 weeks after injury, eventually regaining the capacity for coordinated plantar stepping [90, 114, 283].

2.1.2 Choice of short-term *in vivo* study

The spina cord injury progresses in 3 phases as defined earlier, namely acute, subacute and chronic. Since most patients eligible for an intervention are in chronic stages, and most clinical trials up to date have involved patients in the chronic stage of SCI; the most clinically relevant for studying is the chronic stage [60, 172]. However, when designing experimental models to evaluate several possible treatments in rodents, it is important to consider the objective of the experiment and therefore the time of sacrifice of the animals, which determines the stage of the injury progression. For experiments where an initial hypothesis must be assessed, it is generally preferred to perform a short-term study which gives rise to the possibility of studying the hypothesis in time, as well as verifying the initial hypothesis. For example, to follow in time the effect of providing GDNF in an acute manner after injury, animals were sacrificed at 1 or 4 weeks after injury and treatment with GDNF [284]. Another example is an excellent study over the time course of NPC transplantation in an acute phase (1 week after transplantation), or in a chronic stage (4 months after transplantation) [285]. This trend has also been observed in a study where a biomaterial was inserted along with a NPC transplant as an improved treatment for animals with a SCI; and therefore the animals were sacrificed a week after the insertion of the material and the transplant [286]. For DRG neurons transplant into the SC, a low number of DRG neurons surviving following xenotransplantation was previously reported by the Silver laboratory, where adult mouse DRG neurons transplanted in adult rats displayed a significant decrease in survival two weeks after transplantation [215, 216]. Therefore, in order to study the survival, localization and possible interactions of our

transplanted cells in the study described in Chapter 2, a sub-acute scenario was deemed suitable.

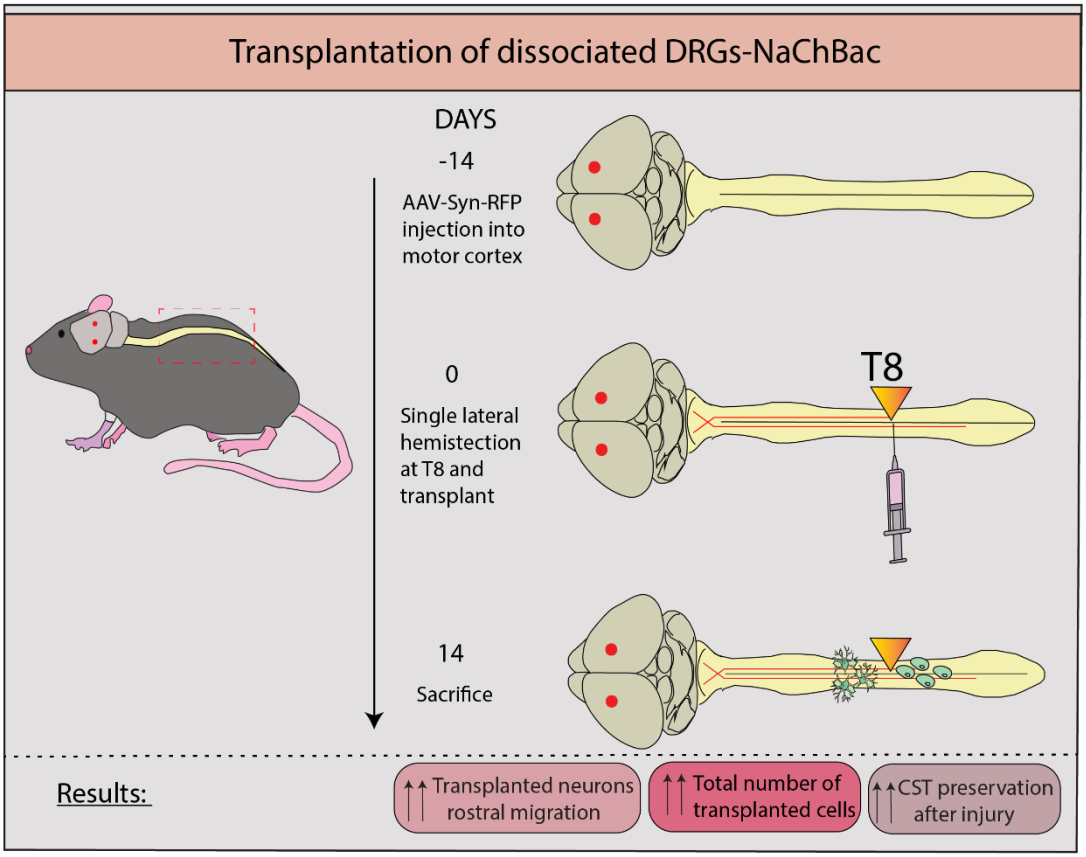

Figure 19: Graphical abstract of Chapter 2.

2.2 Results

2.2.1 Transplantation of NaChBac-expressing DRGs increase survival of total number of cells

NaChBac expression previously revealed an enhanced survival of newly-formed migrating neurons with good integration into existing circuits [228]; then, we hypothesized that NaChBac expression could also alter the survival and/or integration of transplanted DRG neurons. DRGs extracted from neonate rats at P3-P4, as described in **Figure 20A**, were transduced with either pLL3.7 empty vector (Control-GFP) or pLL3.7-NaChBac-eGFP (NaChBac-GFP) and cultured for 5 days prior transplantation into adult mice immediately below a lateral hemisection at the eighth thoracic vertebrae level (T8). Despite being treated

with AraC to avoid glial proliferation, the presence of glia was not completely excluded in the transplanted pool of cells as shown in **Figure 20B;** Green (GFP), yellow (β-III tubulin), blue (DAPI). We confirmed an infection rate of above 90% for both Control-GFP and NaChBac-GFP constructs (**Figure 20B, C**). CST was traced by injecting AAV-Syn-RFP within the motor cortex in all animals two weeks before the injury and transplantation as previously described [237]. Two weeks after transplantation, all animals were sacrificed, and we assessed the localization, survival, and integration of Control-GFP and NaChBac-GFP DRG neurons. **Figure 20A** depicts a schematic representation of the experimental design.

Transplanted DRG neurons, characterized by a large soma and long neurites, part of it positive for neuropeptide calcitonin gene-related peptide (CGRP) expression [287, 288] (**Figure 20E)** were found at the injury site, along with Schwann cells, easily distinguishable by their morphology (**Figure 20F** grey arrows for glial cells; purple arrows for neurons). However, we did not observe significant differences in the number of neurons between mice transplanted with Control-GFP and NaChBac-GFP DRG neurons at this timepoint (**Figure 20D**). However, we counted a higher total number of GFP-positive cells (including neurons and glial cells) in NaChBac-GFP DRG transplanted mice than in Control-GFP DRG transplanted mice as shown in **Figure 20G, H.**

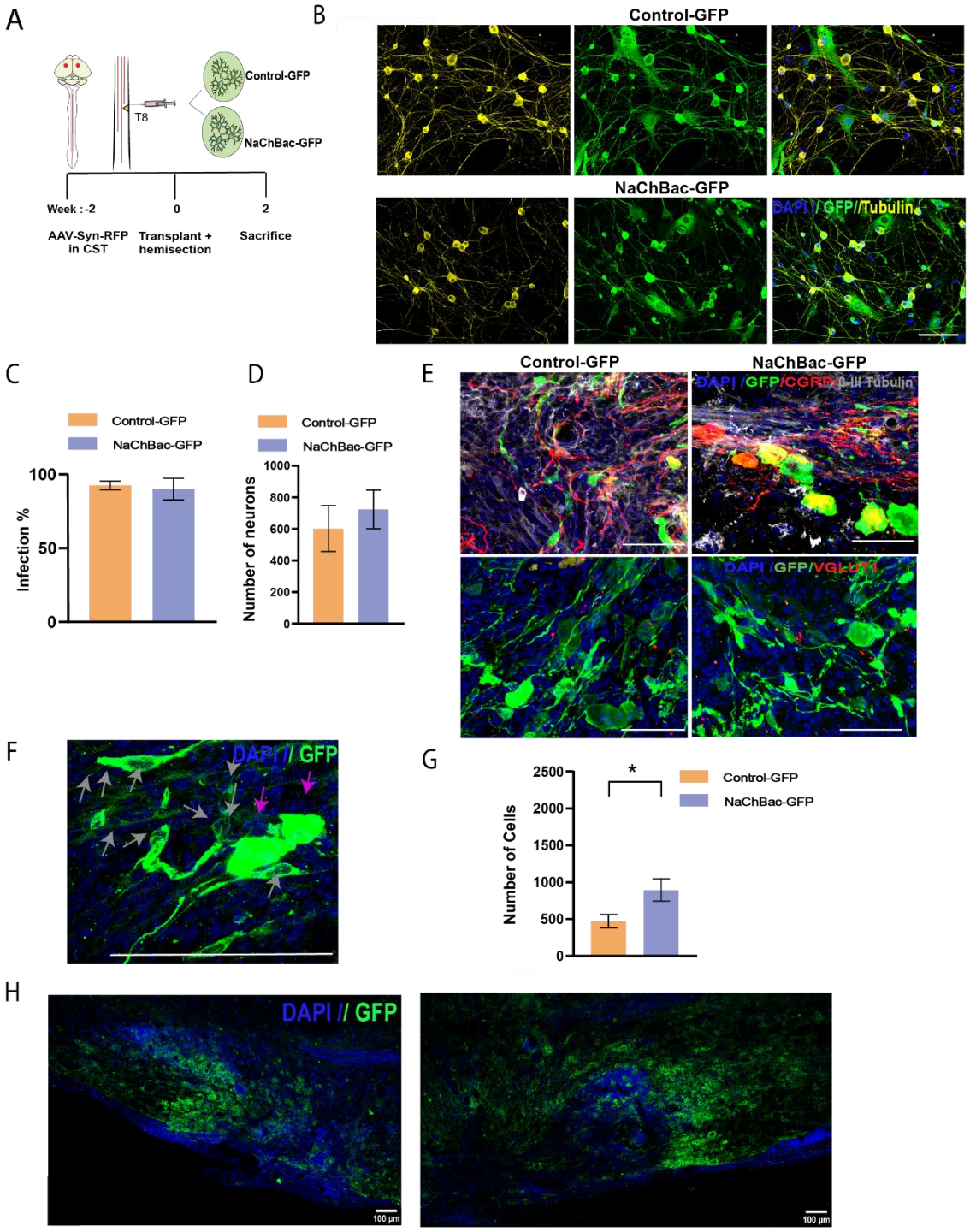

Figure 20: Transplanted NaChBac-expressing DRG neurons show an increase in the survival of total number of transplanted cells. A) Scheme depicting the experimental timeline. **B)** Images of infected dissociated DRG cultures expressing Control-GFP and NaChBac-GFP before transplantation. Green (GFP), yellow (β-III tubulin), blue (DAPI). Scale bar = 100 µm. **C)** Graph showing efficiency of infection in cultures when infected with viral constructs at MoI 10. **D)** Neuron survival measured two weeks after transplantation of Control-DRG or NaChBac-GFP DRG neurons; n=4, unpaired student's t-test. **E)** Longitudinal confocal images of mice two weeks after injury and transplantation of Control-DRG or NaChBac-GFP DRG neurons (green). Green = GFP; Red = CGRP or VGLUT1; Blue = DAPI. Scale bar = 100 µm. **F)** Magnified images of glial cells (grey arrows) and neurons (magenta arrows) after transplantation. Note the

difference in morphology and GFP expression. **G)** Quantification of transplanted cells (green) fourteen days after lesion and transplantation, n=4, *p=0.050, unpaired student's t-test**. H)** Representative images showing the cells within transplanted area. Data presented as mean ± SEM.

2.2.2 Transplantation of NaChBac-expressing DRG neurons increase CST preservation in a mouse model of SCI by single lateral hemisection

Next, we sought to understand other characteristics of NaChBac-expressing cells and the interaction with the endogenous CST.

Interestingly, we discovered that transplanted NaChBac-GFP DRG neurons migrated longer distances from the injection site to rostral locations surrounding the descending CST than Control-GFP DRG neurons (**Figures 21A and B**; clarified spinal cord images and quantification, respectively). This result agrees with previous reports of increased migratory and engraftment capacity in developing neurons in the olfactory system after NaChBac expression [228]. Since endogenous Ca^{2+} and neuronal activity play essential roles in neuronal migration [289], the endogenous activity of DRG neurons may be associated with this increased migrating capacity. Additionally, transplantation at earlier time points correlates with a more rostral migratory phenotype, possibly due to the presence of an inhibitory inflammatory environment at the injury site during the initial stages of SCI [290].

The CST is the central tract involved in skilled voluntary motor functions [291, 292] and CST sprouting after injury has been linked to improved neural activity [293, 294] and enhanced functional recovery after SCI [114, 295]. Since we found transplanted NaChBac-GFP DRG neurons closer to the injured CST rostral projection (**Figure 21A**), we analysed whether transplanted DRG neurons could enhance CST sprouting of injured axons. However, increased proximity of transplanted DRG neurons did not appear to have any effect on the CST sprouting when comparing CST sprouting at the first and second thoracic levels after transplantation of Control-GFP and NaChBac-GFP mice (**Figure 21C**, representative images **and D,** quantification). However, we observed higher frequency of CST axons crossing DRG-NaChBac-grafts than control grafts (p=0.1) suggesting that NaChBac-GFP DRG cells provides a substrate for CST preservation (**Figure 21E**, representative images, dotted line marks area infiltrated by transplanted cells and arrows show the traced CST (yellow) **and F,** quantification). On closer study, we found a significant increase in the amount of RFP-expressing CST fibers preserved at

the injury site in the NaChBac-GFP transplanted group (**Figure 21G,** yellow), measured as the RFP positive pixels extended up to 750 µm after the injury epicenter (marked as 0 in **Figure 21G, H**), in comparison to the near total degeneration of the CST observed in Control-GFP DRG neuron transplanted mice (**Figures 21G** representative images**; 16H,** graph showing CST positive pixels before, at and after injury **21I;** area under the curve of H).

Overall, these findings suggest that NaChBac expression in DRGs enhances their migratory activity and contributes to partially preserve the CST projection at the injury epicenter, without altering the survival of transplanted DRG neurons two weeks after transplantation.

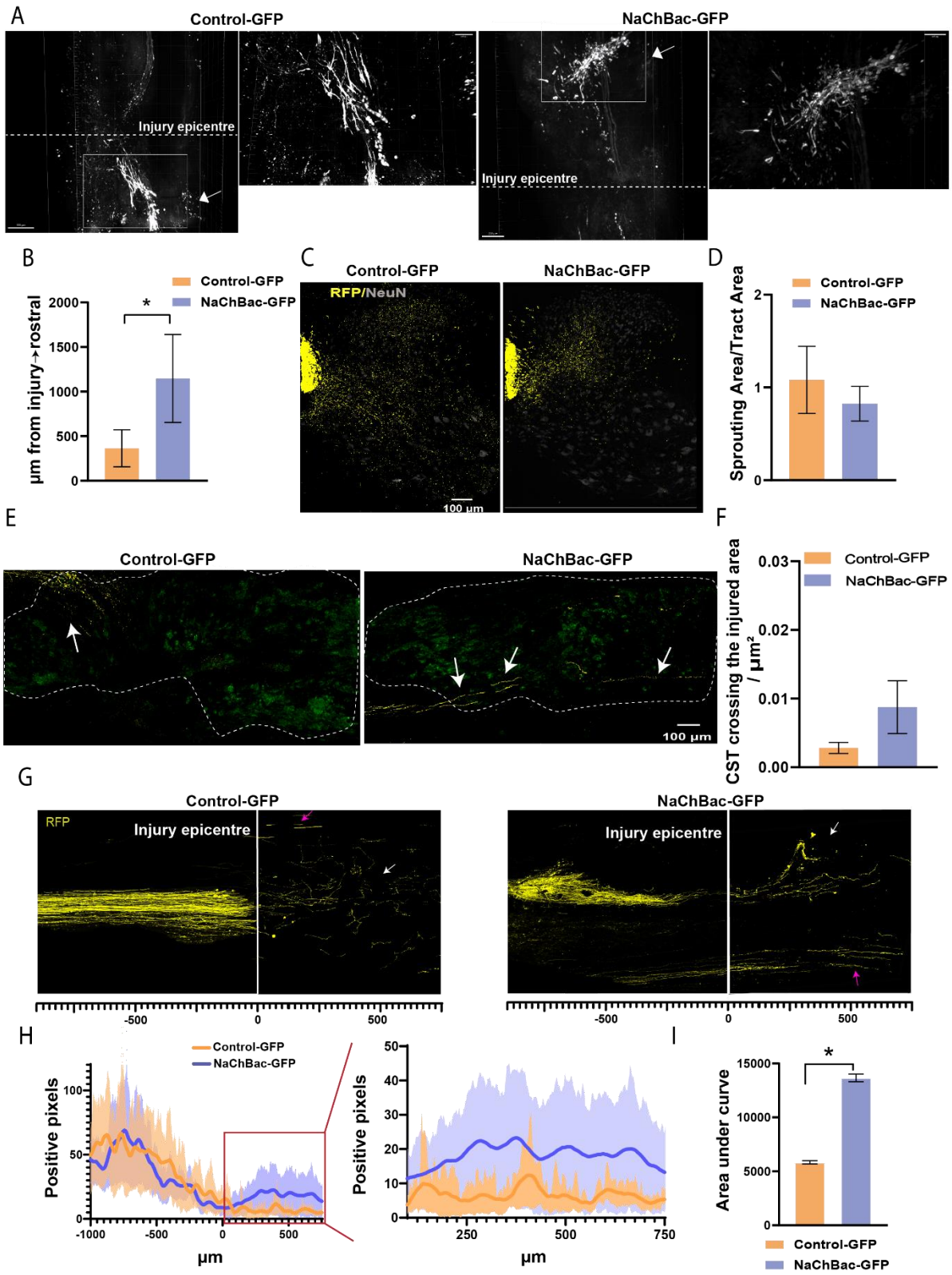

Figure 21: Transplanted NaChBac-expressing DRG neurons display improved migration and CST preservation ability in a lateral hemisection SCI model. A) CUBIC-clarified whole spinal cord-derived images of mice after Control-GFP and NaChBac-GFP DRG neuron transplantation; grey = GFP, ** Injury epicenter. Scale bar = 200 µm. Arrows show the transplanted cells, white boxes mark the amplified images. Scale bar = 50 µm. **B)** Cell migration two weeks after transplantation of Control-GFP and NaChBac-GFP DRG neurons; n=

7-8; *p= 0.05, Mann-Whitney test. **C)** Representative images of CST sprouting rostral to the lesion in Control-GFP and NaChBac-GFP DRG neuron transplanted mice. Yellow = RFP (traced CST), grey = NeuN (neurons). Scale bar = 100 µm. **D)** Quantification of sprouting area normalized to tract area in Control-GFP and NaChBac-GFP DRG neuron transplanted mice; n=7-8, unpaired student's t-test. **G)** Representative RFP-expressing CST fiber (yellow) preservation images after T8 lateral hemisection two weeks after transplant in Control-GFP and NaChBac-GFP DRG neuron transplanted mice. **H)** Quantification of positive RFP-expressing CST pixels (yellow) before and after the injury epicenter (white line) in Control-GFP and NaChBac-GFP DRG neuron transplanted mice. **I)** Area under the curve for CST crossing the injury epicenter up to 750 µm in Control-GFP and NaChBac-GFP DRG neuron transplanted mice, from **I**; n=8-9; *p=0.02, unpaired t-test. Data presented as mean ± SEM.

Chapter 3 - Evaluation of DRGs expressing NaChBac transplant in a chronic, severe injury scenario

3.1 Introduction

Chapter 3 focuses on understanding the effect of transplanting DRGs in a chronic, severe SCI environment, with a special focus on functional locomotor recovery. Additionally, we want to test whether the combination with a non-toxic analog of Blebbistatin, para-amino Blebbistatin (PAB) in a chronic, severe spinal cord injury environment, could further enhance the therapeutical potential of transplanting DRGs expressing NaChBac. For this, we transplanted the cells obtained from the culture immediately after performing the double hemisection injury within the injury site in the relay zone. Additionally, we traced the CST with adenovirus associated virus (AAV) with a specific promoter for neurons, synaptophysin fused to RFP reporter gene on the ipsilateral side of the rostral T7 first hemisection and synaptophysin fused to GFP on the contraleral side, that is, on the side of the T10 hemisection. Therefore, AAV-hSyn-RFP/GFP was injected in the motor cortex of mice two weeks before the injury and transplant.

3.1.1 Double hemisection model

Severe spinal cord injury models are often considered improved models for clinical scenarios given that injury progression in humans is critical and that humas possess inherent lower regeneration capacity than rodents. Therefore, chronic injury models are a good choice for studying functional recovery [280]. One such model is the double staggered hemisection model, which consists of two opposite lateral hemisections separated spatially. Since the role of propriospinal INs has been extensively described as an important target for functional recovery one of the reasons including the capacity of supraspinal tracts such as the CST to sprout and form new connections with the propripospinal INs [296, 297], leading to the formation of “bridge” connections or detour circuits to relay the supraspinal input beneath the injury, the staggered double hemisection injury paradigm provides a good model to enhance the formation of an active relay zone within the two injuries. Essentially, a first lateral hemisection until the spinal cord midline is performed at the desired thoracic level to severe all supraspinal input on the ipsilateral side of the injury, and a second injury is made on the contralateral (mostly rostral) side of the first injury to disrupt all the remaining spared

descending input. Most staggered lesions are done within the thoracic segments of T7-T12 or T7-T10. [90, 296, 298]. Some studies the rostral injury slightly beyond the midline to ensure complete ablation of descending pathways on the ipsilateral side of the injury [110]. Additionally, the double staggered hemisection can be performed simultaneously, or separated temporally, usually up to ten weeks after the first hemisection. The simultaneous double staggered hemisection provides a relay zone that is enough to promote some limited spontaneous functional recovery due to the formation of a "relay" zone whereas when separated temporally the time frame allows for increased remodeling around the single injury even on the ipsilateral side of the injury which were not then affected by the second injury [90]. Therefore, as a model that provides a pro-regenerative background by creating a relay zone but is considered severe and a complete injury due to overall complete ablation of supraspinal input, we chose this model and performed both hemisections simultaneously for this study.

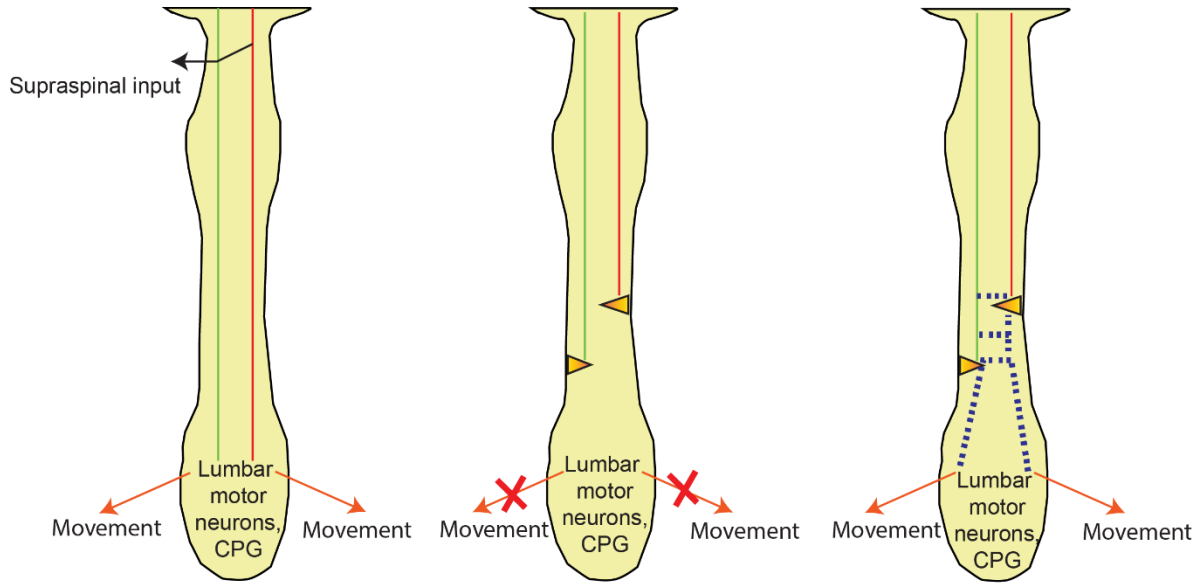

Figure 22: Double hemisection model. Schematic representation of how double hemisection model allows the formation of detour ciruits (blue dotted line) with propriospinal interneurons to relay information to lumbar motor neurons and central pattern generator of the spinal cord.

3.1.2 Choice of long-term *in vivo* study

In patients, a spinal cord injury progresses quickly into the last and most severe stage, the chronic stage, in about six months after injury. As described earlier, the most clinically relevant for exploring the potential therapeutic approach of an intervention is the chronic stage [60, 172]. Therefore, it is essential to study the potential effect of a treatment and its progression until the chronic stage. It is common to consider that the most effective treatments are the ones that can rescue locomotor recovery which is sustained in time. For example, a combinatorial approach study which aimed to understand the role of the administration of a RhoA/ROCK inhibitor fasudil conjugate in combination with NPC transplantation were sacrificed two months after injury [116]. Similarly, in a combinatorial approach to observe the effects of a human iPSC derived NPCs line, and a human MSC together with a sustained curcumin nanoconjugate release, animas were sacrificed 9 weeks post injury to determine the locomotor recovery [299]. Finally, when cytoskeleton modulating drug Epothilone B and D were used as a potential therapy for SCI in combination with rehabilitation, animals were sacrificed 70 days after injury [120]. Additionally, spontaneous recovery mediated by propriospinal INs in the relay zone of a double staggered hemisection requires a minimum of month and a half to exhibit optimum results [90]. In a study where the double hemisection was performed simultaneously, and the effect of KCC2 administration was evaluated, mice were sacrificed seventy days after SCI [110]. Therefore, to perform an adequate study with a range of functional tests of locomotor recovery considering the chosen double staggered hemisection model, we sacrificed the mice about 7 weeks after injury and transplantation.

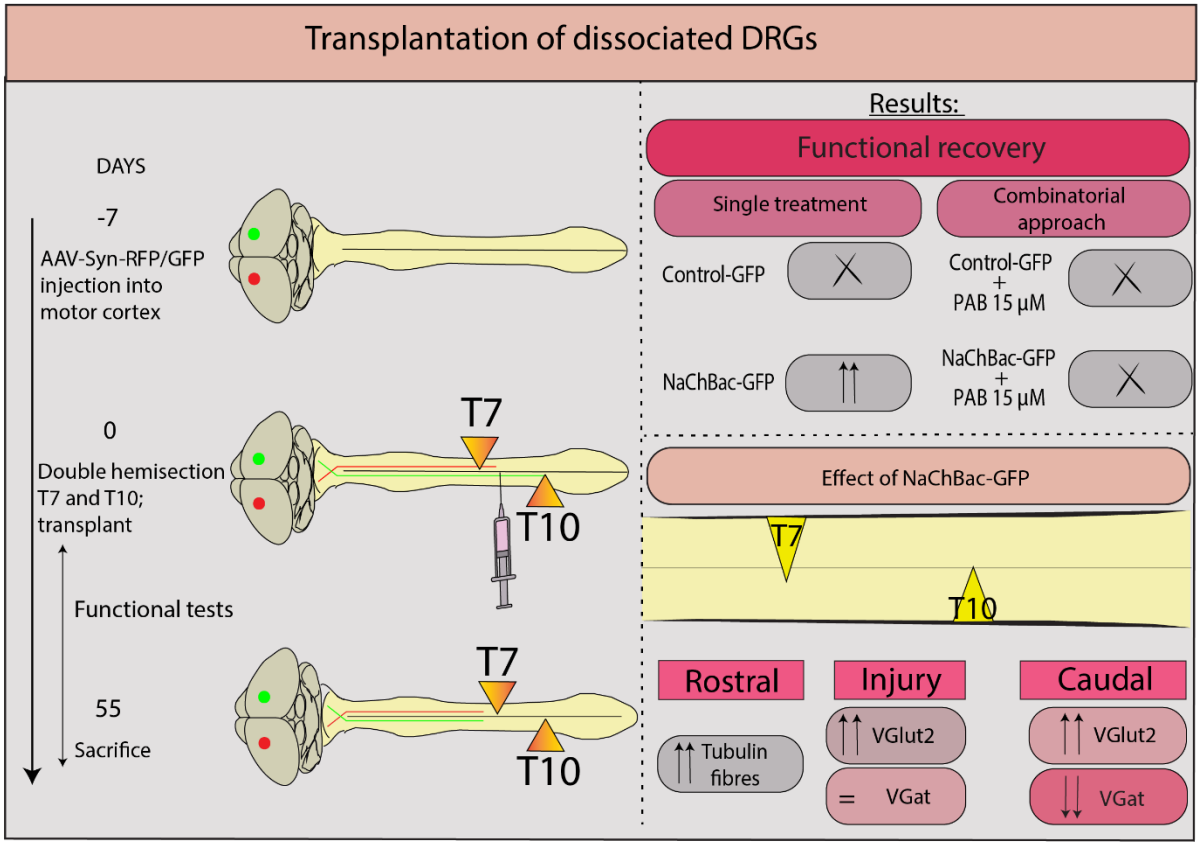

Figure 23: Chapter 3 graphical abstract.

3.2 Results

3.2.1 NaChBac-GFP alone improves BMS score of mice, combinatory treatment does not

We performed a large *in vivo* study to compare several groups in order to evaluate the functional recovery. For this, we performed a double hemisection in animals at T7-T10 levels. Animals were then either injected with only media as control (Non-Transplanted); only the PAB drug at 15 µM (PAB 15 µM) transplanted with DRGs expressing GFP only (Control-GFP); DRGs expressing NaChBac-GFP (NaChBac-GFP); combinatory therapy of with DRGs expressing GFP and the PAB drug at 15 µM (Control-GFP + PAB 15 µM) or DRGs expressing NaChBac-GFP and the PAB drug at 15 µM (NaChBac-GFP + PAB 15 µM) (**Figure 24A**; timeline and groups for the experiment).

We evaluated these BMS performance of the groups (**Figures 24B-E**) and found that the NaChBac-GFP group was the only group with a significantly higher BMS score compared to Control-GFP (**Figure 24C**). Therefore, we hereon focus on the NaChBac-GFP and Control-GFP, compared to the group having received no treatment (Non-Transplanted) groups only.

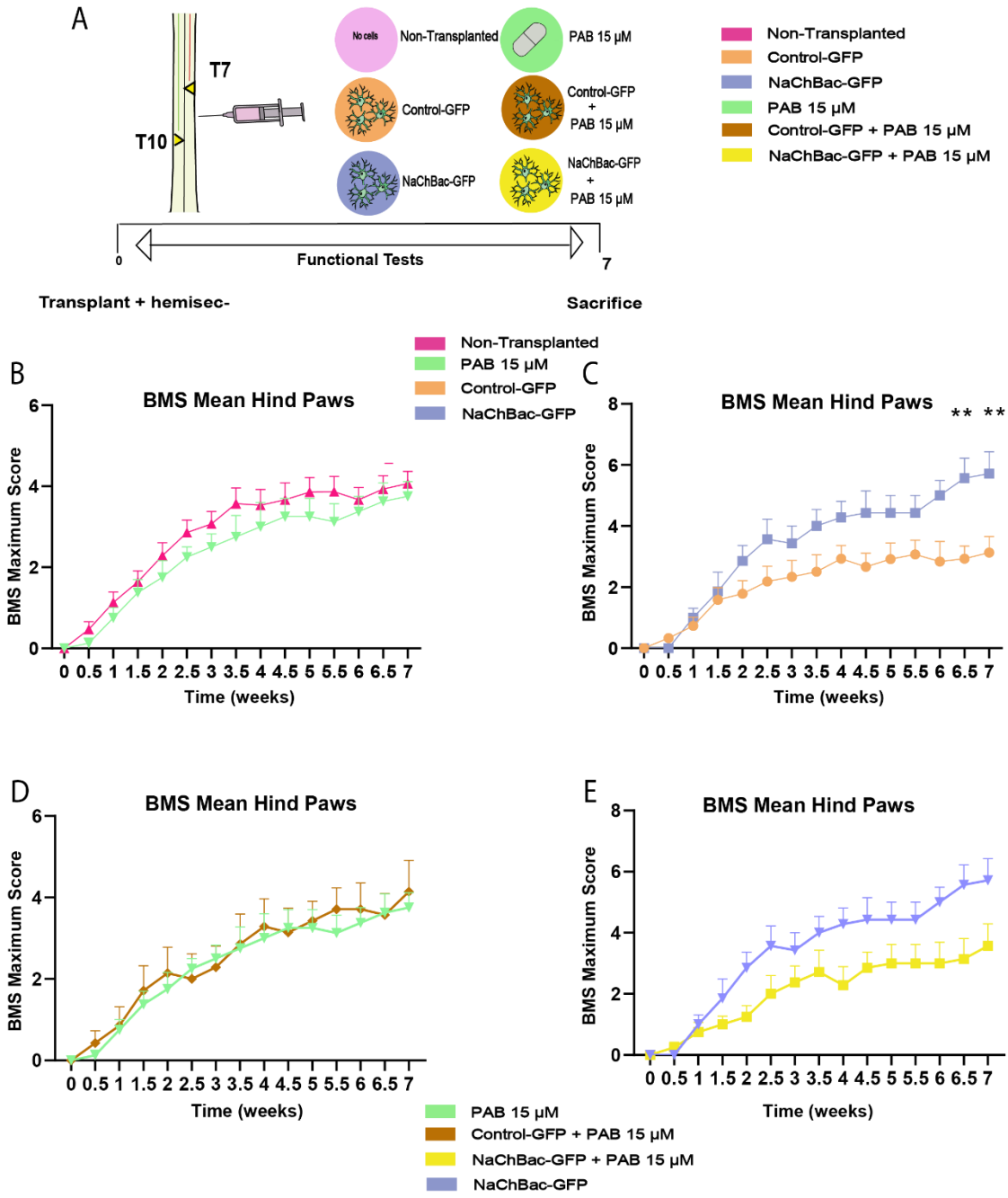

Figure 24: Functional recovery evaluation of combinatory therapy. A) Timeline representing the groups and experiment layout for transplant and injury. **B)** BMS score of Non-Transplanted group and PAB 15 15 µM group. **C)** BMS score of Control-GFP group and NaChBac-GFP groups. Two-way ANOVA followed by Tukey´s test, **p=0.0042, **p=0.0049. D) BMS score of PAB 15 µM group and Control-GFP + PAB 15 µM group. **E)** BMS score of NaChBac-GFP group and NaChBac-GFP + PAB 15 µM group. N=6-8; Data presented as mean ± SEM.

3.2.2 Transplanted NaChBac-expressing DRG transplants improve locomotor function after complete SCI in a double-staggered hemisection SCI mouse model

We next asked whether transplantation of NaChBac-expressing dissociated DRGs could improve connectivity, CST preservation and functional outcome in a clinically relevant, severe,

chronic SCI model. To this end, we performed two lateral thoracic hemisections (right, T7 and left, T10; experimental scheme shown in **Figure 25A**), ensuring the ablation of all descending pathways after the T10 lateral hemisection [300]. This approach allows the evaluation of the pro-regenerative capacity of grafts of DRGs expressing NaChBac-GFP (NaChBac-GFP) when transplanted between hemisections compared to dissociated DRGs expressing Control-GFP (Control-GFP) and non-transplanted animals (Non-Transplanted). We traced the CST one week before injury and transplantation in all animals by injecting AAV-Syn-GFP in the right hemisphere and AAV-Syn-RFP in the left hemisphere of the motor cortex [237] (**Figure 25A**). Functional evaluation using open-field locomotor assessment using the Basso Mouse Scale (BMS) score [239] of all three treatment groups (Non-Transplanted, Control-GFP and NaChBac-GFP DRG transplants) revealed a steady and maintained improvement in the locomotor function of NaChBac-GFP DRG transplanted mice, with significant improvements compared to the Control-GFP DRG transplanted ($p=0.002$) and Non-Transplanted ($p=0.026$) mice after the seventh-week post-injury and transplantation (**Figure 25B**).

We also performed a horizontal ladder beam test to evaluate the locomotion of each hind limb separately [240]. We did not observe any significant differences in the percentage of correct paw placement in the left hind limb (at the T10 hemisection) between the treatment groups (**Figure 25C,** left), nor in the percentage of animals reaching each score point **(Figure 25C,** right). However, we did observe a significant increase in the percentage of correct paw placement in the right hind limb (at the T7 hemisection) in NaChBac-GFP transplanted mice compared to Control-GFP mice (**Figure 25D**, left), and in the percentage of mice reaching a score of 3 in the NaChBac-GFP DRG transplanted group when compared to both control groups (**Figure 25D**, right). When analyzing the percentage of correct paw placement for the mean of both hind limbs (**Figure 25F,** left) rather a significant increase in the percentage of animals reaching score point 3 in NaChBac-GFP mice compared to Control-GFP mice (**Figure 25E,** right). Score 3 of the ladder beam corresponds to toe step and reveals whether mice can support weight and exhibit improved coordination [240]. Finally, although, DRG neuron excitability has been related to nociception, the Von Frey filament test of allodynia revealed that transplantation does not induce significant differences in the response evoking force (g) six weeks after injury and transplantation (**Figure 25F**).

Overall, mice receiving NaChBac-GFP transplant exhibit improved locomotor function without altering nociception compared to animals that received Control-GFP transplant and non-transplanted.

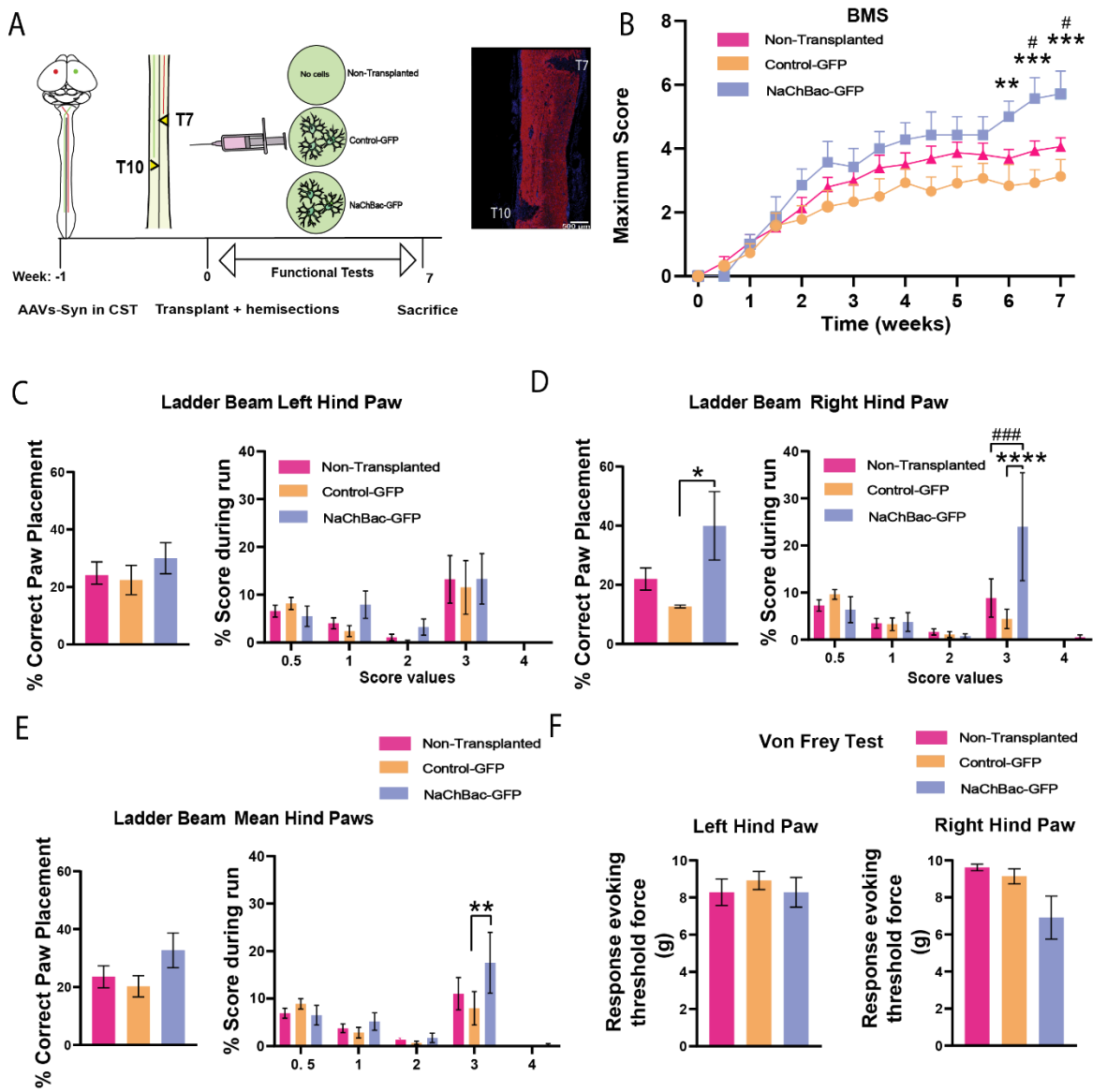

Figure 25: Evaluation of functional recovery in SCI model mice after transplantation of NaChBac-expressing DRG neurons. A) Schematic description of the in vivo experimental timeline: Mice were traced with AAV-SynGFP or RFP, followed by a double lateral hemisection at T7 and T10 and immediately transplanted with NaChBac-GFP transplant, Control-GFP transplant or equivalent media (Non-Transplanted). Tests for functional evaluation were done till sacrifice point (Week 7). **B)** BMS graph depicting scores throughout the experimental timeframe in all treatment groups. Two-way ANOVA followed by Tukey's post hoc test, n= 7-15. Week 6: **Control-GFP vs. NaChBac-GFP p=0.004 Week 6.5: ***Control-GFP vs. NaChBac-GFP, p=0.0002 and $^{\#}$Non-Transplanted vs., NaChBac, p=0.031; Week 7: ***Control-GFP vs. NaChBac-GFP, p=0.002 and $^{\#}$Non-Transplanted vs. NaChBac-GFP, p=0.030. **C)** Graphs depicting the percentage of correct left hind paw placement of animals from all treatment groups in the ladder beam test one day before sacrifice (day 55) (left) and the percentage of animals from

each treatment group receiving the scores for the ladder beam test (right). **D)** Graphs depicting the percentage of correct right hind paw placement of animals from all treatment groups in the ladder beam test one day before sacrifice (day 55) (left) and the percentage of animals from each treatment group receiving the scores for the ladder beam test (right). Left, One-way ANOVA followed by Tukey's post hoc test; *p=0.02. Right, Two-way ANOVA followed by Tukey's post hoc test; $^{\#\#\#}$Non-Transplanted vs. NaChBac-GFP, p= 0.0002; ****Control-GFP vs. NaChBac-GFP, p<0.0001. **E)** Graphs depicting the percentage of correct placement of both hind paws of animals from all treatment groups in the ladder beam test one day before sacrifice (left) and the percentage of animals from each treatment group receiving the scores for the ladder beam test (right). Two-way ANOVA Tukey's post hoc test, **p=0.0095. **F)** Graphs depicting response evoking threshold force (g) at which animals retracted their paws of animals from all treatment groups. One-way ANOVA followed by Tukey´s post hoc test. Data presented as mean ± SEM.

3.2.3 Transplanted NaChBac-expressing dissociated DRGs enhance neuronal fiber preservation rostral to the injury site without long-term CST or serotonergic tract preservation

To identify the mechanisms behind the functional improvement described in NaChBac-GFP transplanted mice we performed histological analysis of the spinal cord seven weeks after injury and treatment. We first evaluated the injured area (negative for GFAP staining) as previously described [299], including the T7 and T10 dual and opposite hemisections (**Figure 26A**). We did not find significant differences in the total injury area between treatment groups, ensuring the homogeneity of the lesion procedure (**Figure 26B**).

Increased sprouting from descending tracts may improve relay circuit activity by innervating propriospinal interneurons in double-staggered hemisection models [90, 236]. Therefore, we asked whether NaChBac-GFP transplant could increase the CST preservation or regeneration between hemisections at the injury site or sprouting rostral to the injury. Mice from all groups displayed complete degeneration of the descending CST labelled with AAV-hSyn-GFP (white arrow), with no GFP expression immediately after the first hemisection at T7 (**Figure 26D**).

Since CST sprouting rostral to the injury relates to improved locomotor function [301, 302], we then studied the CST sprouting area (area of collaterals originating from the CST) immediately rostral to the first hemisection (spinal segments T2 to T7) (**Figure 26C, E**). Similar to previous CST sprouting analysis performed two weeks after simple spinal cord hemisection (**Figure 21C, D**), we did not find differences in the sprouting area of CST axons (**Figure 26C, E**).

The serotonergic (5-HT) descending tracts from the raphe nuclei can contribute to and improve voluntary motor activity after SCI [175, 303]. Therefore, we studied the preservation of 5-HT-positive fibers between hemisections (**Figure 26F**, left, white dotted lines indicate the area taken as rostral and injury) in the three experimental groups. However, we did not observe any significant differences in the density of 5-HT fibers, measured as 5-HT-positive area over total area, between groups (**Figure 26F and G**).

We then explored myelin preservation along the injured area by myelin binding protein (MBP) immunostaining and we found an enhanced myelinated area in NaChBac mice compared to control mice (**Figure 26H**). Accordingly, we found better preservation of neuronal fibers in the spinal cord, detected using β-III tubulin staining, rostral to the injury (**Figure 26I-J**).

Collectively, we find that NaChBac-GFP transplant improves the myelin preservation as well as preservation of other neuronal tracts rostral to the injury but did not observe changes in the preservation or the sprouting of the CST in the chronic, severe stage of SCI, and in the preservation of 5-HT fibers within the injury amongst the groups.

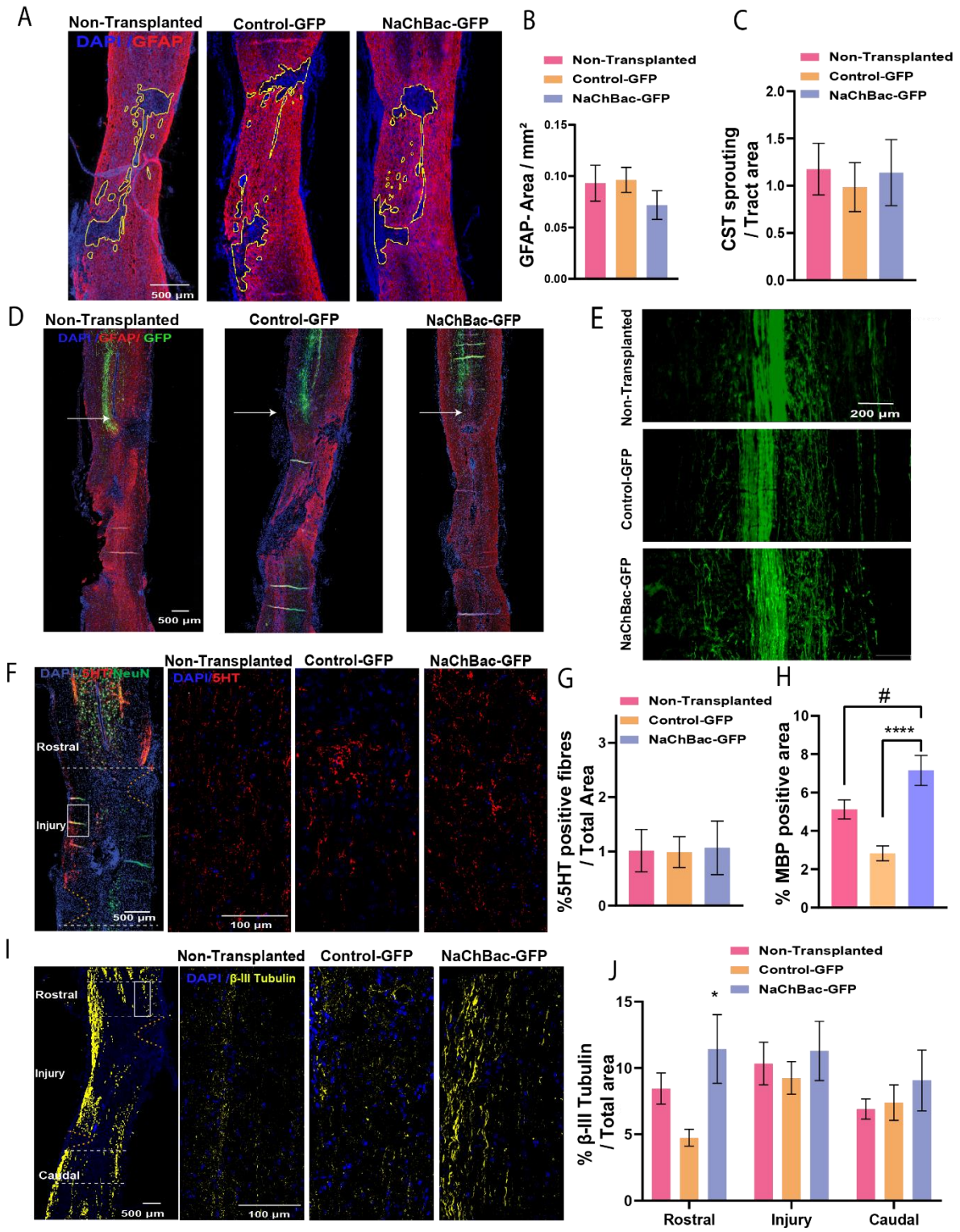

Figure 26: Histological evaluation of the injured area and neuronal fiber preservation in SCI model mice after transplantation of NaChBac-expressing DRGs. A) Representative images of horizontal spinal cord sections for GFAP staining (red) and GFAP-negative injured areas identification (delimited in yellow) in all treatment groups. GFAP = Red; DAPI = blue. Scale bar = 500 µm. **B)** Quantitation of the GFAP-negative injured area normalized to the total area from **A**. One-way ANOVA followed Tukey's post hoc test. **C)** Quantification of CST sprouting normalized to tract area by GFP detection from **E**. One-way ANOVA followed Tukey's post hoc test. **D)** Representative images of GFP (traced CST) rostral to the injury in all treatment groups.

White arrows indicate complete degeneration of traced CST. GFP = green. Scale bar = 500 µm. **E)** Representative images of the CST (center, parallel bundles) and sprouting (collaterals) in all treatment groups. Green = GFP. **F)** Representative images of preserved 5-HT (red) fibers within the SCI in all treatment groups. DAPI = blue; NeuN = green. Scale bars = 500, 100 µm. **G)** Quantification of 5-HT preservation (serotonergic) fibers in the lesion site from **F**. One-way ANOVA followed Tukey's post hoc test. **H)** Graphical representation of MBP staining preservation along the injury, One-way ANOVA followed Tukey's post hoc test, $^{\#}p=0.01$, $^{****}p<0.0002$. **I)** Representative images of β-III-tubulin-positive (yellow) preserved fibers rostral to the injury in all treatment groups. β-III-tubulin = yellow; DAPI = blue. Scale bars = 500, 100 µm. **J**) Graphical representation of preserved β-III-tubulin-positive fibers (yellow) rostral to, within the injury site, and caudal to the injury site from **I**. One-way ANOVA followed Tukey's post hoc test, $^{*}p=0.03$. Unless specified, n= 4-7. Data presented as mean ± SEM.

3.2.4 NaChBac-expressing DRG transplant fails to protect endogenous neurons but increases VGLUT1 excitatory input within relay zone and immediately caudal to the injury

Since improved locomotor function can be a consequence of improved endogenous neuronal survival, we first analysed the effect of DRG transplants on the neuroprotection of host neurons following SCI. No significant differences in endogenous neuronal survival rates between the experimental groups were found when quantified at the rostral, caudal or injured site (as measured by NeuN quantification; **Figure 27A,** representation of zones for NeuN analysis **B,** quantification of NeuN), suggesting that Control-GFP or NaChBac-GFP DRG transplants failed to reduce the neuronal death after SCI.

Since NaChBac-GFP expressing dissociated DRGs displayed increased activity, we wondered whether the transplant was able to modulate activity within the spinal cord, specifically, in the relay zone between hemisections after SCI. Therefore, we began studying the excitatory profile of endogenous neurons within the two hemisections and caudal to the injury by quantifying the number of excitatory vesicular glutamate transporter 1 (VGLUT1). VGLUT1 is a marker of pre-synaptic contacts from the CST and primary afferent fibers [9]. Since our model lacks supraspinal input after the second hemisection, we consider VGLUT1 expression caudal to the injury as almost exclusive to primary afferent fibers. First, we analysed VGLUT1 within the injury site and immediately caudal to the injury site. We found a significant increase in the number of VGLUT1 contacts both within the injury and caudal to the injury in NaChBac-GFP animals compared to both other groups (**Figure 27C**, representative images; **D**, quantification of VGLUT1 contacts per neuron). However, when we analysed VGLUT1 in the

lumbar region (also the central pattern generator), we found no changes in VGLUT1 expression among the groups (**Figure 27E,** quantification of VGLUT1 positive area in layers I-X of the spinal cord**; F,** representative images). Since the VGLUT1 increase caudal to the injury can be considered almost exclusive to afferent fibers, we can say that NaChBac-GFP increases the excitatory input of afferent fibers after the injury but is not maintained in the lumbar zones.

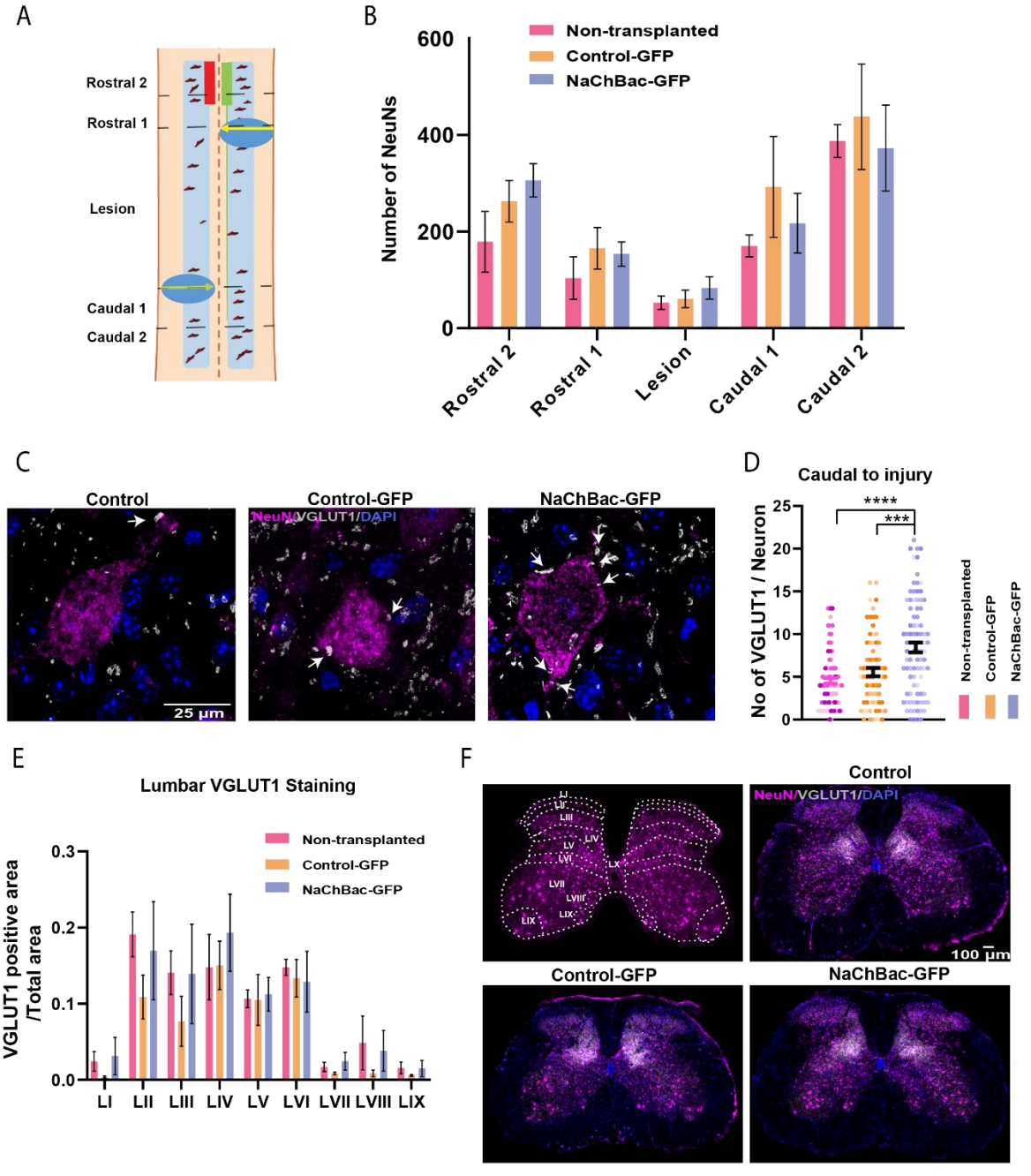

Figure 27: Preservation of endogenous neurons and excitatory VGLUT1 input within and caudal to the injury. A) Schematic representation of the division of the spinal cord to quantify NeuN. **B)** Graph showing quantified NeuN in every zone of the spinal cord. N=4-6, Two-way ANOVA followed by Tukey´s post hoc test. **C)** Images illustrating NeuN (magenta) in the Caudal 1 and 2 areas and VGLUT1 (gray) contacting neurons. Arrows depict VGLUT1 in contact with

neurons. DAPI = blue; Scale bar = 25 µm. **D)** Quantification of VGLUT1 contacts per neuron in Non-Transplanted, Control-GFP, and NaChBac-GFP mice. One-way ANOVA, Tukey´s post-test. **** Non-Transplanted vs. NaChBac-GFP, p=0.0002; ***Control-GFP vs. NaChBac-GFP, p<0.0001. **E)** VGLUT1-positive area relative to total area quantified in the lumbar region of the spinal cord (L1-L6) across nine layers. **F)** Images showing the identified layers of VGLUT1 staining in the lumbar spinal cord; NeuN (magenta), VGLUT1 (gray), DAPI (blue). Scale bar = 100 µm. Data presented as mean ± SEM.

3.2.5 NaChBac-expressing DRG transplant increases the excitatory profile of host neurons within the relay zone and immediately caudal to the injury

Finally, given our previous results with VGLUT1, we further studied whether the reported improved locomotor function in NaChBac-GFP transplanted mice was associated with changes in the synaptic inputs of host neurons and their activity at and below the injured segments.

We explored whether the transplantation of NaChBac-GFP expressing dissociated DRGs could influence neuronal activity within the relay zone between hemisections after SCI. We studied the excitatory and inhibitory profile of endogenous neurons within the two hemisections and caudal to the injury by quantifying the number of excitatory vesicular glutamate transporter 2 (VGLUT2) and inhibitory vesicular GABA transmitter (VGAT) positive contacts, respectively in each neuron. VGLUT2 is a pre-synaptic marker in supraspinal (other than CST) and propriospinal contacts [304]. VGAT functions as a transporter for the primary inhibitory neurotransmitter GABA [305]. Since the double staggered hemisection model disrupts all supraspinal input after the second hemisection, we considered VGLUT2 expression as exclusive to propriospinal neurons [306].

At the injury site, we also uncovered a strong increase in the number of VGLUT2 contacts (**Figure 28A**) per neuron at the SCI in NaChBac expressing DRG transplanted mice compared to control groups (**Figure 28B**). However, no significant change in the number of VGAT contacts (**Figure 28C**) per neuron were detected between the treatment groups (**Figure 28D**). This result indicates that NaChBac-expressing DRG transplant could either induce synaptic contacts between supraspinal (other than CST) with propriospinal neurons, propriospinal with propriospinal neuron or both.

Caudal to the injury, we also observed increased VGLUT2 contacts per neuron in the NaChBac-expressing DRG-transplanted group compared to control groups (**Figure 28E**, **F**). Strikingly, our analysis of VGAT signal immediately caudal to the injury revealed an almost opposite

expression profile to VGLUT2; showing a significant decrease in the number of VGAT contacts per neuron in the NaChBac-expressing DRG-transplanted group compared to control (**Figure 28G, H**).

We also measured the VGLUT1/2 signal further caudal to the injury within the lumbar segments of the spinal cord. Given the specific distribution of VGLUT2 across the laminae [9], we studied the VGLUT2-positive area in cross sections at the lumbar enlargement (L1-L23 segments) differentiating between different spinal cord laminae I-IX, as represented in **Figure 28I** (upper left) but we did not detect differences between treatment groups (**Figure 28J**).

In summary, our findings suggest an altered excitation/inhibition balance biased towards excitation both within the injury relay zone and the immediately caudal-to-injury region in the NaChBac-expressing DRG-transplanted mice. Together with the increased neuronal fiber preservation, we propose that the transplant of NaChBac-expressing DRG neurons stimulates a relay circuit activity, causing a reorganization in the host excitatory/inhibitory input ratio, which is maintained immediately caudal to the injury and contributes to an improvement in the locomotor function after complete SCI.

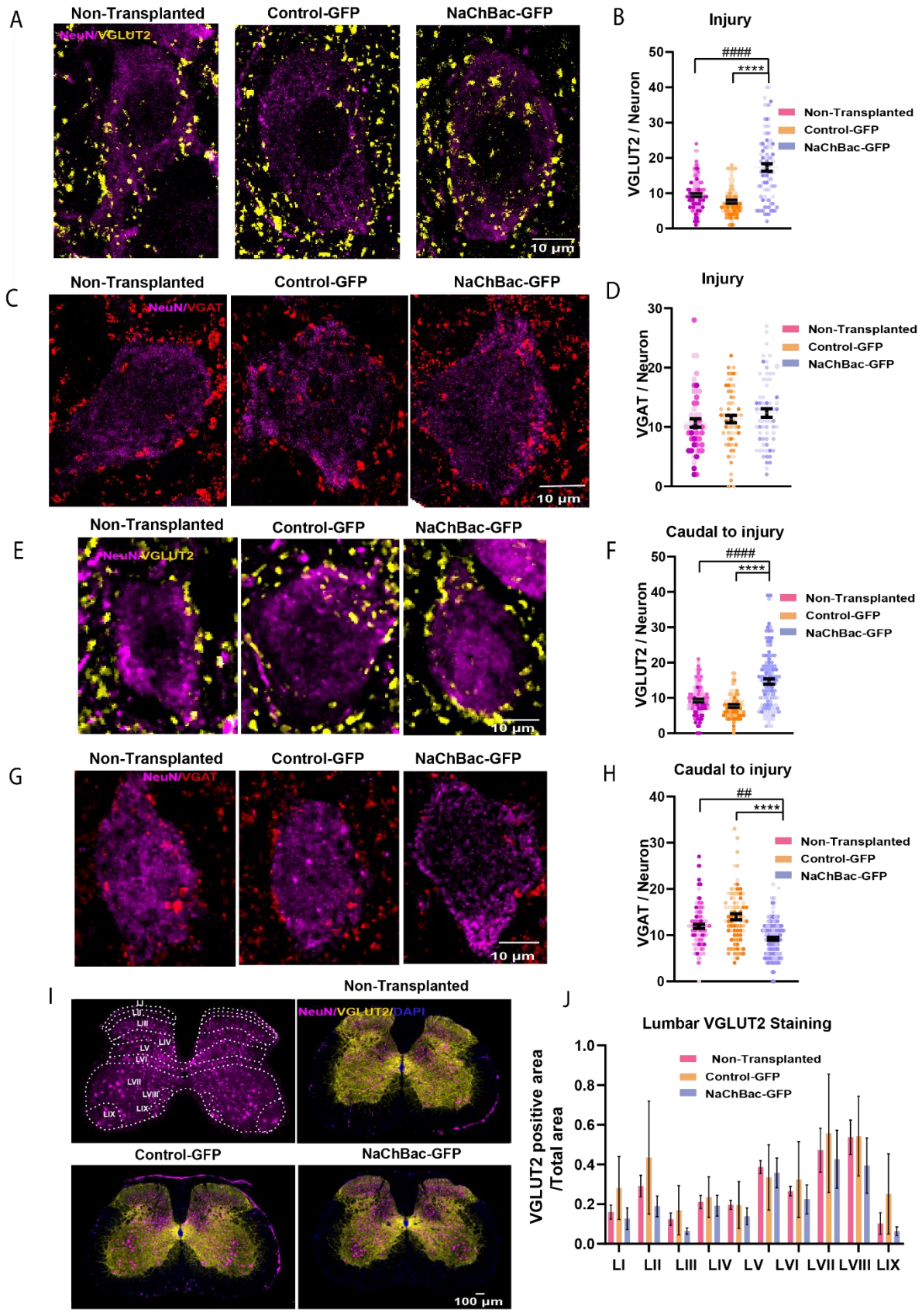

Figure 28: Excitatory and inhibitory synaptic terminals within injury and immediately caudal to injury in SCI model mice after transplantation of NaChBac-expressing DRG neurons. A) Representative images illustrating NeuN (magenta) and VGLUT2 (yellow) contact sites with neurons within the injury site in all treatment groups. Scale bar = 10 µm. **B)** Quantification of

VGLUT2 contacts per neuron, from **A**. One-way ANOVA, Kruskal-Wallis' test. $^{++}$ Non-Transplanted vs. Control-GFP, p=0.004; $^{####}$ Non-Transplanted vs. NaChBac-GFP, p<0.0001; ***Control-GFP vs. NaChBac-GFP, p<0.0001. **C)** Representative images illustrating NeuN (magenta) and VGAT (red) contact sites with neurons within the injury in all treatment groups. Scale bar = 10 µm. **D)** Quantification of VGAT contacts per neuron, from **C**. One-way ANOVA, Kruskal-Wallis' test. **E**) Representative images illustrating NeuN (magenta) and the VGLUT2 (yellow) contacts with neurons immediately caudal to the SCI in all treatment groups. **F)** Quantification of VGLUT2 contacts per neuron immediately caudal to injury, from **E**. One-way ANOVA, Kruskal-Wallis' test. $^{####}$ Non-Transplanted vs. NaChBac-GFP, p<0.0001; ***Control-GFP vs. NaChBac-GFP, p<0.0001. **G)** Representative images illustrating NeuN (magenta) and the VGAT (red) contacts with neurons immediately caudal to the SCI in all treatment groups. **H)** Quantification of VGAT contacts per neuron, from **G**. One-way ANOVA, Kruskal-Wallis' test. $^{##}$ Non-Transplanted vs. NaChBac-GFP, p=0.0038; ***Control-GFP vs. NaChBac-GFP, p<0.0001. Arrows depict examples of VGAT and VGLUT2 contacts with neurons in **A**, **C**, **E**, and **G**. Each dot represents an individual neuron in **B**, **D**, **F**, and **H**. Unless specified otherwise, n=4. **I**) Representative images showing the identified layers of VGLUT2 staining in the lumbar spinal cord in all treatment groups; NeuN = magenta, VGLUT2 = yellow, and DAPI = blue. Scale bar = 100 µm. **J)** VGLUT2-positive area relative to total area quantified in the lumbar region of the spinal cord (L1-L6) across nine layers, from **I** (n=4). Two-way ANOVA followed by Tukey's post hoc test. Data presented as mean ± SEM.

Discussion

Given the multifaceted and multifactorial nature of spinal cord injuries, there is a general consensus for a combinatorial approach towards a possible therapy for SCI [307]. Previous work has shown the synergistic effect of combining a hydrogel with sustained NT-3 release with the peripheral conditioning injury as seen by the increased sprouting of sensory axons across the injury in mice [93]. Researchers from the Tuszynski laboratory showed increased axonal growth and functional recovery in monkey when human induced pluripotent stem cells were grafted along with a cocktail of growth factors such as BDNF, GNDF among others and fibrin to provide a matrix for the transplanted graft [165, 166]. A co-transplant of Schwann cells and NSCs expressing NT-3 significantly increased cortex motor and somatosensory evoked potentials [308]. Similarly, microtubule stabilizing drug Epothilone B failed to improve locomotion but animals received a combinatory therapy of Epothilone B administration and rehabilitation showed significant locomotor recovery [120]. Therefore, we set an initial hypothesis of a triple combinatory treatment involving a cytoskeleton modulating drugs to improve the axonal length of both transplanted cells and local neurons along with a DRG transplant, expressing a sodium channel, NaChBac to improve connectivity and transplant survival.

In Chapter 1, we describe our results when we hypothesized that a combination of cytoskeleton drugs which act upon different components of the growth cone, Epothilone B which acts on microtubules and Blebbistatin, which acts downstream of the RhoA/ROCK pathway, specifically it a NMMII inhibitor should have a synergistic effect and improve axonal length significantly. Additionally, Epothilone B has shown to increase functional recovery in rats after SCI [119, 120], whereas knocking out of NMMII has shown to increase axonal regeneration after optic nerve crush in retinal ganglion cells [251]. However, when plated over non-permissive substrate such as CSPGs to simulate an injury environment, we observed that Blebbistatin alone significantly increased axonal length of DRG neurons, but the combination of Blebbistatin and Epothilone B reverted this effect to significantly shorter axonal lengths. When we studied the growth cone structure of these groups, we found that the growth cone area of DRG neurons plated on non-permissive substrate increased the growth cone area which was reverted by Blebbistatin treatment, but the combination of Epothilone B and Blebbistatin reversed this effect again, increasing the growth cone area. These results are

reminiscent of the “splayed” morphology found in DRG growth cones in the presence of aggrecans, which was reverted by reorganization in actin structure and de-bundling of microtubules by Blebbistatin, effectively overcoming the aggregan “splayed” morphology [117]. Indeed, we find that CSPGs bring about this “splayed” morphology, which is reverted to a functional state by dual action of actin reorganization and consequent microtubule de-bundling by Blebbistatin. However, the combination with Epothilone B possibly inhibits the de-bundling of the microtubules, nullifying the positive effect of Blebbistatin alone.

Therefore, we decided to use Blebbistatin alone for the combination along with the DRG transplant for further *in vivo* study **(Objective 1 (1.1))**.

Additionally in **Chapter 1, Objective (1.2)**; we characterize *in vitro* the expression of NaChBac in dissociated DRGs and N2A cell line. It is known that NaChBac expression decreases the neuronal activation threshold and produces long depolarization waves in CNS neurons [180, 221-224, 228]. In DRG dissociated neurons, we found that NaChBac expression prompted slow activating and inactivating inward current characteristic of this sodium channel at hyperpolarizing voltages around -50 mV. This long inward current also leads to increases the intracellular Ca^{2+} influx in CNS neurons [224]. In our studies, we find and increase in both intracellular Ca^{2+} influx and intracellular cAMP in dissociated cultures. Ca^{2+} and cAMP intracellular influx influence fundamental physiological processes [265], such as cell survival, differentiation, and the initiation/propagation of nerve impulses [309, 310]. Therefore, NaChBac expression may contribute to accelerated neuron maturation [224], neuronal regeneration via regulated growth cone dynamics [264, 266], or modulated neuronal plasticity [311, 312]. In adult neuronal repair, the conditioning lesion paradigm (a well-studied phenomenon where a previous insult to the peripheral axon of DRG neurons leads to a switch in the regenerative capacity of the central axon) is mediated by the upregulated expression of several regeneration-associated genes, including increased levels of intracellular Ca^{2+} and cAMP within DRG neurons [108, 205, 206, 313]. Since NaChBac expression significantly increased both Ca^{2+} and cAMP in sensory DRG neurons in our model, we hypothesized that NaChBac could induce a pro-regenerative state of the DRG neurons transplanted within the SCI. Finally, we aimed to study the effect of the combination of NaChBac expression and Blebbistatin in **Chapter 1, Objective (1.3).** While NaChBac expression did not alter neurite length when compared to Control-GFP counterpart neither over permissive nor non-

permissive substrates. However, over permissive substrates, Blebbistatin increased neurite length of both Control-GFP + Blebbistatin when compared to Control-GFP alone; as well as NaChBac-GFP + Blebbistatin when compared to NaChBac-GFP alone. Furthermore, no differences between Control-GFP + Blebbistatin and NaChBac-GFP + Blebbistatin were found. This suggests that NaChBac expression does not alter neurite length nor the neurite elongating effect of Blebblebistatin observed in results obtained in **Chapter 1, Objective (1.3).** Similar effects are observed over non-permissive substrate, where NaChBac-GFP + Blebbistatin shows significantly higher neurite length when compared to NaChBac-GFP alone. Nevertheless, we fail to see an effect of Blebbistatin in Control-GFP + Blebbistatin group, which can be due to the variability within the sample as seen by the error bars of this group.

It is also known that NaChBac prompts neuronal survival by increasing neuronal excitability and improving their integration in existing circuits [180, 221, 228]. We evaluated whether NaChBac expression influenced proliferation and apoptosis in neuroblastoma cells and found that NaChBac expression promoted cell survival. Bcl-2 regulates Ca^{2+} homeostasis [314], while Ca^{2+} influx can activate AKT signaling [315], which in turn, also modulate the mTOR complex [316]. We confirmed an increase in pAKT and p-mTOR after NaChBac expression in neuroblastoma cells, suggesting the induction of Ca^{2+}-dependent signaling. The mTOR pathway is induced after PTEN downregulation [317], which is associated with increased CST regeneration and functional recovery after SCI [122, 303]. Indeed, mTOR activation represents a relevant pathway for sensory neuron survival and regeneration after SCI [318]. We thus postulate that AKT/mTOR axis activation by NaChBac expression promotes neuron survival and overcomes inhibitory responses in favor of axonal regeneration after transplantation of NaChBac-GFP dissociated DRGs within the SCI.

In fact, our *in vitro* studies in dissociated DRGs revealed a significant increase in the secretion of various neurotrophic factors. This includes an increase in several important neurotrophic factors including NGF, BDNF and GDNF. This is an important aspect since it demonstrates that NaChBac expression alters signaling and transplanted cells expressing NaChBac can actively promote as well as contribute to the formation of more pro-regenerative environment in the injury. Together, an increase of these factors has been shown to significantly improve synaptic plasticity, neuronal regeneration, and functional recovery [319]. An increase in BDNF has previously shown to increase plasticity of the corticospinal tract as well as improve neuronal

survival [320]. NGF has long been known to exert neuroprotective effects. When overexpressed in neural stem cells for transplantation, they could modulate the injury environment and promoting increased functional recovery [321]. It has been studied that VEGF is involved and important for re-vascularization after an injury and promotes improved locomotor function by the prevention of secondary damage after an SCI [322]. Similarly, GDNF improves axonal regeneration, neuronal survival and reduces secondary damage after SCI [323]. On the other hand, IGF-1 exhibited a neuroprotective effect by preventing apoptosis [324] whereas GM-CSF can attenuate glial scar formation [325]. Finally, administration of PDGF-AA can contribute to functional recovery by increasing oligodendrocytes survival thus increasing myelination and motor neuron survival [326].

In *in vivo* models of development and adult neurogenesis, increased endogenous neuronal activity induced by NaChBac-GFP expression improved cell survival during development [180] and integration into adult circuits [228]; however, these studies did not involve a spinal insult. Hence, in **Chapter 2**, we describe the effect of transplanting dissociated DRGs expressing either NaChBac or only GFP in an injury environment as we follow the transplant survival and integration. We found a higher number of NaChBac-expressing cells filling the injured tissue following NaChBac-GFP transplantation compared to Control-GFP transplantation fourteen days after the injury. The DRG neurons transplanted within the injury site survived for at least fourteen days and exhibited long axons, but we did not find any increase in the survival of DRG neurons fourteen days after transplantation. Since NaChBac increased proliferation in N2A cells, and Schwann cells are proliferative in nature, NaChBac-GFP expression could confer increased proliferative nature of glial cells, but not transplanted neurons. This could explain the increase in total number of transplanted cells, but no changes in the number of transplanted neurons only. Interestingly, NaChBac-GFP DRG neurons displayed significantly improved migration rostral to the direction of the injury. Several studies suggest that neuronal activity plays a crucial role in neuron migration during development [327, 328]; therefore, NaChBac-dependent activation could provide additional migratory capacity to neonatal neurons but not glial cells. These enhanced migratory properties could provide additional benefits by maintaining activity near the degenerating CST or other descending tracts rostral to the injury.

Activity-based stimulation can also improve CST remodeling after SCI [293, 294]. Indeed, our findings report promising results, with increased preservation of the injured CST and the formation of a more permissive environment in mice transplanted with NaChBac-expressing DRG neurons. This preservation may occur due to the significant migration of neurons near the CST and a more permissive environment formed by the glial cells transplanted alongside DRG neurons from the dissociated DRG cultures.

Chapter 3 explores the role of transplanted DRGs expressing NaChBac-GFP, GFP alone and with the combinatory treatment with Blebbistatin in a severe, chronic SCI model. However, functional tests revealed that the combinatory treatment with Blebbistatin did not improve locomotor performance, and rather the combination of dissociated DRGs expressing NaChBac showed significant improvement in locomotor assessments. While RhoA/ROCK pathway and its downstream effectors have been studied extensively studied, clinical trials reveal inefficacy as a potential treatment [329]. Recent studies highlighted the importance of RhoA downstream effectors such as NMMII actin arcs which restrict microtubule extension [118]. Later studies have demonstrated the importance of targeting RhoA/ROCK pathway in different cell types. Indeed, this study showed that a knockout model for RhoA does not improve axon extension after SCI, rather inhibits it. This is because RhoA pathway plays an important role in limiting astrogliosis, which increases in a RhoA knockout model, thereby increasing astrocytic reactivity, consequently preventing axonal regeneration. However, selective ablation of RhoA only in neurons led to a significant increase in axonal regeneration after injury, suggesting that the role of RhoA is a dual one [125]. Therefore, we hypothesize a similar effect in the downstream RhoA effector, NMMII and its inhibitor, Blebbistatin. The application of Blebbistatin in our combinatory approach is neither selective nor continuous. Hence, we hypothesize that the immediate effect of Blebbistatin is to increase astrocytic reactivity, preventing other mechanisms of action for improving functional locomotion.

Next, we focus our studies on the groups that showed improved locomotion in a severe, chronic model two months after injury and transplantation.

When transplanted within the injured site, we found that rat neonatal DRGs genetically modified to overexpress NaChBac significantly rescued locomotor function in a severe SCI model. Nevertheless, we did not observe transplanted cells after two months and could not

evaluate potential neuronal or glial survival by NaChBac expression in the long-term scenario. A low number of DRG neurons surviving following xenotransplantation was previously reported by the Silver laboratory, where adult mouse DRG neurons transplanted in adult rats displayed a significant decrease in survival two weeks after transplantation [215, 216]. Transplanted dissociated DRGs promoted early establishment of detour circuits within descending tracts and propriospinal interneurons which relay information as seen with a maintained excitatory input and neuronal activity immediately below the injury.

The double-staggered lateral hemisection injury model offers a robust scenario to study spontaneous recovery since spared axons between the two injured segments can form short detour circuits with propriospinal interneurons that relay information while all descending tracts become severed [90, 236, 300, 330]. We observed a steady and sustained increase in locomotor performance based on the ladder beam assay and BMS scores of mice transplanted with NaChBac-expressing dissociated DRGs up to two months after injury. Although NaChBac-expressing dissociated DRGs enhanced CST sprouting and preservation two weeks after injury, we observed no differences between mice from all treatment groups until two months later. These results indicate that early remodeling with alternative neuronal connections above CST innervation contributed to later functional recovery. As we failed to detect differences between treatment groups upon serotonergic fiber staining, we discarded the raphespinal contribution to functional locomotor recovery. Nevertheless, given the significant increase in the preservation of β-III tubulin fibers rostral to the injury (and a non-significant tendency towards an increase within the injury site; p=0.1), we hypothesized that either the reticulospinal, rubrospinal, and/or vestibulospinal tracts could contribute to the descending input. The improved locomotion observed in mice transplanted with NaChBac-GFP dissociated DRGs could relate to improved neuronal fiber preservation rostral to the injury and increase in VGLUT2 contacts per neuron. We hypothesized that without major descending tracts after SCI, neuronal fibers would form relay connections with propriospinal interneurons.

Increased neuronal activity contributes to neuroplasticity [331], neuronal rewiring [184], and functional recovery after SCI [332]. During development (while circuit arrangements and formation occur), the pruning of connections associates with the loss of neuronal activity [174]. Interestingly, SCI leads to a loss of supraspinal inputs [173] and the remodeling of the neurotransmitter phenotype (switching from excitatory to inhibitory [178]), which is

associated with neuronal inactivation leading to locomotor deficits [176]. However, SCI can induce circuit rearrangements by sprouting and/or forming relay circuits, which can then transmit information below the injury and maintain the neuronal function [90, 114, 175, 295]. Altogether, these findings highlight the importance of maintaining neuronal activity caudal to the injury to support the function caudal to the injury and improve the formation of detour circuits after SCI [333]. Supraspinal neurons that project into the spinal cord (mainly from the reticulospinal, rubrospinal, or vestibulospinal tracts) and propriospinal neurons express VGLUT2 [9, 304]. Since all descending inputs ultimately become interrupted, the double hemisection model enables the formation of relay circuits within the injury site and almost ensures the exclusivity of VGLUT2 expression to propriospinal neurons caudal to the injury and VGLUT1 to primary afferents[306]; in contrast, the inhibitory profile can be studied through VGAT expression [305]. While we demonstrated a lack of alteration to neuron preservation between all treatment groups, the number of VGLUT2 excitatory contacts received by each neuron significantly increased following the transplantation of NaChBac-expressing dissociated DRGs within the relay zone and immediately caudal to the injury compared to both control groups. Additionally, we encountered a similar increase in VGLUT1 excitatory inputs immediately caudal to the injury in mice transplanted with NaChBac-expressing DRG neurons compared to both control groups, which would belong to preserved primary afferents.

Within the relay zone, it remains unclear whether the increase in VGLUT2 contacts derives from an increase in supraspinal input or via an increase in the relay activity of propriospinal neurons. Nevertheless, in case of VGLUT1, since we do not observe preserved CST at this point, we can conclude the contacts either belong to primary afferent or untraced CST. However, our study revealed the maintenance of this increase in VGLUT2 contacts immediately caudal to injury, which is attributed to propriospinal neurons by virtue of this model, and primary afferent fibers in case of VGLUT1.

Notably, we did not observe changes in VGAT expression within the relay zone; instead, we discovered a significant decrease in VGAT expression in mice transplanted with NaChBac-expressing dissociated DRGs neurons immediately caudal to the injury compared to both control groups. These findings suggest that Nachbac-DRG increased the activity in the relay zone thanks to the combination of preserved VGLUT2-positive descending tracts and/or relay

circuit formation with the propriospinal interneurons. Given the maintenance of this profile immediately caudal to the injury, our data suggests a role for short propriospinal neurons in the relay input immediately caudal to the injury. This data suggests that mice transplanted with NaChBac-expressing dissociated DRGs maintain relay activity below the injury, given the decrease in VGAT expression and increase in VGLUT2 expression that could ultimately explain functional improvements.

Severe SCI induces rewiring in denervated spinal cord segments, which can lead to undirected and abnormal plasticity in the lumbar region of the spinal cord [306]. Since we did not observe differences in VGLUT2 staining in the lumbar region between treatment groups, we hypothesized that mice transplanted with NaChBac-expressing DRG neurons only maintain a detour circuit activity immediately caudal to the injury, avoiding denervation of lumbar segments caudal to the injury, thereby preventing undirected plasticity in the lumbar region, and promoting functional recovery.

In conclusion, we describe the effect of transplanting dissociated DRGs with increased intrinsic activity provided by the expression of NaChBac into the SCI. Our findings indicate that NaChBac-expressing dissociated DRGs maintain activity from supraspinal inputs and form detour circuits. Transplantation in a single hemisection model leads to early CST preservation; Transplantation in a double hemisection model has shown a significant preservation of VGLUT2-positive descending inputs, which would be due to an increased relay circuit formation with propriospinal interneurons, maintained immediately below the injury. This study reinforces the importance of maintaining the excitation/inhibition ratio immediately caudal to spinal cord injury, highlighting its role in enhancing the formation of relay circuits and conveys the importance of developing new therapeutical strategies focused on that point.

Conclusions

Chapter 1 :

1. Blebbistatin (at 15 μM concentration) alone increases the total neurite length and percentage of neonatal dorsal root ganglia neurons in culture with neurites, whereas Epothilone B fails to do so.
2. Combination of Blebbistatin and Epothilone (at the tested concentrations) fails to display a synergistic effect on neurite length, instead, reverting the effecting of Blebbistatin.
3. Blebbistatin and Epothilone combined causes growth cones to display "splayed" morphology, explaining the consequent decrease in neurite length of DRG neurons. In contrast, Blebbistatin is able to decrease growth cone area, giving rise to a morphology that is associated with active neurite growth.
4. NaChBac expression leads to an increase in proliferation and pro-survival signalling in Neuro2A cells in culture.
5. The expression of NaChBac in dissociated DRGs leads to the presence of an additional sodium current, which is associated with an overall increase in the intrinsic activity of the DRGs; as seen by a decrease in rheobase or the increase in afterhyperpolarization phase and firing frequency.
6. NaChBac expression does not alter neurite length under permissive and non permissive substrates.
7. NaChBac expression does not significantly modify the effect of Blebbistatin enhancing neurite length although potentiate it.

Chapter 2 :

1. NaChBac expression does not alter transplanted neuronal survival two weeks after injury and transplantation, rather an increase in the overall survival of all transplanted cells, including glia in the spinal cord injury hostile environment.

2. NaChBac expressing DRG neurons migrate further away from the injury site, in a rostral direction.

3. NaChBac expressing DRG transplantation does not alter CST sprouting rostral to the injury, instead, NaChBac expressing DRG transplantation forms a more permissive area for CST preservation.
4. NaChBac expressing DRG transplantation increases the CST preservation caudal to the injury site.

Chapter 3 :

1. Para-blebbistatin local treatment fails to show an effect combined with DRG transplantation on functional locomotion recoveryin a chronic SCI model.
2. NaChBac expressing DRG transplantation shows a significant locomotor recovery when compared to non-modified DRG transplanted and non-transplanted groups.
3. NaChBac expressing DRG transplant does not alter CST sprouting, rostral to the injury, or descending serotonergic fiber preservation in the chronic scenario. However, it does induce preservation of total neuronal fibers rostral to the injury site measured by the beta-III tubulin staining.
4. Transplantation of NaChBac expressing DRGs fails to preserve endogenous neurons.
5. Transplantation of NaChBac expressing DRGs increases the number of excitatory VGLUT1 input within the relay zone and caudal to the injury.
6. Additional excitatory input is due by increased VGLUT2 input within the injury and immediately caudal to the injury, and a decreased inhibitory VGAT input caudal to the injury.
7. Increase in VGLUT2, arising from propriospinal interneurons caudal to the injury, points toward formation of relay connections within the injury site which are maintained immediately caudal to the injury.
8. Coupled with a decrease in VGAT caudal to the injury, there is a maintenance of excitation/inhibition ratio caudal to the injury.
9. In the lumbar segments of the spinal cord, VGLUT1 and VGLUT2 expression is unchanged amongst groups, suggesting the maintenance of activity by short propriospinal interneurons.

Future prospectives

Spinal cord injury research is a complex yet dynamic field which has seen great advance in recent years. Over the last years, the importance of maintaining activity after the injury has been emphasized, especially with increasingly successful studies in human patients by neuromodulation using electric stimulation [198, 332]. Unfortunately, while these studies are extremely exciting and promising, spinal cord injury is still far from cured or restoring complete voluntary locomotor function. Additionally, given the nature of these treatments, patients must undergo complex surgeries that must be performed by skilled neurosurgeons to include foreign devices. Therefore, the race to find possible biological interventions in an attempt to maintain and regain natural functions, especially by cell replacement is still on. On that note, our study highlights the importance of maintaining activity immediately below the injury in order to improve locomotor function by promoting the formation of relay circuits which are active beneath the injury; achieved by the transplantation of dissociated DRGs with increased intrinsic activity. Cell therapy is currently a viable option for the near future as a therapeutic target for SCI. Additionally, use of iPSCs to reprogram desired cell types from the patient is an added advantage. Therefore, the possibility of transplanting neurons from cells obtained from the patient itself could prove an interesting therapeutic approach in the near future. Alternatively, since we also highlight the maintenance of activity and role of propriospinal interneurons in the formation of relay circuits, our work also paves the way for researching the direct stimulation or maintenance of activity endogenous host neurons which are capable relaying information beneath the injury to maintain activity in the spinal cord. Overall, this study provides insight into the complex mechanisms that lie behind a significant locomotor function, while focusing on maintaining activity by direct transplantation of neurons and increasing their intrinsic activity.

Funding

This research was funded by FEDER/Ministerio de Ciencia e Innovación – Agencia Estatal de Investigación PID2021-1243590B-I100 and RISEUP EU grant (Ref. 964562) from FetOpen H2020 program. Part of the equipment employed in this work was funded by Generalitat Valenciana and cofinanced with ERDF funds (OP ERDF of Comunitat Valenciana 2014–2020) and the UE; Fondo Europeo de Desarrollo Regional (FEDER) incluido en el Programa Operativo

FEDER de la Comunidad Valenciana 2014-2020 and the Grisolia program from the GVA supporting Sonia Hingorani Jai Prakash performing her doctoral thesis.

References

1. Jordan, L.M., et al., *Descending command systems for the initiation of locomotion in mammals.* Brain Res Rev, 2008. **57**(1): p. 183-91.
2. Levine, A.J., et al., *Identification of a cellular node for motor control pathways.* Nat Neurosci, 2014. **17**(4): p. 586-93.
3. McCrea, D.A., *Neuronal basis of afferent-evoked enhancement of locomotor activity.* Ann N Y Acad Sci, 1998. **860**: p. 216-25.
4. Cho, T.A., *Spinal cord functional anatomy.* Continuum (Minneap Minn), 2015. **21**(1 Spinal Cord Disorders): p. 13-35.
5. Sengul, G., et al., *Atlas of the spinal cord: Mouse, rat, rhesus, marmoset and human*. 2013, Elsevier Academic Press.
6. Harrow-Mortelliti, M., V. Reddy, and G. Jimsheleishvili, *Physiology, Spinal Cord*, in *StatPearls*. 2023, StatPearls Publishing LLC.: Treasure Island (FL).
7. Ganapathy, M.K., V. Reddy, and P. Tadi, *Neuroanatomy, Spinal Cord Morphology*, in *StatPearls*. 2023, StatPearls Publishing LLC.: Treasure Island (FL).
8. Rexed, B., *A cytoarchitectonic atlas of the spinal cord in the cat.* J Comp Neurol, 1954. **100**(2): p. 297-379.
9. Alvarez, F.J., et al., *Vesicular glutamate transporters in the spinal cord, with special reference to sensory primary afferent synapses.* J Comp Neurol, 2004. **472**(3): p. 257-80.
10. Harrison, M., et al., *Vertebral landmarks for the identification of spinal cord segments in the mouse.* Neuroimage, 2013. **68**: p. 22-9.
11. Saliani, A., et al., *Axon and Myelin Morphology in Animal and Human Spinal Cord.* Front Neuroanat, 2017. **11**: p. 129.
12. Wang, L.H., W.Q. Ding, and Y.G. Sun, *Spinal ascending pathways for somatosensory information processing.* Trends Neurosci, 2022. **45**(8): p. 594-607.
13. Armand, J., *The origin, course and terminations of corticospinal fibers in various mammals.* Prog Brain Res, 1982. **57**: p. 329-60.
14. Kuypers, H., *Anatomy of the Descending Pathways*. 2011.
15. Nathan, P.W., M.C. Smith, and P. Deacon, *The corticospinal tracts in man. Course and location of fibres at different segmental levels.* Brain, 1990. **113 (Pt 2)**: p. 303-24.
16. Uematsu, J., et al., *Development of corticospinal tract fibers and their plasticity I: quantitative analysis of the developing corticospinal tract in mice.* Brain Dev, 1996. **18**(1): p. 29-34.
17. Buys, E.J., et al., *Selective facilitation of different hand muscles by single corticospinal neurones in the conscious monkey.* J Physiol, 1986. **381**: p. 529-49.
18. Porter, R. and R.N. Lemon. *Corticospinal Function and Voluntary Movement*. 1993.
19. Evarts, E.V. and J. Tanji, *Reflex and intended responses in motor cortex pyramidal tract neurons of monkey.* J Neurophysiol, 1976. **39**(5): p. 1069-80.
20. Maier, M.A., et al., *Does a C3-C4 propriospinal system transmit corticospinal excitation in the primate? An investigation in the macaque monkey.* J Physiol, 1998. **511 (Pt 1)**(Pt 1): p. 191-212.

21. Bacon, S.J. and A.D. Smith, *A monosynaptic pathway from an identified vasomotor centre in the medial prefrontal cortex to an autonomic area in the thoracic spinal cord.* Neuroscience, 1993. **54**(3): p. 719-28.

22. Murray, H.M. and M.E. Gurule, *Origin of the rubrospinal tract of the rat.* Neurosci Lett, 1979. **14**(1): p. 19-23.

23. ten Donkelaar, H.J., *Evolution of the red nucleus and rubrospinal tract.* Behav Brain Res, 1988. **28**(1-2): p. 9-20.

24. Whishaw, I.Q., B. Gorny, and J. Sarna, *Paw and limb use in skilled and spontaneous reaching after pyramidal tract, red nucleus and combined lesions in the rat: behavioral and anatomical dissociations.* Behav Brain Res, 1998. **93**(1-2): p. 167-83.

25. Brown, L.T., *Rubrospinal projections in the rat.* J Comp Neurol, 1974. **154**(2): p. 169-87.

26. Bican, O., A. Minagar, and A.A. Pruitt, *The spinal cord: a review of functional neuroanatomy.* Neurol Clin, 2013. **31**(1): p. 1-18.

27. McCurdy, M.L., et al., *Selective projections from the cat red nucleus to digit motor neurons.* J Comp Neurol, 1987. **265**(3): p. 367-79.

28. Kuchler, M., et al., *Red nucleus projections to distinct motor neuron pools in the rat spinal cord.* J Comp Neurol, 2002. **448**(4): p. 349-59.

29. Sakai, S.T., A.G. Davidson, and J.A. Buford, *Reticulospinal neurons in the pontomedullary reticular formation of the monkey (Macaca fascicularis).* Neuroscience, 2009. **163**(4): p. 1158-70.

30. Zaaimi, B., L.R. Dean, and S.N. Baker, *Different contributions of primary motor cortex, reticular formation, and spinal cord to fractionated muscle activation.* J Neurophysiol, 2018. **119**(1): p. 235-250.

31. Peterson, B.W., et al., *Patterns of projection and braching of reticulospinal neurons.* Exp Brain Res, 1975. **23**(4): p. 333-51.

32. Drew, T., S. Prentice, and B. Schepens, *Cortical and brainstem control of locomotion.* Prog Brain Res, 2004. **143**: p. 251-61.

33. Lawrence, D.G. and H.G. Kuypers, *The functional organization of the motor system in the monkey. II. The effects of lesions of the descending brain-stem pathways.* Brain, 1968. **91**(1): p. 15-36.

34. Prentice, S.D. and T. Drew, *Contributions of the reticulospinal system to the postural adjustments occurring during voluntary gait modifications.* J Neurophysiol, 2001. **85**(2): p. 679-98.

35. Carpenter, M.B., *The Vestibular Nuclei and Their Connections, Anatomy and Functional Correlations.* Archives of Neurology, 1963. **8**(3): p. 345-346.

36. Kneisley, L.W., M.P. Biber, and J.H. LaVail, *A study of the origin of brain stem projections to monkey spinal cord using the retrograde transport method.* Exp Neurol, 1978. **60**(1): p. 116-39.

37. Nathan, P.W., M. Smith, and P. Deacon, *Vestibulospinal, reticulospinal and descending propriospinal nerve fibres in man.* Brain, 1996. **119 (Pt 6)**: p. 1809-33.

38. Wilson, V.J., R.M. Wylie, and L.A. Marco, *Projection to the spinal cord from the medial and descending vestibular nuclei of the cat.* Nature, 1967. **215**(5099): p. 429-30.

39. Boyle, R., *Morphology of lumbar-projecting lateral vestibulospinal neurons in the brainstem and cervical spinal cord in the squirrel monkey.* Arch Ital Biol, 2000. **138**(2): p. 107-22.

40. Pompeiano, O., *Spinovestibular relations: anatomical and physiological aspects.* Prog Brain Res, 1972. **37**: p. 263-96.

41. Peterson, B.W. and J.D. Coulter, *A new long spinal projection from the vestibular nuclei in the cat.* Brain Res, 1977. **122**(2): p. 351-6.

42. Goldberg, J.M. and K.E. Cullen, *Vestibular control of the head: possible functions of the vestibulocollic reflex.* Exp Brain Res, 2011. **210**(3-4): p. 331-45.

43. Shamboul, K.M., *Lumbosacral predominance of vestibulospinal fibre projection in the rat.* J Comp Neurol, 1980. **192**(3): p. 519-30.

44. Jang, S.H., J.W. Kwon, and S.S. Yeo, *Three Dimensional Identification of Medial and Lateral Vestibulospinal Tract in the Human Brain: A Diffusion Tensor Imaging Study.* Front Hum Neurosci, 2018. **12**: p. 229.

45. Skagerberg, G. and A. Bjorklund, *Topographic principles in the spinal projections of serotonergic and non-serotonergic brainstem neurons in the rat.* Neuroscience, 1985. **15**(2): p. 445-80.

46. Zhuo, M. and G.F. Gebhart, *Biphasic modulation of spinal nociceptive transmission from the medullary raphe nuclei in the rat.* J Neurophysiol, 1997. **78**(2): p. 746-58.

47. Jones, S.L. and A.R. Light, *Serotoninergic medullary raphespinal projection to the lumbar spinal cord in the rat: a retrograde immunohistochemical study.* J Comp Neurol, 1992. **322**(4): p. 599-610.

48. Liang, H., et al., *Distribution of raphespinal fibers in the mouse spinal cord.* Mol Pain, 2015. **11**: p. 42.

49. Deumens, R., G.C. Koopmans, and E.A. Joosten, *Regeneration of descending axon tracts after spinal cord injury.* Prog Neurobiol, 2005. **77**(1-2): p. 57-89.

50. Mason, P., *Physiological identification of pontomedullary serotonergic neurons in the rat.* J Neurophysiol, 1997. **77**(3): p. 1087-98.

51. Brown, A.R. and M. Martinez, *From cortex to cord: motor circuit plasticity after spinal cord injury.* Neural Regen Res, 2019. **14**(12): p. 2054-2062.

52. Parittotokkaporn, S., et al., *Non-invasive neuromodulation for bowel, bladder and sexual restoration following spinal cord injury: A systematic review.* Clin Neurol Neurosurg, 2020. **194**: p. 105822.

53. Singh, A., et al., *Global prevalence and incidence of traumatic spinal cord injury.* Clin Epidemiol, 2014. **6**: p. 309-31.

54. DeVivo, M.J. and Y. Chen, *Trends in new injuries, prevalent cases, and aging with spinal cord injury.* Arch Phys Med Rehabil, 2011. **92**(3): p. 332-8.

55. Ge, L., et al., *Traumatic and Nontraumatic Spinal Cord Injuries.* World Neurosurg, 2018. **111**: p. e142-e148.

56. Muller-Jensen, L., et al., *Clinical Presentation and Causes of Non-traumatic Spinal Cord Injury: An Observational Study in Emergency Patients.* Front Neurol, 2021. **12**: p. 701927.

57. Khorasanizadeh, M., et al., *Neurological recovery following traumatic spinal cord injury: a systematic review and meta-analysis.* J Neurosurg Spine, 2019: p. 1-17.

58. Scivoletto, G., et al., *The Rehabilitation of Spinal Cord Injury Patients in Europe.* Acta Neurochir Suppl, 2017. **124**: p. 203-210.

59. Cripps, R.A., et al., *A global map for traumatic spinal cord injury epidemiology: towards a living data repository for injury prevention.* Spinal Cord, 2011. **49**(4): p. 493-501.

60. Wilson, J.R., D.W. Cadotte, and M.G. Fehlings, *Clinical predictors of neurological outcome, functional status, and survival after traumatic spinal cord injury: a systematic review.* J Neurosurg Spine, 2012. **17**(1 Suppl): p. 11-26.

61. Badhiwala, J.H., et al., *The influence of timing of surgical decompression for acute spinal cord injury: a pooled analysis of individual patient data.* Lancet Neurol, 2021. **20**(2): p. 117-126.

62. Kirshblum, S., M. Schmidt Read, and R. Rupp, *Classification challenges of the 2019 revised International Standards for Neurological Classification of Spinal Cord Injury (ISNCSCI).* Spinal Cord, 2022. **60**(1): p. 11-17.

63. Fehlings, M.G., et al., *A Clinical Practice Guideline for the Management of Acute Spinal Cord Injury: Introduction, Rationale, and Scope.* Global Spine J, 2017. **7**(3 Suppl): p. 84S-94S.

64. McDonald, J.W. and C. Sadowsky, *Spinal-cord injury.* Lancet, 2002. **359**(9304): p. 417-25.

65. Ahuja, C.S., et al., *Traumatic Spinal Cord Injury-Repair and Regeneration.* Neurosurgery, 2017. **80**(3S): p. S9-S22.

66. Ito, T., et al., *Traumatic spinal cord injury: a neuropathological study on the longitudinal spreading of the lesions.* Acta Neuropathol, 1997. **93**(1): p. 13-8.

67. Pineau, I. and S. Lacroix, *Proinflammatory cytokine synthesis in the injured mouse spinal cord: multiphasic expression pattern and identification of the cell types involved.* J Comp Neurol, 2007. **500**(2): p. 267-85.

68. Doble, A., *The role of excitotoxicity in neurodegenerative disease: implications for therapy.* Pharmacol Ther, 1999. **81**(3): p. 163-221.

69. McAdoo, D.J., et al., *The effect of glutamate receptor blockers on glutamate release following spinal cord injury. Lack of evidence for an ongoing feedback cascade of damage --> glutamate release --> damage --> glutamate release --> etc.* Brain Res, 2005. **1038**(1): p. 92-9.

70. Pivovarova, N.B. and S.B. Andrews, *Calcium-dependent mitochondrial function and dysfunction in neurons.* FEBS J, 2010. **277**(18): p. 3622-36.

71. Hausmann, O.N., *Post-traumatic inflammation following spinal cord injury.* Spinal Cord, 2003. **41**(7): p. 369-78.

72. Kerschensteiner, M., et al., *In vivo imaging of axonal degeneration and regeneration in the injured spinal cord.* Nat Med, 2005. **11**(5): p. 572-7.

73. Totoiu, M.O. and H.S. Keirstead, *Spinal cord injury is accompanied by chronic progressive demyelination.* J Comp Neurol, 2005. **486**(4): p. 373-83.

74. Hall, E.D., et al., *Lipid peroxidation in brain or spinal cord mitochondria after injury.* J Bioenerg Biomembr, 2016. **48**(2): p. 169-74.

75. Dyck, S.M. and S. Karimi-Abdolrezaee, *Chondroitin sulfate proteoglycans: Key modulators in the developing and pathologic central nervous system.* Exp Neurol, 2015. **269**: p. 169-87.

76. Dumont, R.J., et al., *Acute spinal cord injury, part I: pathophysiologic mechanisms.* Clin Neuropharmacol, 2001. **24**(5): p. 254-64.

77. Sofroniew, M.V., *Molecular dissection of reactive astrogliosis and glial scar formation.* Trends Neurosci, 2009. **32**(12): p. 638-47.

78. Silver, J. and J.H. Miller, *Regeneration beyond the glial scar.* Nat Rev Neurosci, 2004. **5**(2): p. 146-56.

79. Hill, C.E., M.S. Beattie, and J.C. Bresnahan, *Degeneration and sprouting of identified descending supraspinal axons after contusive spinal cord injury in the rat.* Exp Neurol, 2001. **171**(1): p. 153-69.

80. Ehlers, M.D., *Deconstructing the axon: Wallerian degeneration and the ubiquitin-proteasome system.* Trends Neurosci, 2004. **27**(1): p. 3-6.

81. Raineteau, O. and M.E. Schwab, *Plasticity of motor systems after incomplete spinal cord injury.* Nat Rev Neurosci, 2001. **2**(4): p. 263-73.

82. Rodriguez-Barrera, R., et al., *Neurogenesis after Spinal Cord Injury: State of the Art.* Cells, 2021. **10**(6).

83. Curtis, R., et al., *Up-regulation of GAP-43 and growth of axons in rat spinal cord after compression injury.* J Neurocytol, 1993. **22**(1): p. 51-64.

84. Chaisuksunt, V., et al., *Axonal regeneration from CNS neurons in the cerebellum and brainstem of adult rats: correlation with the patterns of expression and distribution of messenger RNAs for L1, CHL1, c-jun and growth-associated protein-43.* Neuroscience, 2000. **100**(1): p. 87-108.

85. He, X., et al., *Promotion of spinal cord regeneration by neural stem cell-secreted trimerized cell adhesion molecule L1.* PLoS One, 2012. **7**(9): p. e46223.

86. Di Giovanni, S., et al., *Neuronal plasticity after spinal cord injury: identification of a gene cluster driving neurite outgrowth.* FASEB J, 2005. **19**(1): p. 153-4.

87. Hayashi, M., et al., *Sequential mRNA expression for immediate early genes, cytokines, and neurotrophins in spinal cord injury.* J Neurotrauma, 2000. **17**(3): p. 203-18.

88. Batchelor, P.E., et al., *Macrophages and Microglia Produce Local Trophic Gradients That Stimulate Axonal Sprouting Toward but Not beyond the Wound Edge.* Mol Cell Neurosci, 2002. **21**(3): p. 436-53.

89. Weidner, N., et al., *Spontaneous corticospinal axonal plasticity and functional recovery after adult central nervous system injury.* Proc Natl Acad Sci U S A, 2001. **98**(6): p. 3513-8.

90. Courtine, G., et al., *Recovery of supraspinal control of stepping via indirect propriospinal relay connections after spinal cord injury.* Nat Med, 2008. **14**(1): p. 69-74.

91. Hilton, B.J. and F. Bradke, *Can injured adult CNS axons regenerate by recapitulating development?* Development, 2017. **144**(19): p. 3417-3429.

92. Cregg, J.M., et al., *Functional regeneration beyond the glial scar.* Exp Neurol, 2014. **253**: p. 197-207.

93. Anderson, M.A., et al., *Astrocyte scar formation aids central nervous system axon regeneration.* Nature, 2016. **532**(7598): p. 195-200.

94. Bradbury, E.J. and E.R. Burnside, *Moving beyond the glial scar for spinal cord repair.* Nat Commun, 2019. **10**(1): p. 3879.

95. McKeon, R.J., et al., *Reduction of neurite outgrowth in a model of glial scarring following CNS injury is correlated with the expression of inhibitory molecules on reactive astrocytes.* J Neurosci, 1991. **11**(11): p. 3398-411.

96. Jang, E.H., et al., *Effects of Microtubule Stabilization by Epothilone B Depend on the Type and Age of Neurons.* Neural Plast, 2016. **2016**: p. 5056418.

97. Jones, L.L., R.U. Margolis, and M.H. Tuszynski, *The chondroitin sulfate proteoglycans neurocan, brevican, phosphacan, and versican are differentially regulated following spinal cord injury.* Exp Neurol, 2003. **182**(2): p. 399-411.

98. Brazda, N. and H.W. Muller, *Pharmacological modification of the extracellular matrix to promote regeneration of the injured brain and spinal cord.* Prog Brain Res, 2009. **175**: p. 269-81.

99. Filbin, M.T., *Myelin-associated inhibitors of axonal regeneration in the adult mammalian CNS.* Nat Rev Neurosci, 2003. **4**(9): p. 703-13.

100. Forgione, N. and M.G. Fehlings, *Rho-ROCK inhibition in the treatment of spinal cord injury.* World Neurosurg, 2014. **82**(3-4): p. e535-9.

101. Ramakonar, H. and M.G. Fehlings, *'Time is Spine': new evidence supports decompression within 24 h for acute spinal cord injury.* Spinal Cord, 2021. **59**(8): p. 933-934.

102. Venkatesh, K., et al., *Spinal cord injury: pathophysiology, treatment strategies, associated challenges, and future implications.* Cell Tissue Res, 2019. **377**(2): p. 125-151.

103. Dalal, K.L., E.R. Felix, and D.D. Cardenas, *Pregabalin for the management of neuropathic pain in spinal cord injury.* Pain Manag, 2013. **3**(5): p. 359-67.

104. Warner, F.M., et al., *Early Administration of Gabapentinoids Improves Motor Recovery after Human Spinal Cord Injury.* Cell Rep, 2017. **18**(7): p. 1614-1618.

105. Wang, H.J., et al., *Glutamatergic receptor dysfunction in spinal cord contributes to the exaggerated exercise pressor reflex in heart failure.* Am J Physiol Heart Circ Physiol, 2015. **308**(5): p. H447-55.

106. Liu, S., G.L. Ruenes, and R.P. Yezierski, *NMDA and non-NMDA receptor antagonists protect against excitotoxic injury in the rat spinal cord.* Brain Res, 1997. **756**(1-2): p. 160-7.

107. Costa, L.M., et al., *Rolipram promotes functional recovery after contusive thoracic spinal cord injury in rats.* Behav Brain Res, 2013. **243**: p. 66-73.

108. Qiu, J., et al., *Spinal axon regeneration induced by elevation of cyclic AMP.* Neuron, 2002. **34**(6): p. 895-903.

109. Winkler, T., et al., *An L-type calcium channel blocker, nimodipine influences trauma induced spinal cord conduction and axonal injury in the rat.* Acta Neurochir Suppl, 2003. **86**: p. 425-32.

110. Chen, B., et al., *Reactivation of Dormant Relay Pathways in Injured Spinal Cord by KCC2 Manipulations.* Cell, 2018. **174**(3): p. 521-535 e13.

111. Page, J.C., et al., *Parallel Evaluation of Two Potassium Channel Blockers in Restoring Conduction in Mechanical Spinal Cord Injury in Rat.* J Neurotrauma, 2018. **35**(9): p. 1057-1068.

112. Grijalva, I., et al., *Efficacy and safety of 4-aminopyridine in patients with long-term spinal cord injury: a randomized, double-blind, placebo-controlled trial.* Pharmacotherapy, 2003. **23**(7): p. 823-34.

113. Bradbury, E.J., et al., *Chondroitinase ABC promotes functional recovery after spinal cord injury.* Nature, 2002. **416**(6881): p. 636-40.

114. Rosenzweig, E.S., et al., *Extensive spontaneous plasticity of corticospinal projections after primate spinal cord injury.* Nat Neurosci, 2010. **13**(12): p. 1505-10.

115. Zhang, Y., et al., *Rho Kinase Inhibitor Y27632 Improves Recovery After Spinal Cord Injury by Shifting Astrocyte Phenotype and Morphology via the ROCK/NF-kappaB/C3 Pathway.* Neurochem Res, 2022. **47**(12): p. 3733-3744.

116. Giraldo, E., et al., *A rationally designed self-immolative linker enhances the synergism between a polymer-rock inhibitor conjugate and neural progenitor cells in the treatment of spinal cord injury.* Biomaterials, 2021. **276**: p. 121052.

117. Hur, E.M., et al., *Engineering neuronal growth cones to promote axon regeneration over inhibitory molecules.* Proc Natl Acad Sci U S A, 2011. **108**(12): p. 5057-62.

118. Dupraz, S., et al., *RhoA Controls Axon Extension Independent of Specification in the Developing Brain.* Curr Biol, 2019. **29**(22): p. 3874-3886 e9.

119. Ruschel, J., et al., *Axonal regeneration. Systemic administration of epothilone B promotes axon regeneration after spinal cord injury.* Science, 2015. **348**(6232): p. 347-52.

120. Griffin, J.M., et al., *Rehabilitation enhances epothilone-induced locomotor recovery after spinal cord injury.* Brain Commun, 2023. **5**(1): p. fcad005.

121. Du, K., et al., *Pten Deletion Promotes Regrowth of Corticospinal Tract Axons 1 Year after Spinal Cord Injury.* J Neurosci, 2015. **35**(26): p. 9754-63.

122. Jin, D., et al., *Restoration of skilled locomotion by sprouting corticospinal axons induced by co-deletion of PTEN and SOCS3.* Nat Commun, 2015. **6**: p. 8074.

123. Anderson, M.A., et al., *Required growth facilitators propel axon regeneration across complete spinal cord injury.* Nature, 2018. **561**(7723): p. 396-400.

124. Burnside, E.R., et al., *Immune-evasive gene switch enables regulated delivery of chondroitinase after spinal cord injury.* Brain, 2018. **141**(8): p. 2362-2381.

125. Stern, S., et al., *RhoA drives actin compaction to restrict axon regeneration and astrocyte reactivity after CNS injury.* Neuron, 2021. **109**(21): p. 3436-3455 e9.

126. Chen, J., et al., *Adeno-associated virus-mediated L1 expression promotes functional recovery after spinal cord injury.* Brain, 2007. **130**(Pt 4): p. 954-69.

127. Li, Y., et al., *BDNF guides neural stem cell-derived axons to ventral interneurons and motor neurons after spinal cord injury.* Experimental Neurology, 2023. **359**.

128. Tom, V.J., et al., *Exogenous BDNF enhances the integration of chronically injured axons that regenerate through a peripheral nerve grafted into a chondroitinase-treated spinal cord injury site.* Exp Neurol, 2013. **239**: p. 91-100.

129. Uchida, K., et al., *The retrograde delivery of adenovirus vector carrying the gene for brain-derived neurotrophic factor protects neurons and oligodendrocytes from apoptosis in the chronically compressed spinal cord of twy/twy mice.* Spine (Phila Pa 1976), 2012. **37**(26): p. 2125-35.

130. *Successful Brain Grafting.* Science, 1890. **16**(392): p. 78-9.

131. Ranson, S.W., *Transplantation of the spinal ganglion into the brain.* Q Bull Northwest Univ Med Sch, 1909. **11**: p. 176-178.

132. Perlow, M.J., et al., *Brain grafts reduce motor abnormalities produced by destruction of nigrostriatal dopamine system.* Science, 1979. **204**(4393): p. 643-7.

133. Cajal, S.R., J. DeFelipe, and E.G. Jones, *Cajal's Degeneration and Regeneration of the Nervous System*. 1991: Oxford University Press.

134. Brown, J.O. and C.G. Mc, *Abortive regeneration of the transected spinal cord.* J Comp Neurol, 1947. **87**(2): p. 131-7.

135. Barnard, J.W. and W. Carpenter, *Lack of regeneration in spinal cord of rat.* J Neurophysiol, 1950. **13**(3): p. 223-28.

136. David, S. and A.J. Aguayo, *Axonal elongation into peripheral nervous system "bridges" after central nervous system injury in adult rats.* Science, 1981. **214**(4523): p. 931-3.

137. Richardson, P.M., U.M. McGuinness, and A.J. Aguayo, *Axons from CNS neurons regenerate into PNS grafts.* Nature, 1980. **284**(5753): p. 264-5.

138. Bernstein-Goral, H. and B.S. Bregman, *Spinal cord transplants support the regeneration of axotomized neurons after spinal cord lesions at birth: a quantitative double-labeling study.* Exp Neurol, 1993. **123**(1): p. 118-32.

139. Bregman, B.S., *Spinal cord transplants permit the growth of serotonergic axons across the site of neonatal spinal cord transection.* Brain Res, 1987. **431**(2): p. 265-79.

140. Jakeman, L.B. and P.J. Reier, *Axonal projections between fetal spinal cord transplants and the adult rat spinal cord: a neuroanatomical tracing study of local interactions.* J Comp Neurol, 1991. **307**(2): p. 311-34.

141. Skoff, R.P. and J.E. Vaughn, *An autoradiographic study of cellular proliferation in degenerating rat optic nerve.* J Comp Neurol, 1971. **141**(2): p. 133-55.

142. Levine, J.M., R. Reynolds, and J.W. Fawcett, *The oligodendrocyte precursor cell in health and disease.* Trends Neurosci, 2001. **24**(1): p. 39-47.

143. Lee, K.H., et al., *Effects of glial transplantation on functional recovery following acute spinal cord injury.* J Neurotrauma, 2005. **22**(5): p. 575-89.

144. Keirstead, H.S., et al., *Human embryonic stem cell-derived oligodendrocyte progenitor cell transplants remyelinate and restore locomotion after spinal cord injury.* J Neurosci, 2005. **25**(19): p. 4694-705.

145. Sharp, J., et al., *Human embryonic stem cell-derived oligodendrocyte progenitor cell transplants improve recovery after cervical spinal cord injury.* Stem Cells, 2010. **28**(1): p. 152-63.

146. Czepiel, M., et al., *Differentiation of induced pluripotent stem cells into functional oligodendrocytes.* Glia, 2011. **59**(6): p. 882-92.

147. All, A.H., et al., *Early intervention for spinal cord injury with human induced pluripotent stem cells oligodendrocyte progenitors.* PLoS One, 2015. **10**(1): p. e0116933.

148. Rasouli, A., et al., *Resection of glial scar following spinal cord injury.* J Orthop Res, 2009. **27**(7): p. 931-6.

149. Fawcett, J.W. and R.A. Asher, *The glial scar and central nervous system repair.* Brain Res Bull, 1999. **49**(6): p. 377-91.

150. Li, N. and G.K. Leung, *Oligodendrocyte Precursor Cells in Spinal Cord Injury: A Review and Update.* Biomed Res Int, 2015. **2015**: p. 235195.

151. Lu, L., et al., *Isolation and characterization of human umbilical cord mesenchymal stem cells with hematopoiesis-supportive function and other potentials.* Haematologica, 2006. **91 8**: p. 1017-26.

152. Fischer, I., J.N. Dulin, and M.A. Lane, *Transplanting neural progenitor cells to restore connectivity after spinal cord injury.* Nat Rev Neurosci, 2020. **21**(7): p. 366-383.

153. Cofano, F., et al., *Mesenchymal Stem Cells for Spinal Cord Injury: Current Options, Limitations, and Future of Cell Therapy.* Int J Mol Sci, 2019. **20**(11).

154. Qi, X., et al., *In vitro differentiation of bone marrow stromal cells into neurons and glial cells and differential protein expression in a two-compartment bone marrow stromal cell/neuron co-culture system.* J Clin Neurosci, 2010. **17**(7): p. 908-13.

155. Kim, G.U., et al., *Therapeutic Potential of Mesenchymal Stem Cells (MSCs) and MSC-Derived Extracellular Vesicles for the Treatment of Spinal Cord Injury.* Int J Mol Sci, 2021. **22**(24).

156. Sorrell, J.M., M.A. Baber, and A.I. Caplan, *Influence of adult mesenchymal stem cells on in vitro vascular formation.* Tissue Eng Part A, 2009. **15**(7): p. 1751-61.

157. Avanzini, M.A., et al., *Generation of mesenchymal stromal cells in the presence of platelet lysate: a phenotypic and functional comparison of umbilical cord blood- and bone marrow-derived progenitors.* Haematologica, 2009. **94**(12): p. 1649-60.

158. Xia, Y., et al., *Application of chitosan-based materials in surgical or postoperative hemostasis.* Frontiers in Materials, 2022. **9**.

159. Han, J., Y. Li, and Y. Li, *Strategies to Enhance Mesenchymal Stem Cell-Based Therapies for Acute Respiratory Distress Syndrome.* Stem Cells Int, 2019. **2019**: p. 5432134.

160. Lane, M.A., A.C. Lepore, and I. Fischer, *Improving the therapeutic efficacy of neural progenitor cell transplantation following spinal cord injury.* Expert Rev Neurother, 2017. **17**(5): p. 433-440.

161. Mayer-Proschel, M., et al., *Isolation of lineage-restricted neuronal precursors from multipotent neuroepithelial stem cells.* Neuron, 1997. **19**(4): p. 773-85.

162. Weiss, S., et al., *Multipotent CNS stem cells are present in the adult mammalian spinal cord and ventricular neuroaxis.* J Neurosci, 1996. **16**(23): p. 7599-609.

163. Altman, J. and G.D. Das, *Autoradiographic and histological evidence of postnatal hippocampal neurogenesis in rats.* J Comp Neurol, 1965. **124**(3): p. 319-35.

164. Zholudeva, L.V., et al., *Transplantation of Neural Progenitors and V2a Interneurons after Spinal Cord Injury.* J Neurotrauma, 2018. **35**(24): p. 2883-2903.

165. Lu, P., et al., *Long-distance growth and connectivity of neural stem cells after severe spinal cord injury.* Cell, 2012. **150**(6): p. 1264-73.

166. Rosenzweig, E.S., et al., *Restorative effects of human neural stem cell grafts on the primate spinal cord.* Nat Med, 2018. **24**(4): p. 484-490.

167. Kadoya, K., et al., *Spinal cord reconstitution with homologous neural grafts enables robust corticospinal regeneration.* Nat Med, 2016. **22**(5): p. 479-87.

168. Ceto, S., et al., *Neural Stem Cell Grafts Form Extensive Synaptic Networks that Integrate with Host Circuits after Spinal Cord Injury.* Cell Stem Cell, 2020. **27**(3): p. 430-440 e5.

169. Requejo-Aguilar, R., et al., *Combined polymer-curcumin conjugate and ependymal progenitor/stem cell treatment enhances spinal cord injury functional recovery.* Biomaterials, 2017. **113**: p. 18-30.

170. Lepore, A.C. and I. Fischer, *Lineage-restricted neural precursors survive, migrate, and differentiate following transplantation into the injured adult spinal cord.* Exp Neurol, 2005. **194**(1): p. 230-42.

171. Khazaei, M., et al., *GDNF rescues the fate of neural progenitor grafts by attenuating Notch signals in the injured spinal cord in rodents.* Sci Transl Med, 2020. **12**(525).

172. Steeves, J.D., et al., *Guidelines for the conduct of clinical trials for spinal cord injury (SCI) as developed by the ICCP panel: clinical trial outcome measures.* Spinal Cord, 2007. **45**(3): p. 206-21.

173. Dietz, V. and R. Muller, *Degradation of neuronal function following a spinal cord injury: mechanisms and countermeasures.* Brain, 2004. **127**(Pt 10): p. 2221-31.

174. Faust, T.E., G. Gunner, and D.P. Schafer, *Mechanisms governing activity-dependent synaptic pruning in the developing mammalian CNS.* Nat Rev Neurosci, 2021. **22**(11): p. 657-673.

175. Ballermann, M. and K. Fouad, *Spontaneous locomotor recovery in spinal cord injured rats is accompanied by anatomical plasticity of reticulospinal fibers.* Eur J Neurosci, 2006. **23**(8): p. 1988-96.

176. Yokota, K., et al., *Pathological changes of distal motor neurons after complete spinal cord injury.* Mol Brain, 2019. **12**(1): p. 4.

177. Satkunendrarajah, K., et al., *Cervical excitatory neurons sustain breathing after spinal cord injury.* Nature, 2018. **562**(7727): p. 419-422.

178. Bertels, H., et al., *Neurotransmitter phenotype switching by spinal excitatory interneurons regulates locomotor recovery after spinal cord injury.* Nat Neurosci, 2022. **25**(5): p. 617-629.

179. Molteni, R., et al., *Voluntary exercise increases axonal regeneration from sensory neurons.* Proc Natl Acad Sci U S A, 2004. **101**(22): p. 8473-8.

180. Priya, R., et al., *Activity Regulates Cell Death within Cortical Interneurons through a Calcineurin-Dependent Mechanism.* Cell Rep, 2018. **22**(7): p. 1695-1709.

181. Warm, D., et al., *Spontaneous Activity Predicts Survival of Developing Cortical Neurons.* Front Cell Dev Biol, 2022. **10**: p. 937761.

182. Duan, Z.R.S., et al., *GABAergic Restriction of Network Dynamics Regulates Interneuron Survival in the Developing Cortex.* Neuron, 2020. **105**(1): p. 75-92 e5.

183. Fouad, K. and W. Tetzlaff, *Rehabilitative training and plasticity following spinal cord injury.* Experimental Neurology, 2012. **235**(1): p. 91-99.

184. Goldshmit, Y., et al., *Treadmill training after spinal cord hemisection in mice promotes axonal sprouting and synapse formation and improves motor recovery.* J Neurotrauma, 2008. **25**(5): p. 449-65.

185. Ying, Z., et al., *Exercise restores levels of neurotrophins and synaptic plasticity following spinal cord injury.* Exp Neurol, 2005. **193**(2): p. 411-9.

186. Sanchez-Ventura, J., et al., *Voluntary wheel running preserves lumbar perineuronal nets, enhances motor functions and prevents hyperreflexia after spinal cord injury.* Exp Neurol, 2021. **336**: p. 113533.

187. Noble, B.T., et al., *Thoracic VGluT2(+) Spinal Interneurons Regulate Structural and Functional Plasticity of Sympathetic Networks after High-Level Spinal Cord Injury.* J Neurosci, 2022. **42**(17): p. 3659-3675.

188. Engesser-Cesar, C., et al., *Wheel running following spinal cord injury improves locomotor recovery and stimulates serotonergic fiber growth.* Eur J Neurosci, 2007. **25**(7): p. 1931-9.

189. Asboth, L., et al., *Cortico-reticulo-spinal circuit reorganization enables functional recovery after severe spinal cord contusion.* Nat Neurosci, 2018. **21**(4): p. 576-588.

190. Li, S., et al., *Promoting axon regeneration in the adult CNS by modulation of the melanopsin/GPCR signaling.* Proc Natl Acad Sci U S A, 2016. **113**(7): p. 1937-42.

191. Petruska, J.C., et al., *Changes in motoneuron properties and synaptic inputs related to step training after spinal cord transection in rats.* J Neurosci, 2007. **27**(16): p. 4460-71.

192. Kobayakawa, K., et al., *Locomotor Training Increases Synaptic Structure With High NGL-2 Expression After Spinal Cord Hemisection.* Neurorehabil Neural Repair, 2019. **33**(3): p. 225-231.

193. Iwahara, T., et al., *Spinal cord stimulation-induced locomotion in the adult cat.* Brain Res Bull, 1992. **28**(1): p. 99-105.

194. Musienko, P.E., I.N. Bogacheva, and Y.P. Gerasimenko, *Significance of peripheral feedback in the generation of stepping movements during epidural stimulation of the spinal cord.* Neurosci Behav Physiol, 2007. **37**(2): p. 181-90.

195. Lavrov, I., et al., *Facilitation of stepping with epidural stimulation in spinal rats: role of sensory input.* J Neurosci, 2008. **28**(31): p. 7774-80.

196. Courtine, G., et al., *Transformation of nonfunctional spinal circuits into functional states after the loss of brain input.* Nat Neurosci, 2009. **12**(10): p. 1333-42.

197. Barra, B., et al., *Epidural electrical stimulation of the cervical dorsal roots restores voluntary upper limb control in paralyzed monkeys.* Nat Neurosci, 2022. **25**(7): p. 924-934.

198. Kathe, C., et al., *The neurons that restore walking after paralysis.* Nature, 2022. **611**(7936): p. 540-547.

199. Tornero, D., et al., *Human induced pluripotent stem cell-derived cortical neurons integrate in stroke-injured cortex and improve functional recovery.* Brain, 2013. **136**(Pt 12): p. 3561-77.

200. Michelsen, K.A., et al., *Area-specific reestablishment of damaged circuits in the adult cerebral cortex by cortical neurons derived from mouse embryonic stem cells.* Neuron, 2015. **85**(5): p. 982-97.

201. Bjorklund, A. and O. Lindvall, *Replacing Dopamine Neurons in Parkinson's Disease: How did it happen?* J Parkinsons Dis, 2017. **7**(s1): p. S21-S31.

202. Braz, J.M., et al., *Transplant-mediated enhancement of spinal cord GABAergic inhibition reverses paclitaxel-induced mechanical and heat hypersensitivity.* Pain, 2015. **156**(6): p. 1084-1091.

203. Braz, J.M., et al., *Forebrain GABAergic neuron precursors integrate into adult spinal cord and reduce injury-induced neuropathic pain.* Neuron, 2012. **74**(4): p. 663-75.

204. Zheng, X., et al., *Human spinal GABA neurons survive and mature in the injured nonhuman primate spinal cord.* Stem Cell Reports, 2023. **18**(2): p. 439-448.

205. Neumann, S. and C.J. Woolf, *Regeneration of dorsal column fibers into and beyond the lesion site following adult spinal cord injury.* Neuron, 1999. **23**(1): p. 83-91.

206. Neumann, S., et al., *Regeneration of sensory axons within the injured spinal cord induced by intraganglionic cAMP elevation.* Neuron, 2002. **34**(6): p. 885-93.

207. Horvat, J.C., et al., *Co-transplantation of embryonic neural tissue and autologous peripheral nerve segments to severe spinal cord injury of the adult rat. Guided axogenesis from transplanted neurons.* Restor Neurol Neurosci, 1991. **2**(4): p. 289-98.

208. Ye, J.H., et al., *Co-transplantation of fetal or adult dorsal root ganglia and of autologous peripheral nerve segments to the adult rat spinal cord: extensive reinnervation of the grafted nerves by the transplanted DRG cells.* Dev Neurosci, 1992. **14**(2): p. 123-9.

209. Rhrich-Haddout, F., et al., *Expression of peripherin in solid transplants of foetal spinal cord and dorsal root ganglia grafted to the injured cervical spinal cord of adult rats.* Neurosci Lett, 1994. **170**(1): p. 59-62.

210. Zalewski, A.A., H.G. Goshgarian, and W.K. Silvers, *The fate of neurons and neurilemmal cells in allografts of ganglia in the spinal cord of normal and immunologically tolerant rats.* Exp Neurol, 1978. **59**(2): p. 322-30.

211. Rosario, C.M., et al., *Centrifugal growth in orthotopic grafts of allogeneic dorsal root ganglia in adult rats: evidence for possible central ingrowth?* Exp Neurol, 1992. **115**(1): p. 158-62.

212. Rosario, C.M., et al., *Differentiation and axonal outgrowth pattern of fetal dorsal root ganglion cells orthotopically allografted into adult rats.* Exp Neurol, 1993. **120**(1): p. 16-31.

213. Rosario, C.M., et al., *Peripheral target reinnervation following orthotopic grafting of fetal allogeneic and xenogeneic dorsal root ganglia.* Exp Neurol, 1995. **132**(2): p. 251-61.

214. Kozlova, E.N., et al., *Peripherally grafted human foetal dorsal root ganglion cells extend axons into the spinal cord of adult host rats by circumventing dorsal root entry zone astrocytes.* Neuroreport, 1995. **6**(2): p. 269-72.

215. Davies, S.J., et al., *Regeneration of adult axons in white matter tracts of the central nervous system.* Nature, 1997. **390**(6661): p. 680-3.

216. Davies, S.J., et al., *Robust regeneration of adult sensory axons in degenerating white matter of the adult rat spinal cord.* J Neurosci, 1999. **19**(14): p. 5810-22.

217. Ren, D., et al., *A prokaryotic voltage-gated sodium channel.* Science, 2001. **294**(5550): p. 2372-5.

218. Charalambous, K. and B.A. Wallace, *NaChBac: the long lost sodium channel ancestor.* Biochemistry, 2011. **50**(32): p. 6742-52.

219. Chahine, M., et al., *Role of arginine residues on the S4 segment of the Bacillus halodurans Na+ channel in voltage-sensing.* J Membr Biol, 2004. **201**(1): p. 9-24.

220. Bean, B.P., *The action potential in mammalian central neurons.* Nat Rev Neurosci, 2007. **8**(6): p. 451-65.

221. Kelsch, W., et al., *A critical period for activity-dependent synaptic development during olfactory bulb adult neurogenesis.* J Neurosci, 2009. **29**(38): p. 11852-8.

222. Xue, M., B.V. Atallah, and M. Scanziani, *Equalizing excitation-inhibition ratios across visual cortical neurons.* Nature, 2014. **511**(7511): p. 596-600.

223. Zhu, C., et al., *Profound and redundant functions of arcuate neurons in obesity development.* Nat Metab, 2020. **2**(8): p. 763-774.

224. Bando, Y., et al., *Control of Spontaneous Ca2+ Transients Is Critical for Neuronal Maturation in the Developing Neocortex.* Cereb Cortex, 2016. **26**(1): p. 106-117.

225. Pfisterer, U. and K. Khodosevich, *Neuronal survival in the brain: neuron type-specific mechanisms.* Cell Death Dis, 2017. **8**(3): p. e2643.

226. Wong Fong Sang, I.E., et al., *Optogenetically Controlled Activity Pattern Determines Survival Rate of Developing Neocortical Neurons.* Int J Mol Sci, 2021. **22**(12).

227. Mouret, A., et al., *Learning and survival of newly generated neurons: when time matters.* J Neurosci, 2008. **28**(45): p. 11511-6.

228. Lin, C.W., et al., *Genetically increased cell-intrinsic excitability enhances neuronal integration into adult brain circuits.* Neuron, 2010. **65**(1): p. 32-9.

229. Ding, B. and D.L. Kilpatrick, *Lentiviral vector production, titration, and transduction of primary neurons.* Methods Mol Biol, 2013. **1018**: p. 119-31.

230. Sanchez-Huertas, C., et al., *Non-centrosomal nucleation mediated by augmin organizes microtubules in post-mitotic neurons and controls axonal microtubule polarity.* Nat Commun, 2016. **7**: p. 12187.

231. Rubinson, D.A., et al., *A lentivirus-based system to functionally silence genes in primary mammalian cells, stem cells and transgenic mice by RNA interference.* Nat Genet, 2003. **33**(3): p. 401-6.

232. Monreal-Trigo, J., et al., *Optogenetic Stimulation Array for Confocal Microscopy Fast Transient Monitoring.* IEEE Trans Biomed Circuits Syst, 2022. **PP**.

233. Virtanen, S.S., et al., *Adenosine inhibits tumor cell invasion via receptor-independent mechanisms.* Mol Cancer Res, 2014. **12**(12): p. 1863-74.

234. Wojnicz, A., et al., *Simultaneous monitoring of monoamines, amino acids, nucleotides and neuropeptides by liquid chromatography-tandem mass spectrometry and its application to neurosecretion in bovine chromaffin cells.* J Mass Spectrom, 2016. **51**(8): p. 651-664.

235. Lilley, E., et al., *Refining rodent models of spinal cord injury.* Exp Neurol, 2020. **328**: p. 113273.

236. Chen, B., et al., *Reactivation of Dormant Relay Pathways in Injured Spinal Cord by KCC2 Manipulations.* Cell, 2018. **174**(6): p. 1599.

237. Hilton, B.J., et al., *High-resolution 3D imaging and analysis of axon regeneration in unsectioned spinal cord with or without tissue clearing.* Nat Protoc, 2019. **14**(4): p. 1235-1260.

238. Ahmed, R.U., M. Alam, and Y.P. Zheng, *Experimental spinal cord injury and behavioral tests in laboratory rats.* Heliyon, 2019. **5**(3): p. e01324.

239. Basso, D.M., et al., *Basso Mouse Scale for locomotion detects differences in recovery after spinal cord injury in five common mouse strains.* J Neurotrauma, 2006. **23**(5): p. 635-59.

240. Cummings, B.J., et al., *Adaptation of a ladder beam walking task to assess locomotor recovery in mice following spinal cord injury.* Behav Brain Res, 2007. **177**(2): p. 232-41.

241. Metz, G.A. and I.Q. Whishaw, *Cortical and subcortical lesions impair skilled walking in the ladder rung walking test: a new task to evaluate fore- and hindlimb stepping, placing, and co-ordination.* J Neurosci Methods, 2002. **115**(2): p. 169-79.

242. Deuis, J.R., L.S. Dvorakova, and I. Vetter, *Methods Used to Evaluate Pain Behaviors in Rodents.* Frontiers in Molecular Neuroscience, 2017. **10**.

243. Giraldo, E., et al., *Transplantation of Human-Fetal-Spinal-Cord-Derived NPCs Primed with a Polyglutamate-Conjugated Rho/Rock Inhibitor in Acute Spinal Cord Injury.* Cells, 2022. **11**(20).

244. Stuart, D.A. and D.E. Oorschot, *Embedding, sectioning, immunocytochemical and stereological methods that optimise research on the lesioned adult rat spinal cord.* J Neurosci Methods, 1995. **61**(1-2): p. 5-14.

245. Adzemovic, M.Z., et al., *Immunohistochemical Analysis in the Rat Central Nervous System and Peripheral Lymph Node Tissue Sections.* J Vis Exp, 2016(117).

246. Xia, L., et al., *Continual Deletion of Spinal Microglia Reforms Astrocyte Scar Favoring Axonal Regeneration.* Front Pharmacol, 2022. **13**: p. 881195.

247. Schaal, S.M., et al., *The therapeutic profile of rolipram, PDE target and mechanism of action as a neuroprotectant following spinal cord injury.* PLoS One, 2012. **7**(9): p. e43634.

248. Franze, K. and J. Guck, *The biophysics of neuronal growth.* Reports on Progress in Physics, 2010. **73**(9).

249. Leite, S.C., R. Pinto-Costa, and M.M. Sousa, *Actin dynamics in the growth cone: a key player in axon regeneration.* Curr Opin Neurobiol, 2021. **69**: p. 11-18.

250. Yu, P., et al., *Myosin II activity regulates neurite outgrowth and guidance in response to chondroitin sulfate proteoglycans.* J Neurochem, 2012. **120**(6): p. 1117-28.

251. Wang, X.W., et al., *Knocking Out Non-muscle Myosin II in Retinal Ganglion Cells Promotes Long-Distance Optic Nerve Regeneration.* Cell Rep, 2020. **31**(3): p. 107537.

252. Geraldo, S. and P.R. Gordon-Weeks, *Cytoskeletal dynamics in growth-cone steering.* J Cell Sci, 2009. **122**(Pt 20): p. 3595-604.

253. Buck, K.B. and J.Q. Zheng, *Growth cone turning induced by direct local modification of microtubule dynamics.* J Neurosci, 2002. **22**(21): p. 9358-67.

254. Ruschel, J. and F. Bradke, *Systemic administration of epothilone D improves functional recovery of walking after rat spinal cord contusion injury.* Exp Neurol, 2018. **306**: p. 243-249.

255. Kaplan, A., et al., *Neurite outgrowth and growth cone collapse assays to assess neuronal responses to extracellular cues.* Methods Mol Biol, 2014. **1162**: p. 43-56.

256. Jin, J., et al., *Effect of chondroitin sulfate proteoglycans on neuronal cell adhesion, spreading and neurite growth in culture.* Neural Regen Res, 2018. **13**(2): p. 289-297.

257. Bonner, J. and T.P. O'Connor, *The permissive cue laminin is essential for growth cone turning in vivo.* J Neurosci, 2001. **21**(24): p. 9782-91.

258. Lemmon, V., et al., *Neurite growth on different substrates: permissive versus instructive influences and the role of adhesive strength.* J Neurosci, 1992. **12**(3): p. 818-26.

259. Zhao, Y., et al., *Patch clamp technique: Review of the current state of the art and potential contributions from nanoengineering.* Proceedings of the Institution of Mechanical Engineers, Part N: Journal of Nanoengineering and Nanosystems, 2009. **222**(1): p. 1-11.

260. Verkhratsky, A., et al., *Crosslink between calcium and sodium signalling.* Exp Physiol, 2018. **103**(2): p. 157-169.

261. Yu, X.M., et al., *THE ROLE OF INTRACELLULAR SODIUM (Na) IN THE REGULATION OF CALCIUM (Ca)-MEDIATED SIGNALING AND TOXICITY.* Health (Irvine Calif), 2010. **2**(1): p. 8-15.

262. Sukumaran, P., et al., *Calcium Signaling Regulates Autophagy and Apoptosis.* Cells, 2021. **10**(8).

263. Kumar, S., et al., *Mechanisms controlling neurite outgrowth in a pheochromocytoma cell line: the role of TRPC channels.* J Cell Physiol, 2012. **227**(4): p. 1408-19.

264. Gasperini, R.J., et al., *How does calcium interact with the cytoskeleton to regulate growth cone motility during axon pathfinding?* Mol Cell Neurosci, 2017. **84**: p. 29-35.

265. Halls, M.L. and D.M. Cooper, *Regulation by Ca2+-signaling pathways of adenylyl cyclases.* Cold Spring Harb Perspect Biol, 2011. **3**(1): p. a004143.

266. Forbes, E.M., et al., *Calcium and cAMP levels interact to determine attraction versus repulsion in axon guidance.* Neuron, 2012. **74**(3): p. 490-503.

267. Evangelopoulos, M.E., J. Weis, and A. Kruttgen, *Signalling pathways leading to neuroblastoma differentiation after serum withdrawal: HDL blocks neuroblastoma differentiation by inhibition of EGFR.* Oncogene, 2005. **24**(20): p. 3309-18.

268. Namsi, A., et al., *Induction of Neuronal Differentiation of Murine N2a Cells by Two Polyphenols Present in the Mediterranean Diet Mimicking Neurotrophins Activities: Resveratrol and Apigenin.* Diseases, 2018. **6**(3).

269. Tremblay, R.G., et al., *Differentiation of mouse Neuro 2A cells into dopamine neurons.* J Neurosci Methods, 2010. **186**(1): p. 60-7.

270. Kim, M.S., et al., *Ginsenoside Re and Rd enhance the expression of cholinergic markers and neuronal differentiation in Neuro-2a cells.* Biol Pharm Bull, 2014. **37**(5): p. 826-33.

271. Martin, D., et al., *DC electrical stimulation enhances proliferation and differentiation on N2a and MC3T3 cell lines.* J Biol Eng, 2022. **16**(1): p. 27.

272. Yadav, Y., M. Sharma, and C.S. Dey, *PP1gamma regulates neuronal insulin signaling and aggravates insulin resistance leading to AD-like phenotypes.* Cell Commun Signal, 2023. **21**(1): p. 82.

273. Blanco, V., J. Lopez Camelo, and N.G. Carri, *Growth inhibition, morphological differentiation and stimulation of survival in neuronal cell type (Neuro-2a) treated with trophic molecules.* Cell Biol Int, 2001. **25**(9): p. 909-17.

274. Hou, Y., et al., *Resveratrol provides neuroprotection by regulating the JAK2/STAT3/PI3K/AKT/mTOR pathway after stroke in rats.* Genes Dis, 2018. **5**(3): p. 245-255.

275. Deng, H., et al., *B-Cell Lymphoma 2 (Bcl-2) and Regulation of Apoptosis after Traumatic Brain Injury: A Clinical Perspective.* Medicina (Kaunas), 2020. **56**(6).

276. Pemberton, J.M., J.P. Pogmore, and D.W. Andrews, *Neuronal cell life, death, and axonal degeneration as regulated by the BCL-2 family proteins.* Cell Death Differ, 2021. **28**(1): p. 108-122.

277. Deogracias, R., et al., *Expression of the neurotrophin receptor trkB is regulated by the cAMP/CREB pathway in neurons.* Mol Cell Neurosci, 2004. **26**(3): p. 470-80.

278. Fearnley, G.W., et al., *VEGF-A isoform-specific regulation of calcium ion flux, transcriptional activation and endothelial cell migration.* Biol Open, 2015. **4**(6): p. 731-42.

279. Perez-Garcia, M.J., et al., *Glial cell line-derived neurotrophic factor increases intracellular calcium concentration. Role of calcium/calmodulin in the activation of the phosphatidylinositol 3-kinase pathway.* J Biol Chem, 2004. **279**(7): p. 6132-42.

280. Cheriyan, T., et al., *Spinal cord injury models: a review.* Spinal Cord, 2014. **52**(8): p. 588-95.

281. Roth, E.J., et al., *Traumatic cervical Brown-Sequard and Brown-Sequard-plus syndromes: the spectrum of presentations and outcomes.* Paraplegia, 1991. **29**(9): p. 582-9.

282. Steward, O. and R. Willenberg, *Rodent spinal cord injury models for studies of axon regeneration.* Exp Neurol, 2017. **287**(Pt 3): p. 374-383.

283. Anderson, K.D., M. Abdul, and O. Steward, *Quantitative assessment of deficits and recovery of forelimb motor function after cervical spinal cord injury in mice.* Exp Neurol, 2004. **190**(1): p. 184-91.

284. Dolbeare, D. and J.D. Houle, *Restriction of axonal retraction and promotion of axonal regeneration by chronically injured neurons after intraspinal treatment with glial cell line-derived neurotrophic factor (GDNF).* J Neurotrauma, 2003. **20**(11): p. 1251-61.

285. Li, X., et al., *Regenerative Potential of Ependymal Cells for Spinal Cord Injuries Over Time.* EBioMedicine, 2016. **13**: p. 55-65.

286. Elkhenany, H., et al., *A Hyaluronic Acid Demilune Scaffold and Polypyrrole-Coated Fibers Carrying Embedded Human Neural Precursor Cells and Curcumin for Surface Capping of Spinal Cord Injuries.* Biomedicines, 2021. **9**(12).

287. Usoskin, D., et al., *Unbiased classification of sensory neuron types by large-scale single-cell RNA sequencing.* Nat Neurosci, 2015. **18**(1): p. 145-53.

288. Zheng, Y., et al., *Deep Sequencing of Somatosensory Neurons Reveals Molecular Determinants of Intrinsic Physiological Properties.* Neuron, 2019. **103**(4): p. 598-616 e7.

289. Li, K., et al., *Endogenous but not sensory-driven activity controls migration, morphogenesis and survival of adult-born juxtaglomerular neurons in the mouse olfactory bulb.* Cell Mol Life Sci, 2023. **80**(4): p. 98.

290. Piltti, K.M., et al., *Transplantation dose alters the dynamics of human neural stem cell engraftment, proliferation and migration after spinal cord injury.* Stem Cell Res, 2015. **15**(2): p. 341-53.

291. Courtine, G., et al., *Performance of locomotion and foot grasping following a unilateral thoracic corticospinal tract lesion in monkeys (Macaca mulatta).* Brain, 2005. **128**(Pt 10): p. 2338-58.

292. Poplawski, G.H. and M.H. Tuszynski, *Regeneration of Corticospinal Axons into Neural Progenitor Cell Grafts After Spinal Cord Injury.* Neurosci Insights, 2020. **15**: p. 2633105520974000.

293. Carmichael, S.T. and M.F. Chesselet, *Synchronous neuronal activity is a signal for axonal sprouting after cortical lesions in the adult.* J Neurosci, 2002. **22**(14): p. 6062-70.

294. Zareen, N., et al., *Stimulation-dependent remodeling of the corticospinal tract requires reactivation of growth-promoting developmental signaling pathways.* Exp Neurol, 2018. **307**: p. 133-144.

295. Cao, Y., et al., *Contralateral Axon Sprouting but Not Ipsilateral Regeneration Is Responsible for Spontaneous Locomotor Recovery Post Spinal Cord Hemisection.* Front Cell Neurosci, 2021. **15**: p. 730348.

296. Barriere, G., et al., *Prominent role of the spinal central pattern generator in the recovery of locomotion after partial spinal cord injuries.* J Neurosci, 2008. **28**(15): p. 3976-87.

297. Flynn, J.R., et al., *The role of propriospinal interneurons in recovery from spinal cord injury.* Neuropharmacology, 2011. **60**(5): p. 809-22.

298. May, Z., et al., *Following Spinal Cord Injury Transected Reticulospinal Tract Axons Develop New Collateral Inputs to Spinal Interneurons in Parallel with Locomotor Recovery.* Neural Plast, 2017. **2017**: p. 1932875.

299. Bonilla, P., et al., *Human-Induced Neural and Mesenchymal Stem Cell Therapy Combined with a Curcumin Nanoconjugate as a Spinal Cord Injury Treatment.* Int J Mol Sci, 2021. **22**(11).

300. Fouad, K., et al., *Locomotion after spinal cord injury depends on constitutive activity in serotonin receptors.* J Neurophysiol, 2010. **104**(6): p. 2975-84.

301. Fouad, K., et al., *Cervical sprouting of corticospinal fibers after thoracic spinal cord injury accompanies shifts in evoked motor responses.* Curr Biol, 2001. **11**(22): p. 1766-70.

302. Onifer, S.M., G.M. Smith, and K. Fouad, *Plasticity after spinal cord injury: relevance to recovery and approaches to facilitate it.* Neurotherapeutics, 2011. **8**(2): p. 283-93.

303. Bhowmick, S. and P.M. Abdul-Muneer, *PTEN Blocking Stimulates Corticospinal and Raphespinal Axonal Regeneration and Promotes Functional Recovery After Spinal Cord Injury.* J Neuropathol Exp Neurol, 2021. **80**(2): p. 169-181.

304. Du Beau, A., et al., *Neurotransmitter phenotypes of descending systems in the rat lumbar spinal cord.* Neuroscience, 2012. **227**: p. 67-79.

305. Chaudhry, F.A., et al., *The vesicular GABA transporter, VGAT, localizes to synaptic vesicles in sets of glycinergic as well as GABAergic neurons.* J Neurosci, 1998. **18**(23): p. 9733-50.

306. Beauparlant, J., et al., *Undirected compensatory plasticity contributes to neuronal dysfunction after severe spinal cord injury.* Brain, 2013. **136**(Pt 11): p. 3347-61.

307. Griffin, J.M. and F. Bradke, *Therapeutic repair for spinal cord injury: combinatory approaches to address a multifaceted problem.* EMBO Mol Med, 2020. **12**(3): p. e11505.

308. Wang, J.M., et al., *Cograft of neural stem cells and schwann cells overexpressing TrkC and neurotrophin-3 respectively after rat spinal cord transection.* Biomaterials, 2011. **32**(30): p. 7454-68.

309. Brini, M., et al., *Neuronal calcium signaling: function and dysfunction.* Cell Mol Life Sci, 2014. **71**(15): p. 2787-814.

310. Cameron, E.G. and M.S. Kapiloff, *Intracellular compartmentation of cAMP promotes neuroprotection and regeneration of CNS neurons.* Neural Regen Res, 2017. **12**(2): p. 201-202.

311. Inglebert, Y. and D. Debanne, *Calcium and Spike Timing-Dependent Plasticity.* Front Cell Neurosci, 2021. **15**: p. 727336.

312. Shahoha, M., et al., *cAMP-Dependent Synaptic Plasticity at the Hippocampal Mossy Fiber Terminal.* Front Synaptic Neurosci, 2022. **14**: p. 861215.

313. Pearse, D.D., et al., *cAMP and Schwann cells promote axonal growth and functional recovery after spinal cord injury.* Nat Med, 2004. **10**(6): p. 610-6.

314. Bonneau, B., et al., *Non-apoptotic roles of Bcl-2 family: the calcium connection.* Biochim Biophys Acta, 2013. **1833**(7): p. 1755-65.

315. Kourti, M., et al., *Enhanced Ca(2+) Entry Sustains the Activation of Akt in Glucose Deprived SH-SY5Y Cells.* Int J Mol Sci, 2022. **23**(3).

316. Amemiya, Y., et al., *New Insights into the Regulation of mTOR Signaling via Ca(2+)-Binding Proteins.* Int J Mol Sci, 2023. **24**(4).

317. Duan, X., et al., *Subtype-specific regeneration of retinal ganglion cells following axotomy: effects of osteopontin and mTOR signaling.* Neuron, 2015. **85**(6): p. 1244-56.

318. Chen, N., et al., *Overexpression of Rictor in the injured spinal cord promotes functional recovery in a rat model of spinal cord injury.* FASEB J, 2020. **34**(5): p. 6984-6998.

319. Harvey, A.R., et al., *Neurotrophic factors for spinal cord repair: Which, where, how and when to apply, and for what period of time?* Brain Res, 2015. **1619**: p. 36-71.

320. Weishaupt, N., A. Blesch, and K. Fouad, *BDNF: the career of a multifaceted neurotrophin in spinal cord injury.* Exp Neurol, 2012. **238**(2): p. 254-64.

321. Wang, L., et al., *Neural Stem Cells Overexpressing Nerve Growth Factor Improve Functional Recovery in Rats Following Spinal Cord Injury via Modulating Microenvironment and Enhancing Endogenous Neurogenesis.* Front Cell Neurosci, 2021. **15**: p. 773375.

322. Widenfalk, J., et al., *Vascular endothelial growth factor improves functional outcome and decreases secondary degeneration in experimental spinal cord contusion injury.* Neuroscience, 2003. **120**(4): p. 951-60.

323. Ortmann, S.D. and D.J. Hellenbrand, *Glial cell line-derived neurotrophic factor as a treatment after spinal cord injury.* Neural Regen Res, 2018. **13**(10): p. 1733-1734.

324. Zhang, D., et al., *Insulin-like growth factor 1 promotes neurological functional recovery after spinal cord injury through inhibition of autophagy via the PI3K/Akt/mTOR signaling pathway.* Exp Ther Med, 2021. **22**(5): p. 1265.

325. Huang, X., et al., *GM-CSF inhibits glial scar formation and shows long-term protective effect after spinal cord injury.* J Neurol Sci, 2009. **277**(1-2): p. 87-97.

326. Guo, X.Y., et al., *Subcutaneous Administration of PDGF-AA Improves the Functional Recovery After Spinal Cord Injury.* Front Neurosci, 2019. **13**: p. 6.

327. Spitzer, N.C., *Electrical activity in early neuronal development.* Nature, 2006. **444**(7120): p. 707-12.

328. Itoh, K., et al., *Activity-dependent regulation of N-cadherin in DRG neurons: Differential regulation of N-cadherin, NCAM, and L1 by distinct patterns of action potentials.* Journal of Neurobiology, 1997. **33**(6): p. 735-748.

329. Fehlings, M.G., et al., *A Randomized Controlled Trial of Local Delivery of a Rho Inhibitor (VX-210) in Patients with Acute Traumatic Cervical Spinal Cord Injury.* J Neurotrauma, 2021. **38**(15): p. 2065-2072.

330. van den Brand, R., et al., *Restoring voluntary control of locomotion after paralyzing spinal cord injury.* Science, 2012. **336**(6085): p. 1182-5.

331. Girgis, J., et al., *Reaching training in rats with spinal cord injury promotes plasticity and task specific recovery.* Brain, 2007. **130**(Pt 11): p. 2993-3003.

332. Rowald, A., et al., *Activity-dependent spinal cord neuromodulation rapidly restores trunk and leg motor functions after complete paralysis.* Nat Med, 2022. **28**(2): p. 260-271.

333. Fouad, K. and W. Tetzlaff, *Rehabilitative training and plasticity following spinal cord injury.* Exp Neurol, 2012. **235**(1): p. 91-9.